REAL-TIME AND RELIABLE COMMUNICATION IN WIRELESS SENSOR AND ACTOR NETWORKS

A Thesis
Presented to
The Academic Faculty

by

Vehbi Cagri Gungor

In Partial Fulfillment
of the Requirements for the Degree
Doctor of Philosophy in Electrical and Computer Engineering in the
School of Electrical and Computer Engineering

Georgia Institute of Technology
August 2007

REAL-TIME AND RELIABLE COMMUNICATION IN WIRELESS SENSOR AND ACTOR NETWORKS

Approved by:

Professor Ian F. Akyildiz, Advisor
School of Electrical and Computer Engineering
Georgia Institute of Technology

Professor Bonnie S. Heck
School of Electrical and Computer Engineering
Georgia Institute of Technology

Professor John Copeland
School of Electrical and Computer Engineering
Georgia Institute of Technology

Professor Richard Fujimoto
College of Computing
Georgia Institute of Technology

Professor Henry Owen
School of Electrical and Computer Engineering
Georgia Institute of Technology

Date Approved: June 6 2007

To my mother Ayten,

and to my love Burcu

ACKNOWLEDGEMENTS

First and foremost, I would like to express my gratitude and sincere thanks to my advisor, Dr. Ian F. Akyildiz. I am indebted to Dr. Akyildiz for his invaluable and seamless support, guidance, friendship, and trust throughout my doctoral study. This work would not have been possible without all the insightful discussions with him. Not only did Dr. Akyildiz lead me into the world of networking research, he has also taught me in many other ways that could lead me to success in my future career.

My cordial thanks also extend to Dr. John Copeland, Dr. Henry Owen, Dr. Bonnie S. Heck, and Dr. Richard Fujimoto for being on my dissertation defense committee. Their invaluable comments and enlightening suggestions have helped me to achieve a solid research path towards this thesis.

I would also like to acknowledge the members of the Broadband and Wireless Networking Laboratory (BWN-Lab) due to the excellent atmosphere they created. I am especially thankful to Ozgur B. Akan and Mehmet C. Vuran for their friendship and support.

Finally, I would like to express my deep gratitude to my mother Ayten and my love Burcu, for their patience, continuous support and encouragement throughout this thesis.

TABLE OF CONTENTS

LIST OF TABLES

LIST OF FIGURES

ABBREVIATIONS

LQI	Link Quality Indicator
MAC	Medium Access Control
MEMS	Micro Electro-Mechanical Systems
LOS	Line-Of-Sight
NGWI	Next Generation Wireless Internet
NLOS	Non Line-Of-Sight
QoS	Quality of Service
PRR	Packet Reception Rate
RLQ	Resource-aware and Link-Quality-based
RSSI	Received Signal Strength Indicator
$(RT)^2$	Real-Time and Reliable Transport
RTT	Round Trip Time
SACK	Selective Acknowledgment
TCP	Transmission Control Protocol
WAMR	Wireless Automatic Meter Reading
WSN	Wireless Sensor Network
WSAN	Wireless Sensor and Actor Network

SUMMARY

Wireless Sensor and Actor Networks (WSANs) are composed of heterogeneous nodes referred to as *sensors* and *actors*. Sensors are low-cost, low-power, multi-functional devices that communicate untethered in short distances. Actors collect and process sensor data and perform appropriate actions on the environment. Hence, actors are resource-rich devices equipped with higher processing and transmission capabilities, and longer battery life.

In WSANs, the collaborative operation of the sensors enables the distributed sensing of a physical phenomenon. After sensors detect an event in the deployment field, the event data is distributively processed and transmitted to the actors, which gather, process, and eventually reconstruct the event data. WSANs can be considered a distributed control system designed to react to sensor information with an effective and timely action. For this reason, in WSANs it is important to provide real-time coordination and communication to guarantee timely execution of the right actions. The energy efficiency of the networking protocols is also a major concern, since sensors are resource-constrained devices. Hence, the unique characteristics and challenges coupled with the limitations of wireless environments call for novel networking protocols for WSANs.

The objective of this research is to develop new communication protocols to support real-time and reliable event data delivery with minimum energy consumption in WSANs. The proposed solutions dynamically adjust their protocol configurations to adapt to the heterogenous characteristics of WSANs. Specifically, the interactions between contention resolution and congestion control mechanisms as well as the physical layer effects in WSANs are investigated. Next, a real-time and reliable transport

protocol is proposed to achieve reliable and timely event detection with congestion avoidance in WSANs. In addition, a resource-aware and link-quality-based routing protocol is presented to address energy limitations and link quality variations in WSANs. Finally, the WSAN applications are presented for electric utilities and the propagation characteristics of wireless channel in different utility environments are investigated.

CHAPTER I

INTRODUCTION

Wireless Sensor and Actor Networks (WSANs) [16] are composed of heterogeneous nodes referred to as *sensors* and *actors*. Sensors are low-cost, low-power, multi-functional devices that communicate untethered in short distances. Actors collect and process sensor data and perform appropriate actions on the environment. Hence, actors are resource-rich devices equipped with higher processing and transmission capabilities, and longer battery life. A typical network architecture of WSANs is shown in Figure 1.

In WSANs, the collaborative operation of the sensors enables the *distributed sensing* of a physical phenomenon. After sensors detect an event that is occurring in the environment, the event data is distributively processed and transmitted to the actors, which gather, process, and eventually reconstruct the event data. The process of establishing data paths between sensors and actors is referred to as *sensor-actor communication* [16]. Once the event has been detected, the actors coordinate to reconstruct it, to estimate its characteristics, and make a collaborative decision on how to perform the action. This process is referred to as *actor-actor communication* [16]. Therefore, the operation of the WSANs can be considered as a timely event detection, decision, and acting loop.

The existing and potential applications of WSANs span a wide range, including real-time target tracking, homeland security, battlefield surveillance, and biological or chemical attack detection [16], [43], [28], [40]. For example, in fire detection applications, sensors can relay the exact origin and intensity of the fire to water sprinkler actors so that the fire can be extinguished before it spreads. Similarly, motion and

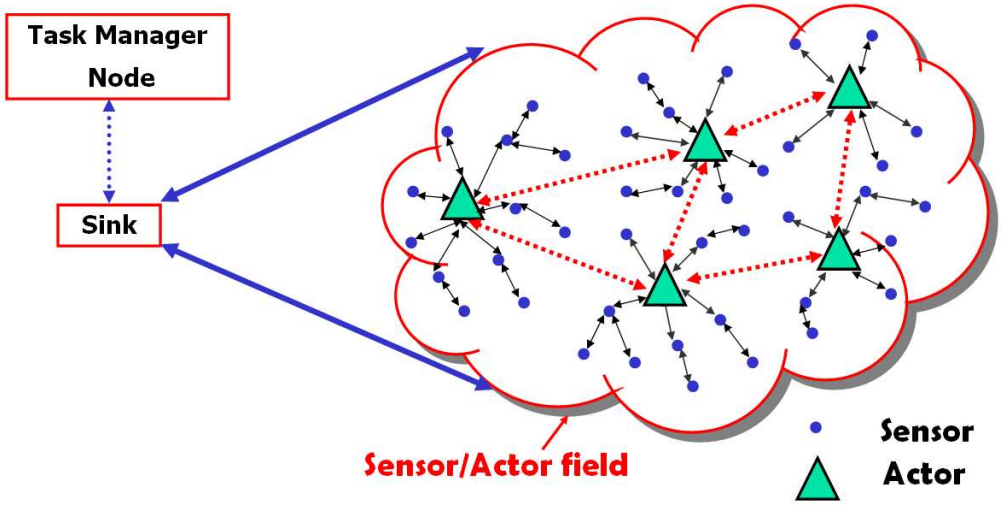

Figure 1: An illustration of an integrated architecture of WSANs.

light sensors in a building can detect the presence of intruders and command cameras or other instrumentations to track them. Furthermore, sensors for structural health monitoring in airplanes or spaceships can drive instruments to timely take countermeasures against critical mechanical stress or structural faults. However, the realization of these currently designed and envisioned applications directly depends on the real-time and reliable communication capabilities of the deployed sensor/actor network.

Recently, considerable research efforts have yielded many promising communication protocols for wireless sensor networks (WSNs) [18]. The common feature of these protocols is that they mainly address the energy-efficient and reliable data communication requirements of WSNs. However, in addition to the energy-efficiency and communication reliability, many proposed WSAN applications have strict delay bounds and hence mandate timely transport of the event features from the sensor field to the actor nodes [16]. Consequently, the unique features and application requirements of WSANs require a real-time and reliable data communication solution. The major communication challenges for the realization of a real-time and reliable communication in WSANs can be outlined as follows:

- *Heterogeneous reliability requirements:* The transport paradigms of WSANs have different reliability requirements because of the node heterogeneities in the deployment field [16]. For example, while sensor-actor communication may not require 100% reliability because of the correlation among the sensor readings [15],[56], actor-actor communication requires 100% reliability in order to make a collaborative decision on how to perform the action.

- *Delay bounds:* In WSANs, actor nodes need to immediately react to sensor data based on the application-specific requirements. Hence, real-time communication within certain delay bounds is a crucial concern to guarantee timely execution of the right actions.

- *Wireless channel errors:* The wireless channel errors in WSANs lead to bursts of packet loss [16]. Despite the existence of channel coding schemes, packet-level transport layer reliability mechanisms are required. Furthermore, new congestion detection and control algorithms are necessary to avoid erroneous congestion decisions resulting from channel-related packet losses.

- *Energy efficiency:* Although the primary objective of the communication protocols in WSANs is reliable event detection and timely execution of the right actions, this must be accomplished with minimum energy consumption because of limited energy resources of sensor nodes.

All the above communication challenges, coupled with the limitations of wireless environments, call for novel real-time and reliable communication protocols for WSANs. To address this need, real-time and reliable communication solutions are proposed in this proposal. The proposed solutions dynamically adjust their protocol configurations to adapt to the heterogenous characteristics of WSANs and support reliable event data delivery with minimum energy consumption in order for actor nodes to initiate the right actions timely.

1.1 Research Objectives and Solutions

In this research, first the characteristics and challenges of wireless sensor and actor networks (WSANs) are investigated and then based on these characteristics, new and efficient communication protocols are proposed. Specifically, the following four areas are investigated under this research:

1. On the Cross-Layer Interactions between Congestion and Contention in WSANs
2. Real-Time and Reliable Transport in WSANs
3. Resource-Aware and Link-Quality-Based Routing in WSANs
4. WSAN Applications and Experiments for Electric Utility Automation

1.1.1 On the Cross-Layer Interactions between Congestion and Contention in WSANs

Recently, a number of congestion detection and control algorithms have been proposed for wireless sensor networks [15],[34], and [59]. The majority of these algorithms state that cross-layer interactions between transport layer and MAC layer are imperative for efficient congestion detection and hence congestion control. Despite the considerable amount of research on several aspects of congestion detection and control in sensor networks, the interdependence of congestion and contention in WSANs is yet to be efficiently studied and addressed.

In this thesis, the interactions between contention resolution and congestion control mechanisms as well as the physical layer effects in wireless sensor and actor networks (WSANs) were investigated in detail. An extensive set of simulations was performed in order to quantify the impacts of several network parameters on the overall network performance. In addition, the main sources of network congestion in WSANs were identified as (i) channel contention and interference, (ii) source reporting rates, (iii), many-to-one network nature, (iv) number of event sources, and (v)

packet collisions. The results of this analysis confirm the urgent need for a delay-constrained reliable event transport solution with an efficient congestion detection and control mechanism in WSANs.

1.1.2 Real-Time and Reliable Transport in WSANs

The existing and potential applications of WSANs span a very wide range, including real-time target tracking and surveillance, homeland security, and biological or chemical attack detection [16]. Realization of these currently designed and envisioned applications, however, directly depends on real-time and reliable communication capabilities of the deployed sensor/actor network.

In this thesis, a real-time and reliable transport $(RT)^2$ protocol was proposed to address the communication challenges introduced by the coexistence of sensors and actors in WSANs. The $(RT)^2$ protocol is a novel transport solution that seeks to achieve reliable and timely event detection with minimum possible energy consumption. It includes a combined congestion control mechanism that serves the dual purpose of achieving reliability and conserving energy. The $(RT)^2$ protocol operation is determined by the current network state based on the delay-constrained event reliability and congestion condition in the network. If the delay-constrained event reliability is lower than required, $(RT)^2$ adjusts the reporting frequency of source nodes aggressively to reach the desired reliability level as soon as possible. If the reliability is higher than required, then $(RT)^2$ reduces the reporting frequency conservatively to conserve energy while still maintaining reliability. This self-configuring nature of $(RT)^2$ makes it robust to random, dynamic topology in WSANs. Furthermore, to address the different reliability requirements of actor-actor communication, $(RT)^2$ incorporates adaptive rate-based transmission control and (SACK)-based reliability mechanism during actor-actor communication. Performance evaluation via simulation experiments shows that $(RT)^2$ achieves high performance in terms of reliable

event detection, communication latency and energy consumption in WSANs.

1.1.3 Resource-Aware and Link-Quality-Based Routing in WSANs

Recent experimental studies [37], [65], [52] and [66] have shown that in WSANs, wireless link quality varies over space and time, deviating to a large extent from the idealized unit disc graph models used in network simulation tools. These studies provide valuable and solid foundations for several sensor network protocols [50], [19] and [62] and have guided design decisions and tradeoffs for a wide range of sensor network applications [18]. Although these early studies made many important observations for the problems of reliable data transmission in WSNs, the challenges of integrating battery-powered sensors with resource-rich actor nodes are yet to be efficiently studied and addressed.

In this thesis, to address energy limitations and link quality variations in WSANs, a resource-aware and link-quality-based (RLQ) routing protocol was developed for WSANs. The RLQ routing protocol uses a link-cost metric, which is based on both energy efficiency and link quality statistics. The primary objective of the RLQ routing protocol is to adapt to varying wireless channel conditions, while exploiting the heterogeneous capabilities in WSANs. To accomplish this objective, the RLQ routing protocol biases the use of resource-rich actor nodes over energy-constrained sensor nodes for packet forwarding and processing in the network. Specifically, the proposed link cost metric captures the expected energy cost to transmit, receive and retransmit a packet, while considering the residual energy levels of the sensor nodes. Moreover, for nodes that have high energy resources, e.g., actor nodes, the transmission and reception of packets have negligible energy cost, which is also reflected in the link cost metric. Unlike most of the existing simulation-based studies, this research effort is guided by extensive field experiments of link-quality dynamics at various locations over a long period of time using recent sensor/actor network platforms. Through

these experiments, significant performance improvements of the RLQ protocol over existing routing protocols have been demonstrated in terms of packet reception rate, throughput, and network lifetime.

1.1.4 WSAN Applications and Experiments for Electric Utility Automation

In today's competitive electric utility marketplace, electric utilities face growing demands to produce reliable power, comply with environmental regulations and meet corporate financial objectives. Given the increasing age of many electrical systems and the dynamic electric utility market, intelligent and low cost monitoring and control systems are required in order to improve the productivity and efficiency of such systems.

With the recent advances in wireless sensor and actor networks (WSANs), the realization of low-cost embedded electric utility monitoring systems have become feasible. In this regard, accurate wireless channel models are extremely important for the design of WSAN-based electric utility communication architectures. These channel models provide utility network designers with the ability to predict the performance of the communication system for specific propagation environment, channel modulation, and frequency band. Although there exists radio propagation measurements in urban areas, office buildings, and factories [46], [67], the propagation characteristics in utility systems are yet to be efficiently studied and addressed.

In this thesis, a statistical characterization of the wireless channel in different electric utility environments is presented. Field tests have been performed on 802.15.4 compliant wireless sensor/actor networks in both a 500 kV substation as well as an underground network transformer vault to measure background noise, channel characteristics, and attenuation in the 2.4 GHz frequency band. Various communication links, including both line-of-sight (LOS) and non-LOS (NLOS) scenarios, are also considered. In addition, the use of external antennas in WSANs is investigated to

improve the communication range in the network. In this context, extensive measurements are made to quantify the use of external antennas in indoor, outdoor and underground utility environments.

1.2 Thesis Outline

This thesis is organized as follows. Chapter 2 investigates the interactions between contention resolution and congestion control mechanisms as well as the physical layer effects in WSANs. Chapter 3 introduces a new real-time and reliable transport protocol, which achieves reliable and timely event detection with minimum energy expenditure in WSANs. Chapter 4 presents a resource-aware and link-quality-based routing protocol, which addresses energy limitations and link-quality variations in WSANs. Chapter 5 presents the WSAN applications for electric utilities and investigates the propagation characteristics of wireless channel in different utility environments. Finally, Chapter 6 summarizes the research results and suggests a number of problems for future investigation.

CHAPTER II

ON THE CROSS-LAYER INTERACTIONS BETWEEN CONGESTION AND CONTENTION IN WIRELESS SENSOR AND ACTOR NETWORKS

In this chapter, the interactions between contention resolution and congestion control mechanisms in wireless sensor and actor networks (WSANs) are comprehensively investigated. An extensive set of simulations is performed in order to quantify the impacts of several network parameters on the overall network performance. This study was first presented in [29]. In Section 5.1, a comprehensive review of the related work on congestion detection and control algorithms in WSANs is described. In Section 2.2, an overview of the performance metrics and the evaluation environment are described. The main results of our analysis are presented in Section 2.3.

2.1 Motivation and Related Work

In WSANs, because of the memory limitations of the sensor nodes and limited capacity of shared wireless medium, congestion might be experienced in the network. Congestion leads to both waste of communication and energy resources of the sensor nodes and also hampers the event detection reliability because of packet losses [25]. Hence, it is mandatory to address the congestion in the sensor field to prolong the network lifetime, and to provide the required quality of service (QoS) that WSAN applications demand.

Unlike the congestion cases in conventional wired networks, many potential reasons may lead to overall network congestion in WSANs. Communication in a shared wireless medium in WSANs constitutes one of the main sources of congestion, which

has not been considered in conventional congestion control approaches. Moreover, the multi-hop nature of the WSAN amplifies the likelihood as well as the severity of network congestion. In general, the main sources for network congestion in WSANs can be classified as follows:

- *Channel Contention and Interference:* In WSANs, the local channel contention in the shared communication medium may result in network congestion. This channel contention can occur between different flows passing through the same vicinity and between different packets of the same flow.

- *Number of Event Sources:* WSANs are specialized in informing events observed by the sensor nodes and acting upon the observed event by the actor nodes. Hence, the number of nodes transmitting event features directly affects both the efficiency of the network protocols and the accuracy of the event information [29]. Although higher number of event sources can improve the accuracy of the event information, the multi-hop nature and the local interactions between sensor nodes can degrade the overall network performance.

- *Packet Collisions:* High network contention increases the probability of packet collisions in the wireless medium. Based on the underlying medium access control (MAC) mechanism, after several unsuccessful transmission attempts, these packets are dropped at the sender node. Hence, the decrease in buffer length due to these drops may inaccurately indicate lower congestion when only buffer length is considered for congestion detection.

- *Reporting Rate:* Mainly, WSAN applications can be classified into two classes, i.e., event-driven and periodic [16]. In both cases, as a result of increased reporting rate, network congestion occurs even if local contention is minimized. This conventional reason for network congestion has a different meaning in WSAN since the sink (or the actor node based on the assumed WSAN architecture [16])

is interested only in the collective information from multiple sensors rather than individual flows. Therefore, a collaborative approach is required in controlling flow rates.

- *Many to One Nature:* Due to the collaborative nature of the WSANs, the packet transmission about an event from multiple sensors to few number of actor nodes or to a single sink (depending on the WSAN architecture assumed [16]) may create a bottleneck, especially around the receiving architectural element (sink or the actor node). Hence, this many-to-one nature also creates congestion in the network.

The reasons for congestion in WSANs, as briefly explained above, are directly related to the local interactions of sensor nodes in the network. In other words, local interactions among sensor nodes influence the overall network performance. For example, controlling contention between sensor nodes has positive effects in reducing the end-to-end network congestion. Furthermore, it has been demonstrated that for efficient congestion detection in WSNs, the sensor nodes should be aware of the network channel condition around them [34],[59]. Therefore, it is also clear that the channel conditions and physical layer effects are also important factors which may affect the contention, congestion levels and hence the overall network performance [16], [46].

Majority of the congestion control algorithms proposed for sensor networks [15],[34], and [59] state that cross-layer interactions between transport layer and MAC layer is imperative for efficient congestion detection and hence congestion control in multi-hop sensor networking paradigm. In [59], channel load information from the MAC layer is incorporated into congestion detection and control mechanisms. In a converse approach, the authors in [61] transmission control scheme for use at the MAC layer in WSN is proposed. In [15], congestion detection is performed through buffer

occupancy measurements. In [14], the backoff window of each node is linked to its local congestion state. Furthermore, [34] compares the buffer occupancy-based and channel load-based congestion detection mechanisms. Moreover, it has been experimentally shown that a hybrid approach would lead to most efficient results. It has been advocated in [34] that MAC layer support is beneficial in congestion detection and control algorithms.

In [57], the analysis of the relation between channel contention and network congestion has been performed for wireless sensor networks with the assumption that the sensor nodes send their readings to a single sink, which clearly does not apply to WSANs. Therefore, this analysis does not consider the co-existence of sensor and actor nodes as well as the effects of having multiple actors, all of which are to receive data from sensor nodes. Furthermore, the analysis in [57] does not also investigate the effects of physical layer issues on the local contention and network congestion in WSAN.

Overall, it is clear that cross layer approaches in congestion detection and control are necessary in WSAN due to the tight relation between local contention and network-wide congestion. Despite the considerable amount of research on several aspects of congestion control in sensor networks, the interdependence of congestion and contention in WSAN is yet to be efficiently studied and addressed. Therefore, the unique characteristics of WSAN call for a comprehensive analysis of the network congestion and contention under various network conditions.

2.2 Network Model and Performance Metrics

The objective of this study is to investigate the interactions between local contention and network-wide congestion in WSANs. As discussed in the previous section, a thorough analysis of contention resolution and congestion control mechanisms are

Table 1: Simulation parameters.

Parameter	Value
Area of sensor field	100x100 m^2
Number of sensor nodes	100
Radio range of a sensor node	40 m
Packet length	30 bytes
IFQ length	50 packets
Retransmission Limit	7
Transmit Power	0.660 W
Receive Power	0.395 W
Sleep Power	0.035 W
Event radius	30 m
Simulation Time	100 s

required. To provide such an analysis, we set up an evaluation environment using *ns-2* [8]. The simulations are performed using this environment in a 100x100m^2 sensor field. 100 sensors are randomly deployed in this field. Moreover, 16 actors are placed evenly on a circle of radius 50m. A sensor node transmits its information to the closest actor when an event occurs in its sensing range. A sample network topology is shown in Figure 2, while the parameters used in the simulations are shown in Table 2.1. Unless otherwise specified, these parameters are used in the simulations. We vary the number of actors that are active to illustrate the effect of number of actors collecting an information. The number of actors are selected as 1, 2, 4, 8, and 16 and their locations are indicated by their numbers in Figure 2. In each simulation, events are generated at the center of the topology and nodes inside a certain event radius, R_{ev}, become source nodes and start to send information to the actors. During the simulations, the locations of the actors are fixed and 5 different topologies with random sensor placement are used. The results are the average of these simulations.

Using this evaluation environment, the following performance metrics are investigated:

Delivery Ratio (DR): WSAN requires a collective event reliability notion rather

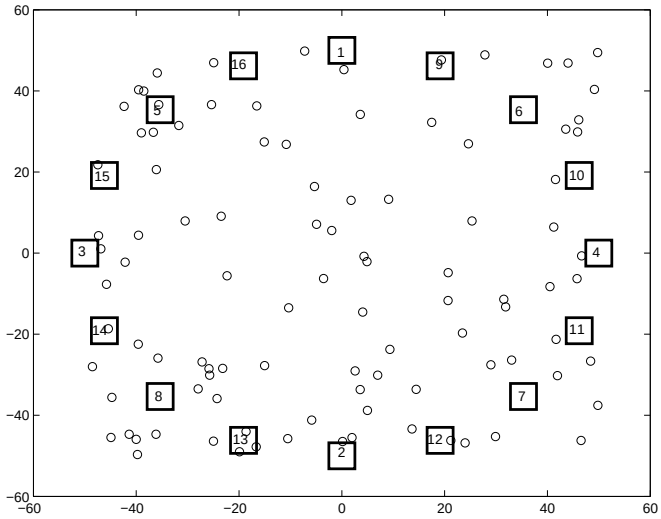

Figure 2: Sample topology used in the simulations. The circles represent the sensors while the squares represent the actors.

than traditional end-to-end reliability [25]. Therefore, the total number of packets received about an event from all the nodes inside the event radius is of importance in WSAN. We define the delivery ratio as the percentage of total sent packets that are received at the actor nodes.

Collisions: The performance of the WSAN depends on the efficient usage of the wireless medium. Hence, the underlying MAC layer performance directly affects the overall performance including the reliability and energy efficiency. The number of collisions represent the contention level around the sensor nodes.

MAC Layer Errors: One of the main reasons for packet losses in wireless networks is due to MAC layer errors. The packets that cannot be transmitted due to excessive contention in the wireless medium and wireless channel errors are investigated using this performance metric. Along with the number of collisions, the MAC layer errors represent the local contention level around the sensor nodes. In our results, the percentage of total sent packets lost due to MAC layer errors are given to investigate the effect of MAC layer performance based on the traffic load.

Buffer Overflows: The memory limitations of the sensor nodes necessitate limited

sized buffers to be used. As the network load increases, the packets are dropped due to excessive incoming traffic. The factors influencing this phenomenon are investigated through the percentage of the total sent packets lost due to buffer overflow. Moreover, the effect of the buffer size on the overall network performance is investigated.

End-to-end Latency: Several WSAN applications such as tracking, intrusion detection and surveillance require that the observed event is reliably detected at the actor within a certain delay bound. Hence, the impact of various network characteristics such as sensor reporting rate, number of sources, buffer size, and contention window on the average end-to-end latency of data packets is also shown to study the tradeoffs related to latency.

Energy Efficiency: In WSANs, energy efficiency of the developed protocols is also crucial due to the constrained energy resources of the sensors. Therefore, the average energy consumption per sent packet is also investigated.

All above performance metrics help us to determine the interactions between the overall network congestion and local contention resolution mechanisms. In the following sections, we describe our comprehensive analysis, which reveals the effects of network parameters on congestion and contention in detail.

2.3 Analysis

2.3.1 Effect of Number of Actors

In this section, the effect of number of actors that collect information from sensors is investigated. As explained in Section 2.2, each sensor sends information to the closest actor if it is inside the event radius corresponding to an event generated randomly inside the sensor field. Increasing the number of actors that collect this information disperses the traffic from the event area to multiple directions. This dispersion may lead to less congestion in the WSAN. However, since more sensor nodes are used for routing traffic from multiple sensors, the energy consumption may increase if

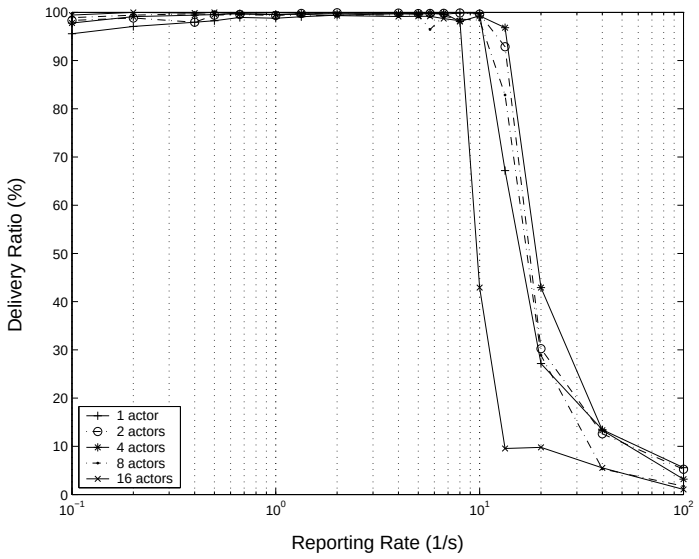

Figure 3: Delivery ratio vs. reporting rate for different number of actors.

too many actors are used. Our investigations show that there is a tradeoff in the number of actors and an arbitrary number may lead to performance degradation when compared to single sink topologies. In order to present the effect of number of actors, we performed simulations for various number of actors, i.e., 1, 2, 4, 8, 16, that are evenly located around a circle of radius 50m.

The impact of number of actors on the overall packet delivery ratio is shown in Figure 3. The x- and y-axes in Figure 3 represent the reporting rate of the source nodes and the delivery ratio, respectively. The delivery ratio corresponds to the percentage of the total sent packets received at all the actors throughout the simulation duration. As shown in Figure 3, irrespective of the number of actors, the packet delivery ratio is almost 100% when the reporting rate is low and decreases sharply above a certain reporting rate. This decrease is also saturated as the reporting rate is further increased. This behavior is also observed throughout the results that will be presented in the following. For the sake of clarity in our discussions, here we introduce some definitions regarding this unique behavior in WSANs.

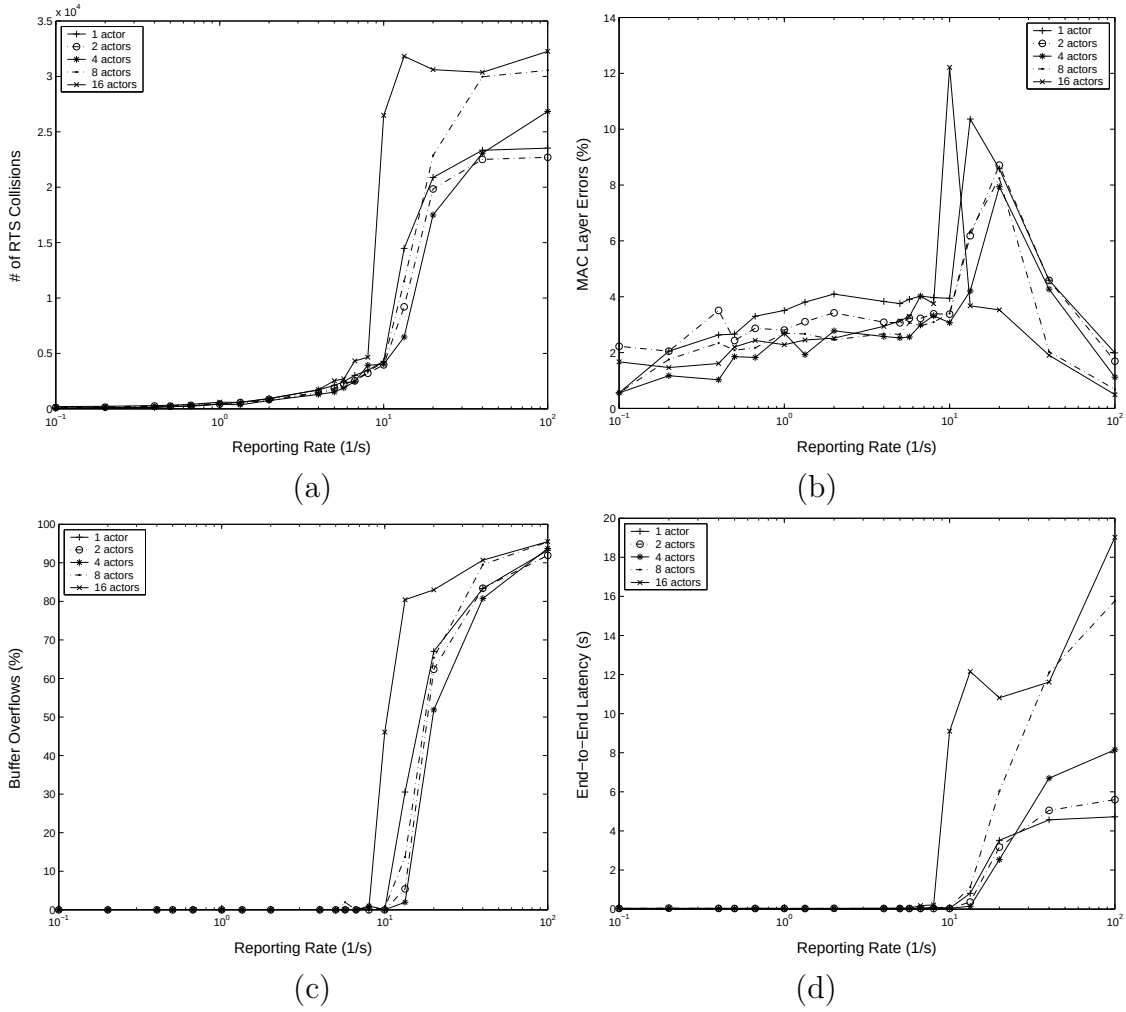

Figure 4: (a) Number of RTS collisions, (b) MAC layer errors, (c) Buffer overflows, and (d) End-to-end latency vs. reporting rate for different number of actors.

We define two reporting rate thresholds, denoted as dr_{th}^{low} and dr_{th}^{high}, which represent the threshold for reporting rate when the network behavior is observed to change significantly. The actual values of these thresholds change based on the network configuration, such as number of actors and source nodes, buffer length and the maximum retransmission limit. The first threshold, dr_{th}^{low} represents the reporting rate above which the network congestion starts to build up. As an example, dr_{th}^{low} is found to be around $8s^{-1}$ when 16 actors collect information from the sensor nodes from Figure 5. The region below dr_{th}^{low} where the packet delivery ratio is relatively constant is referred to as the ***non-congested region***. This regime, the buffer occupancy of the

nodes is low enough that the traffic load is accommodated without causing congestion. Above dr_{th}^{low}, a sharp transition phase is observed which is referred to as the ***transition region***. This phase is where the network congestion builds up due to both traffic load increase and local contentions. Beyond a second threshold, dr_{th}^{high}, the packet delivery ratio saturates which is referred to as ***highly-congested region***. Similarly, dr_{th}^{high} is found to be $13s^{-1}$ for 16 actors. The discussions in the following will be based on these definitions.

As shown in Figure 3, irrespective of the number of actors, highly-congested region is always observed. This is due to the excessive number of packets injected into the network which cannot be supported by the underlying wireless medium capacity. The packet delivery ratio is kept at a fairly high value, i.e., $DR > 95\%$, while $r > r_{th}^{low}$. However, as the reporting rate, r, is increased above dr_{th}^{high}, the packet delivery ratio drops to significantly low values, i.e., $DR < 10\%$. The number of actors affect this behavior, by shifting the delivery ratio-reporting rate graph to left or right. It can be observed that there is an optimal number for actors that should collect sensor information that maximizes the packet delivery ratio. In our experiments, this value is found to be 4. It is observed that when the number of actors is increased from 1 to 4, the delivery ratio graph shifts to right, which results in higher dr_{th}^{low} and dr_{th}^{high} values. As a result, the network can be operated at higher reporting rates without affecting the reliability of the network. Higher reporting rates may lead to higher resolution for event estimation at the actors and more accurate actions being taken. However, increasing the number of actors beyond this point has adverse affects on delivery ratio. As an example, delivery ratio drops by 85%, when the number of actors is increased from 4 to 16 at $r = 13s^{-1}$.

In order to further investigate the reasons for the sharp decrease beyond dr_{th}^{low} and the effect of number of actors, we first present focus on local interactions of the sensor nodes. For this purpose, the number of RTS collisions and the percentage of

MAC layer errors are shown in Figure 4 (a) and Figure 4 (b), respectively. These figures clearly reveal the effect of increased network load on the local channel contention. As shown in Figure 4 (a), the number of RTS collisions starts to increase at a lower reporting rate than the dr_{th}^{low} value found in Figure 3. This shows that the local contention increases before the network is congested. However, through the contention resolution mechanism, this contention is controlled and the delivery ratio is not affected up to some point. Whenever the reporting rate is further increased, the increased contention leads to packet drops at the MAC layer as shown in Figure 4 (b). It is interesting to note that, the maximum values of the percentage of packet losses due to MAC layer errors correspond to the dr_{th}^{low} values when compared to Figure 3. Moreover, above this critical reporting rate, the percentage of packet drops due to MAC layer errors starts to decrease[1]. This is due to the fact that when the network capacity is exceeded, the packet losses are mostly resulting from buffer overflows in the network as shown in Figure 4 (c). It is also important to note that as the tradeoff caused by number of actors is still evident here. 16 actors cause the most number of RTS collisions when compared to other values for actors. This is mainly due to the fact that multiple routes need to be constructed to reach each of the actors. Since more nodes participate in routing when the number of actors is increased, these nodes cause contention among each other. While dispersing the traffic to multiple actors minimize the congestion, the contention is increased due to the local interactions of these multiple routes to the actors.

To further investigate the effect of number of actors on the overall network parameters, the percentage of sent packets lost due to buffer overflow is shown in Figure 4 (c). These results show that buffer overflow is the major factor affecting the event

[1]In fact, when the network capacity is exceeded, the number of MAC layer errors becomes approximately constant which results in decrease in the percentage of packet drops due to MAC layer errors.

delivery ratio. Note that, the three regions, i.e., non-congested, transition and highly-congested regions are clearly observed also from Figure 4 (c). When Figure 4 (a) and Figure 4 (b) are also considered, we observe that there is a close relation between buffer overflows and local contention. As the packets are dropped due to higher traffic load at the network buffer, the collisions and MAC layer errors start to saturate[2]. Since the node buffer is filled, MAC layer is supported with constant rate leading to saturation in local contention. As a result, it can be stated that network buffer size can control the saturated contention level in WSAN. As the number of actors is increased to 4, buffer overflows are decreased leading to higher delivery ratio. Since congestion is controlled by dispersing the traffic to multiple actors, the network is congested at higher reporting rates. However, increasing the number of actors above 4 leads to higher percentage of buffer overflows than observed by the single actor scenario.

In Figure 4 (d) we show the average end-to-end latency of the event packets from sensor field to the actors. As seen in Figure 4 (d), the average end-to-end packet latency is low in the non-congested region. Beyond dr_{th}^{low}, the average packet latency starts to increase. This is obvious because the increased network load due to higher reporting rate leads to increase in the buffer occupancy and network channel contention. Thus, the average forwarding packet delay along the path from the sensors field to the actor node starts to increase. Moreover, increasing collisions lead to retransmissions, which also increase the MAC layer delay. Note that, the increase in the average packet delay is observed regardless of the number of actors.

Based on the results presented above, it can be stated that selecting the number of actors in a WSAN significantly affects the network performance. The performance results show that an optimal number of actors is necessary for efficient communication

[2]Note that, in Figure 4 (b) the percentage of sent packets lost due to MAC layer errors is shown. Hence, the decrease in this value corresponds to a constant MAC layer error value.

and increasing the actors above this number leads to degradation in overall network performance. Especially higher number of actors leads to degradation in delivery ratio, congestion, local contention as well as end-to-end latency. In our experiments, we have found that 4 actors leads to the best performance among other number of actors. Hence, in the following, we present the results for 1 and 4 actors to investigate the various factors that affect the performance of WSANs.

2.3.2 Effect of Number of Sources

The network congestion and local contention is directly related to the traffic in the network. As discussed in the previous section, reporting rate of sensor nodes is one of the factors that influence the network traffic. In addition to the reporting rate of a sensor node, the number of sensors that report their observations to their associated actors is also a major factor. In this section, we investigate the effect of this factor on various network performance metrics. As explained in Section 2.2, each sensor sends information if it is inside the event radius corresponding to an event. In order to present the effect of number of source in a WSAN, we performed simulations using various event radius, R_{ev}, values, i.e., 20m, 30m, and 40m. In each figure results for 1 and 4 actors are shown.

The impact of number of sources on the overall packet delivery ratio is shown in Figure 5. A similar trend as discussed in Section 2.3.1 is also observed irrespective of the number of source nodes. Moreover, the delivery ratio-reporting rate graph shifts to left as the number of source nodes are increased, leading to lower dr_{th}^{low} values. The reasons for this shift is twofold. First reason is the increased number of packets injected into the network because of the increased number of sources. Second, higher contention is experienced in the network since more nodes contend to send their information. An interesting result is the effect of number of actors when the event radius is changed. for $R_{ev} < 40$m, 4 actors result in higher delivery ratio values in the

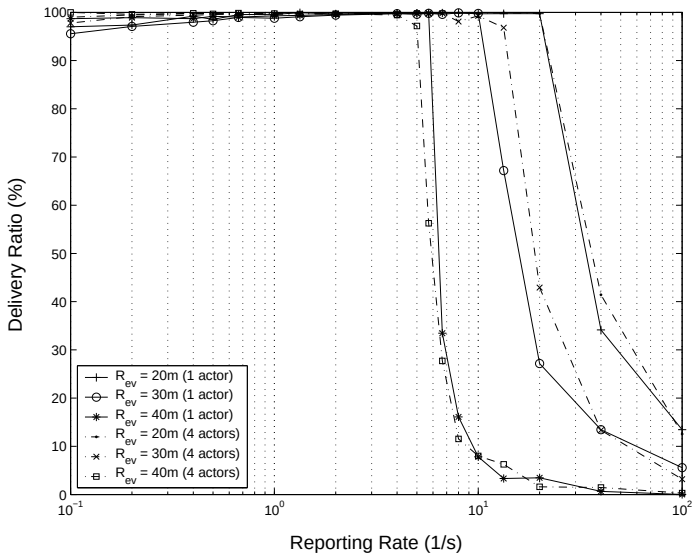

Figure 5: Delivery ratio vs. reporting rate for different values of event radius, R_{ev}.

transition region and the network congestion is observed at higher reporting rates. However, for $R_{ev} = 40$m, increasing the number of actors slightly increases congestion. This important result is due to the effect of contention as we will investigate next.

In Figure 6 (a) and Figure 6 (b), we present the number of RTS collisions and the percentage of MAC layer errors, respectively. These figures clearly reveal the effect of increased network load on the local network channel contention. It is observed that as the number of source nodes increases, the maximum of the percentage of packet losses due to MAC layer errors occur at lower reporting rate values. This observation is also consistent with the packet delivery ratio observations shown in Figure 5. Moreover, the reason for lower delivery ratio for $R_{ev} = 40$m with 4 actors can be seen in Figure 6 (b). MAC errors constitute a higher percentage of sent packets since higher number of routes are generated and more nodes contend for access to the medium when the number of actors is increased.

To further investigate the effect of number of source nodes on the overall network parameters, the percentage of sent packets lost due to buffer overflow is shown in Figure 6 (c). As the number of source nodes are increased, contention level is also

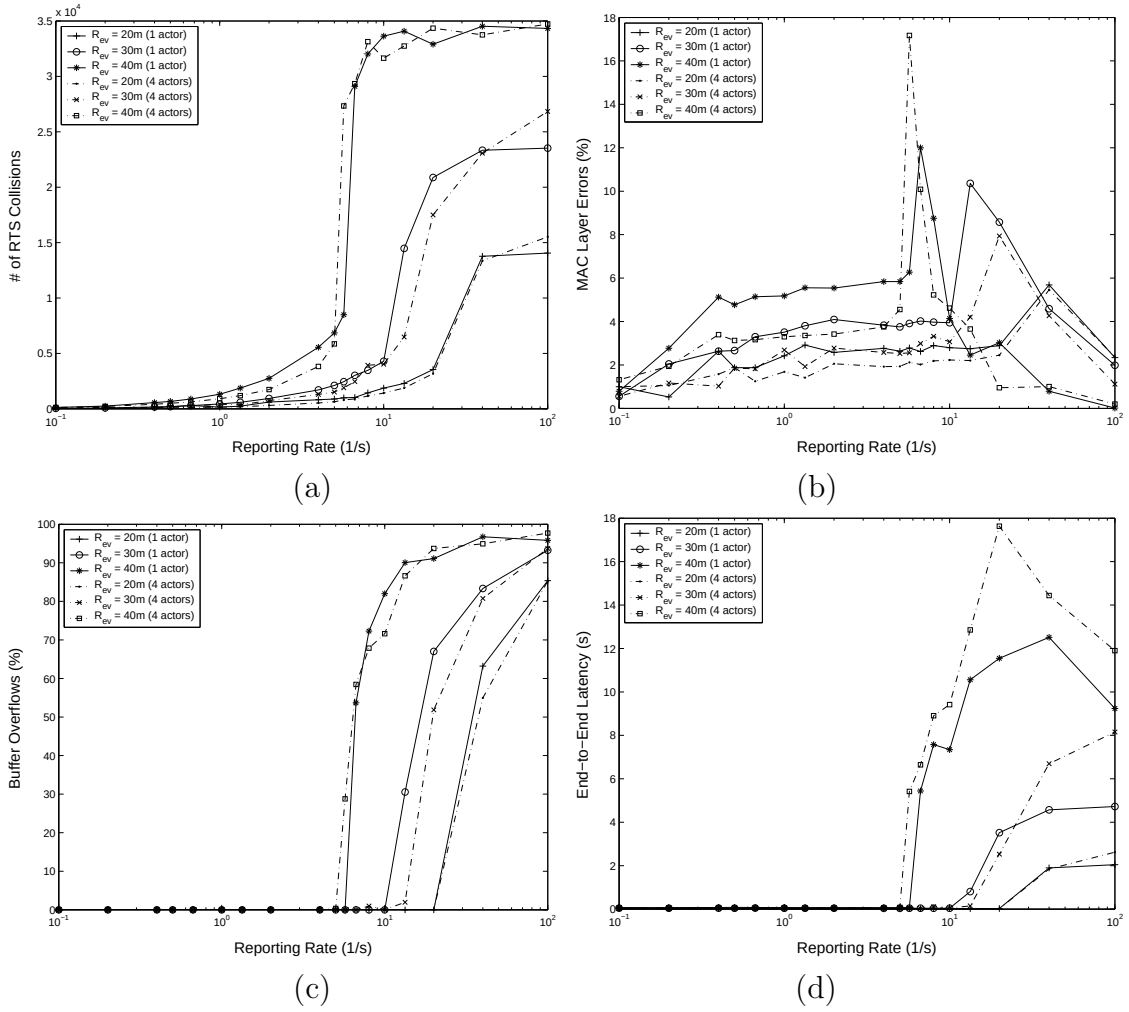

Figure 6: (a) Number of RTS collisions, (b) MAC layer errors, (c) Buffer overflows, and (d) End-to-end latency vs. reporting rate for different values of event radius, R_{ev}.

increased. Since congestion builds up due to higher number of nodes sending information to the actor, the network is congested at lower reporting rates. In Figure 6 (d) we present the average end-to-end latency of the event packets from sensor field to the actor node. Note that, the increase in the average packet delay is observed regardless of the number of source nodes and the increase in average packet latency occurs at higher reporting rates as the number of source nodes decreases. An interesting result is that in the congested region, the latency for 4 actors is higher than 1 actor. Although distributed event transmission is assumed to decrease end-to-end latency, this is not the case when network is congested. However, it is important to

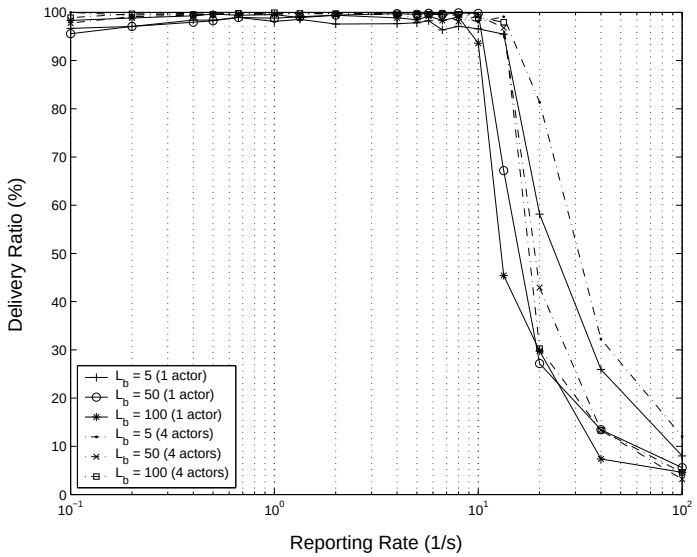

Figure 7: Delivery ratio vs. reporting rate for different values of buffer length.

note that in the transition region, the latency for 4 actors is slightly less than the case for 1 actors for $R_{ev} < 40$m. This result motivated the need for multiple actors in an event area since non-congested and transition regions are of interest for practical operation.

Based on the results presented above, it can be stated that the number of sources in a WSAN clearly affects the network performance. Especially higher number of source nodes leads to degradation in delivery ratio, congestion, local contention as well as end-to-end latency. However, more sources in the case of an event correspond to a spatial increase in the observed information, which may be crucial for the accuracy of event estimation and timeliness of actions for the WSAN application. Hence, the tradeoff between network performance and the application performance in terms of number of sources should be carefully engineered.

2.3.3 Effect of Buffer Size

In this section, the impact of buffer size for the sensor nodes on the network performance is investigated. For this purpose, we performed simulations using different buffer sizes, L_b, for the sensors, i.e., 5, 50, and 100.

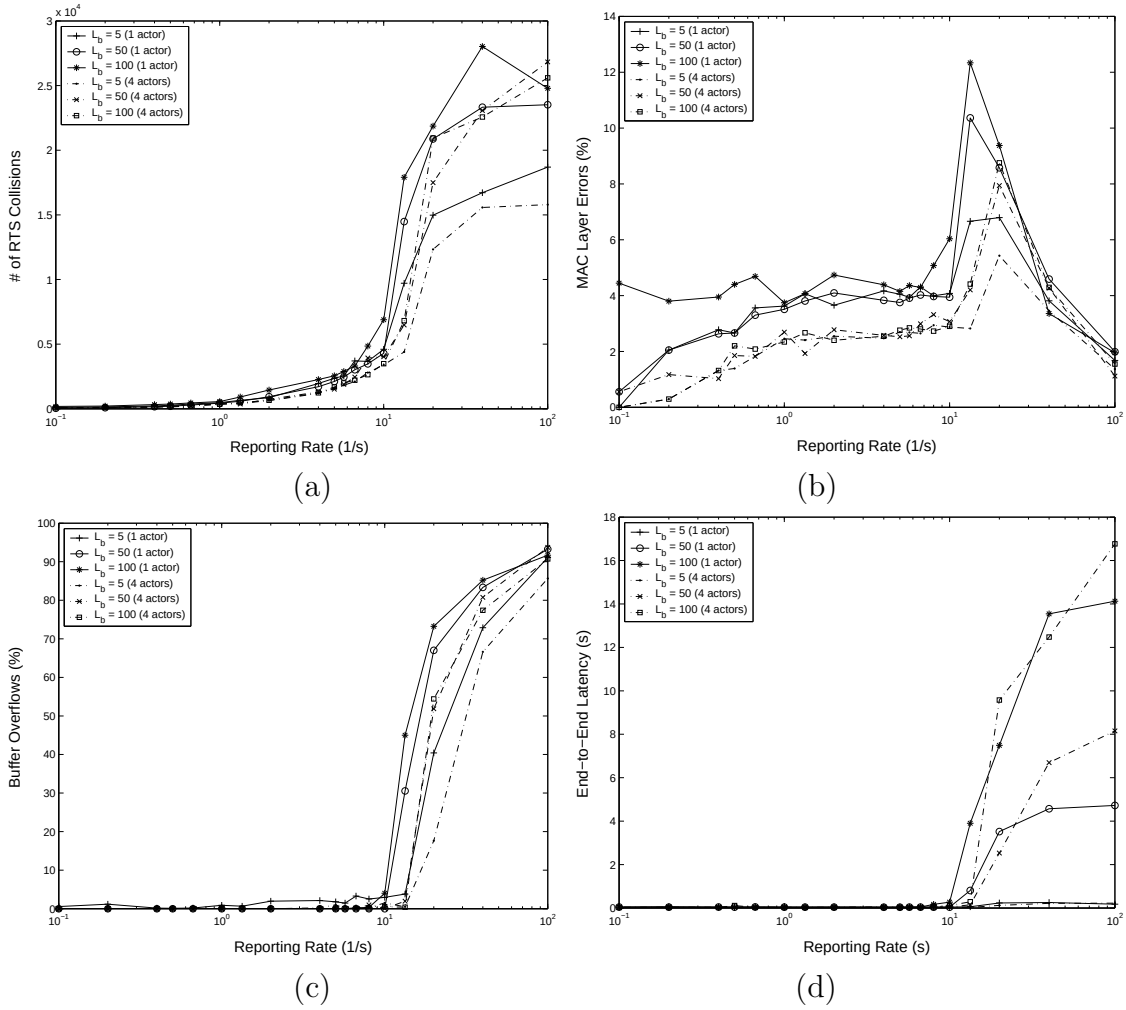

Figure 8: (a) Number of RTS collisions, (b) MAC layer errors, (c) Buffer overflows, and (d) End-to-end latency vs. reporting rate for different values of buffer length.

To investigate the effects of different buffer sizes of sensor nodes on the delivery ratio, in Figure 7, we have observed the packet delivery ratio for different buffer sizes of the sensors for 1 and 4 actors. It is clear that similar shape as observed in Figure 5 is seen in Figure 7. Moreover, the change in buffer size has minimal effect on the delivery ratio. Note that, as the network load increases, although the buffer size of the sensors is large, e.g., 100, the delivery ratio cannot be maximized due to the limited capacity of shared wireless medium. It is also important to note that increasing the number of actors to 4 improves the delivery ratio especially when the buffer length, L_b is small.

Increasing buffer size in WSAN has a negative effect on the local contention level as shown in Figure 8 (a) and Figure 8 (b). As the buffer size is increased, both the number of collisions and the percentage of sent packets lost due to MAC layer errors increase. The increase in collisions is due to increased number of packets waiting to be transmitted in each sensor node when the wireless channel capacity is exceeded. When the buffer size is low, these packets are already dropped and are not passed to the MAC layer, leading to lower contention. This interesting result is also evident from Figure 8 (c), where the percentage of sent packets lost due to buffer overflow is shown for different buffer sizes and number of actors. When the reporting rate is low, a decrease in buffer size leads to increase in buffer overflows as expected. However, in the transition region, lower buffer sizes lead to lower buffer overflows. As a result, the MAC layer errors decrease as shown in Figure 8 (b), which leads to the conclusion that lower buffer sizes can help decrease the local contention. Furthermore, increasing the number of actors also positively influence the buffer overflow performance of WSANs.

Another interesting tradeoff is observed when average end-to-end latency of the event packets from sensor field to the actor node is investigated. As seen in Figure 8 (d), the average end-to-end packet latency starts to increase as the reporting rate increases regardless of the buffer sizes. Note that, decreasing the buffer size significantly decreases the end-to-end latency in the network. This is due to the fact that as the buffer size of the sensors increases, the queuing delay of the packets increases significantly. Moreover, for low buffer size values, buffer overflows lead to a larger number of packet losses in the network, which results in lower channel contention and lower end-to-end packet latency values compared to those values of higher buffer sizes. Finally, increasing the number of actors increase the end-to-end latency in the congested region, as expected according to the previous discussions.

As a result, the above discussions on the effects of buffer size reveals that, in the case of applications where packet delivery ratio can be afforded to be low, i.e.,

$DR \simeq 90\%$, and end-to-end latency is important, lower buffer sizes can be selected. This interesting result is contradictory to the conventional belief that limited storage capabilities of sensor nodes always leads to performance degradation. However, when coupled with the effect of local interactions, this property is shown to be advantageous for a specific class of applications.

2.3.4 Effect of MAC Layer Retransmissions

One of the main factors affecting the delivery ratio in a multi-hop network is the local delivery ratio mechanism which is implemented in the MAC layer. The MAC layer aims to provide hop-by-hop reliability by performing ARQ-based reliability mechanism. The performance of this mechanism mainly depends on the maximum number of retransmissions for packet failures. In this section, we investigate the effect of local reliability mechanism on the overall network performance. In the following figures, we present the effect of maximum retransmission limit, Rtx_{max}, on the network performance metrics introduced in Section 2.2. The results are shown for Rtx_{max} values of 4, 7, and 10. It is clear that increasing the retransmission limit results in more reliable links being established. On the other hand, since retransmissions increase the MAC layer delay, buffer overflows and end-to-end latency may increase. Accordingly, we indicate interesting tradeoffs which occur due to the interaction of different mechanisms at different layers of the network stack.

The overall packet delivery ratio is shown in Figure 9 (a). The effect of hop-by-hop reliability is evident when the network is congested, i.e., reporting rate exceeds dr_{th}^{high}. For lower values of Rtx_{max}, the packet delivery ratio begins to decrease at lower dr_{th}^{low}. This decrease is also sharper when the local reliability is lower as shown with the $Rtx_{max} = 4$ graph. Note also that, although there exists significant difference between $Rtx_{max} = 4$ and $Rtx_{max} = 7$, further increase in the maximum retransmission limit to $Rtx_{max} = 10$, does not effect the overall network reliability significantly.

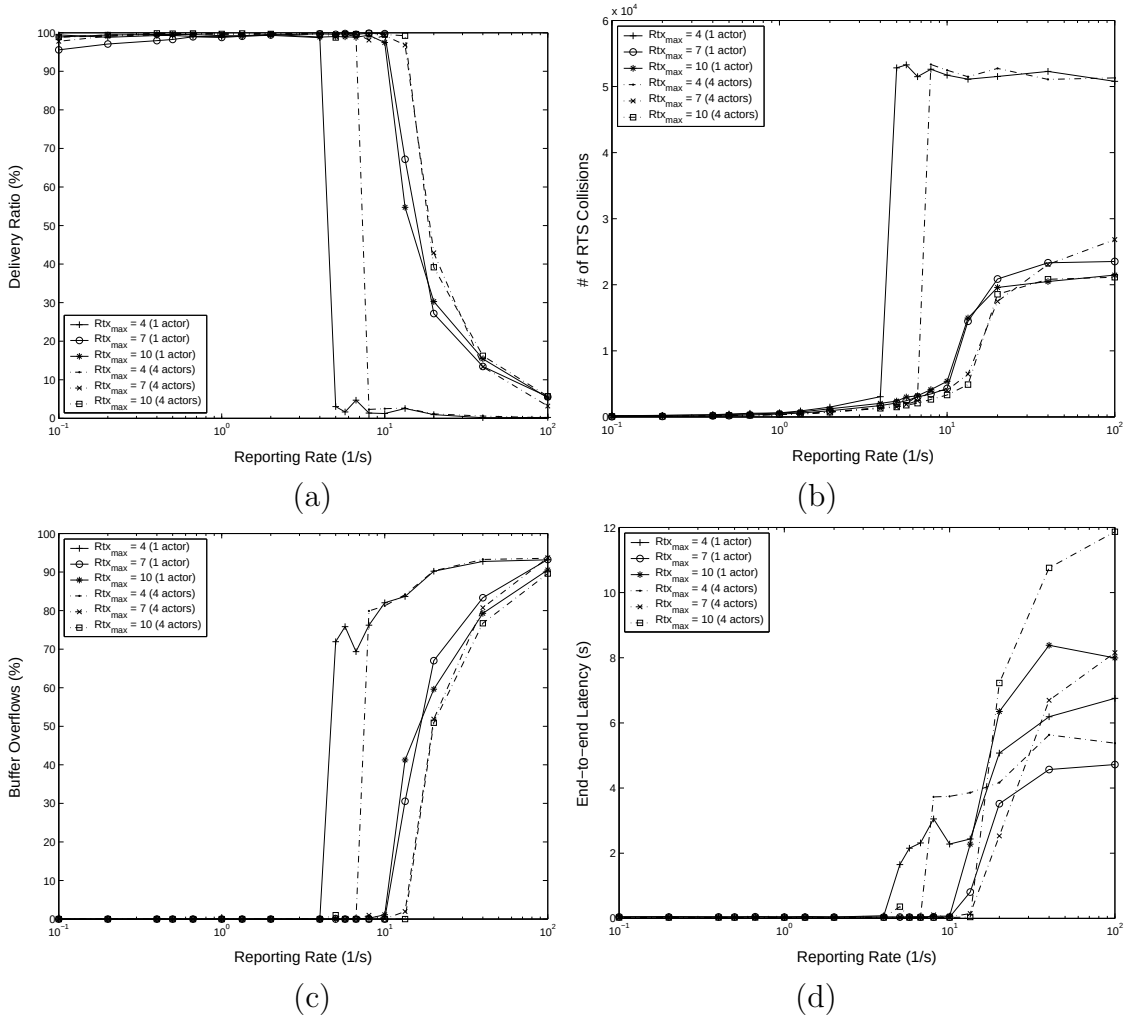

Figure 9: (a)Delivery ratio, (b) number of RTS collisions, (c) buffer overflows, and (d) end-to-end latency vs. reporting rate for different values of retransmission limit, Rtx_{max}.

Overall, the results show that by adjusting local reliability mechanism, higher reporting rates can be supported by the network efficiently. Another way to improve the network reliability when local reliability is low is to increase the number of actors. The delivery ratio graphs for 4 actors result in higher dr_{th}^{low} values. However, the effect of retransmission limit is more important when the curves for $Rtx_{max} = 4$ (4 actors) and $Rtx_{max} = 7$ (1 actors) are compared. A higher retransmission limit leads to higher delivery ratio even though a single actor is used for data collection.

To investigate the effects of maximum retransmission limit on the overall network

performance, we also present number of RTS collisions in Figure 9 (b). As shown in Figure 9 (b), for lower values of Rtx_{max}, we observe higher MAC layer drops in the network in the transition and congested regions, which leads to lower packet delivery ratio values. Consequently, when the network capacity is highly exceeded, in addition to local reliability mechanisms, end-to-end congestion control and reliability mechanisms should be performed.

One of the tradeoffs in supporting higher delivery ratio by adjusting the retransmission limit, Rtx_{max} is shown in Figure 9 (d), where the end-to-end latency is shown. In the non-congested region, the end-to-end latency is in the range of 100 ms irrespective of the retransmission limit. Since the local contention level is low in this region, retransmission mechanism is not used. However, as the congestion level builds up, significant increase in the latency is observed. This increase starts at lower reporting rate values when Rtx_{max} is small. In the highly-congested region, the latency is saturated. This is due to the buffer overflows at higher layers. Since these packets cannot reach the MAC layer, the end-to-end latency is kept at a relatively constant level. This interesting result is also evident from Figure 9 (c), where the percentage of sent packets lost due to buffer overflow is shown for different Rtx_{max} values. As shown in Figure 9 (c), after dr_{th}^{high} value, irrespective of Rtx_{max} values, most of the packets are dropped due to buffer overflows before reaching the MAC layer which leads to above mentioned relatively constant latency in highly-congested region. Increasing the number of active actors in the event area also increases the end-to-end latency irrespective of the retransmission limit. This effect, however, is high for higher retransmission limit values.

2.3.5 Contention Window

As discussed in Section 2.3.4, local contention and hence collisions constitute one of the major sources for packet drops in WSN. Thus, contention resolution mechanisms

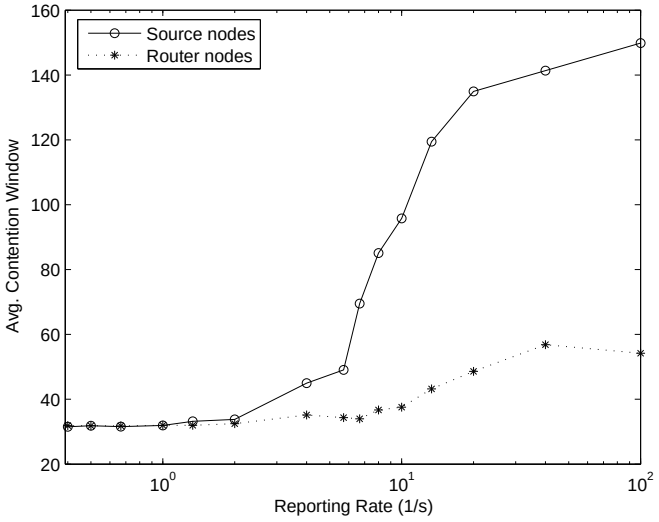

Figure 10: Average contention window size for source nodes and router nodes.

are required in MAC protocols. In contention-based MAC protocols, the contention resolution mechanism is performed via contention window adjustments [10]. Each node determines its random backoff time, which is selected randomly between $(0, cw)$, where cw represents the contention window size. The contention window size, cw, is initially set to a minimum contention window size CW_{min}. Moreover, cw is increased as the contention level is increased in the vicinity of the node. Hence, the value of cw during the operation of a sensor node is representative of the local contention. In Figure 10, the average cw values two types of sensor nodes in the WSAN are presented. These types of nodes are determined based on their roles in the transmission of event information. The nodes that generate the event information are referred to as *source nodes*, while the nodes that participate in forwarding the packets to the actor in the multi-hop network are referred to as *router nodes*.

As shown in Figure 10, average contention window size of the source nodes increases significantly in the transition region. An interesting result to note is that there is a huge difference between the average cw values for source and router nodes. This reveals that there is a high contention in the vicinity of source nodes, since multiple

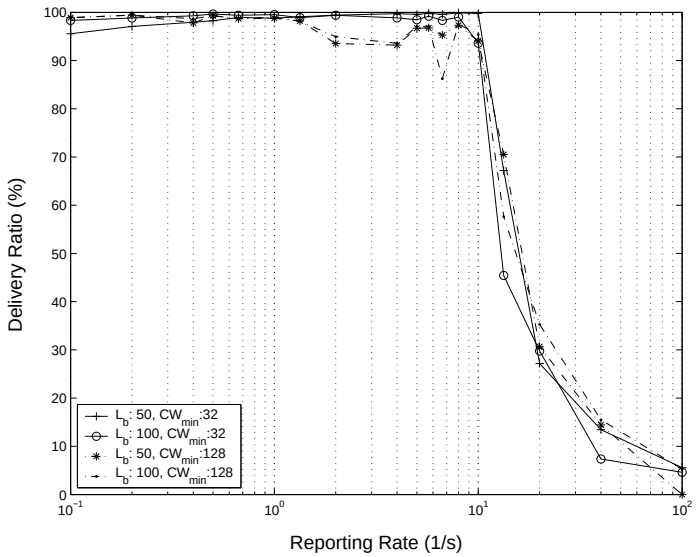

Figure 11: Delivery ratio vs. reporting rate for different combinations of buffer size and contention window.

nodes try to send information about the same event at the same time. Moreover, as the reporting rate is increased, the average *cw* value increases. This implies that a higher *cw* value can be initially determined for applications that require higher reporting rate in order to increase the efficiency of the network.

In order to investigate the effect of initial contention window size, CW_{min}, on the network performance metrics, we performed simulations by varying the initial contention window size, CW_{min} and buffer size. In our simulations, the CW_{min} is first chosen as 32 and then increased to 128 since this value is observed in Figure 10 for high reporting rates. Moreover, the buffer size is chosen as 50 and 100. Since the number of actors play a similar role as explained in the previous discussions, we do not include them in this section for space considerations.

In Figure 11, the packet delivery ratio for 4 different combination of buffer sizes and CW_{min} values is shown. It is observed that when the reporting rate is very low, the packet delivery ratio is higher for lower CW_{min} value. The difference in delivery ratio increases as the reporting rate is increased in the non-congested region. This is due the unnecessary long contention window size at this region. However, in the

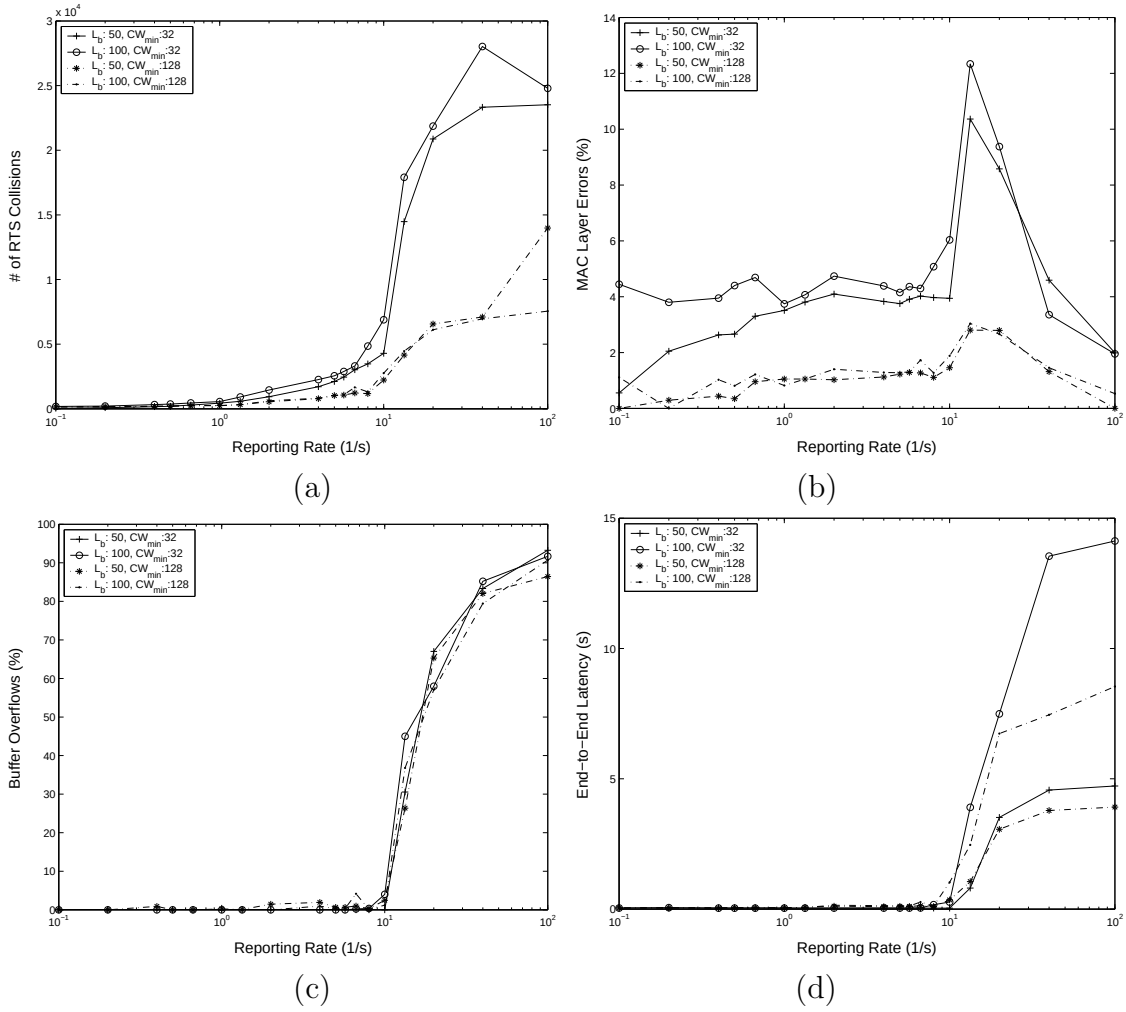

Figure 12: (a) Number of RTS collisions, (b) MAC layer errors, (c) Buffer overflows, and (d) End-to-end latency vs. reporting rate for different combinations of buffer size and contention window.

transition region and the highly-congested region, similar values are observed.

The effect of initial contention window size CW_{min} on RTS collisions, MAC errors, and buffer overflows are shown in Figure 12 (a), 12 (b), and 12 (c), respectively. As shown in these figures, increasing CW_{min} has positive effect on MAC layer collisions and MAC layer errors. However, buffer overflows are generally independent of the initial contention window size. Another advantage of increasing the initial contention window size can be observed from Figure 12 (d), where the average end-to-end latency is shown. Higher initial contention window size results in slightly higher latency in

the transition region while it decreases the end-to-end latency in the congested region. This is explained by Figure 12 (a) and 12 (b). Since higher contention window size decreases collisions, less number of retransmissions is required for successful delivery of packets. As a result, the access delay is reduced resulting in lower end-to-end latency. However, higher contention window size leads to higher backoff durations. As a result, the buffer overflows are not affected. Consequently, adaptive contention window mechanisms are required to improve overall network performance. It is clear that the existing contention resolution mechanisms adaptively increase the contention window size based on the local contention level. However, the knowledge of overall network condition can also be exploited. For example an increase in the reporting rate can be exploited in the contention resolution mechanism to achieve higher efficiency.

2.3.6 Wireless Channel Effects

When a radio signal propagates through the wireless environment, it is affected by reflection, diffraction and scattering [46] and [31]. In addition to these, in WSANs, low antenna heights of the sensor nodes (10s of cms) and near ground communication channels cause signal distortions due to ground reflection. In this section, we investigate the effects of wireless channel on network congestion and channel contention in terms of delivery ratio and latency. For this purpose, we model a realistic physical layer using log-normal shadowing path loss model [46]. This model is used for large and small coverage systems and moreover, experimental studies have shown that it provides more accurate multi-path channel models than Nakagami and Rayleigh models for indoor wireless environments with obstructions [67]. In this model, the signal to noise ratio $\gamma(d)$ at a distance d from the transmitter is given by:

$$\gamma(d)_{dB} = P_t - PL(d_0) - 10\eta log_{10}\Big(\frac{d}{d_0}\Big) - X_\sigma - P_n \qquad (1)$$

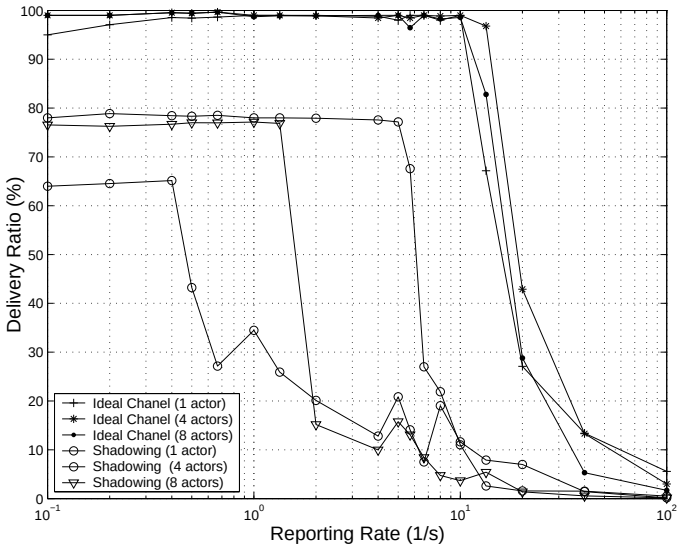

Figure 13: Delivery ratio vs. reporting rate in case of realistic wireless channel.

where P_t is the transmit power in dBm, $PL(d_0)$ is the path loss at a reference distance d_0, η is the path loss exponent, X_σ is a zero mean Gaussian random variable with standard deviation σ, and P_n is the noise power in dBm. In practice, the values of path loss exponent (η) and the standard deviation (σ) are computed from experimentally measured data. For example, η is 2 to 3 for indoor environments with obstructions and σ ranges from 2 to 5 based on different environment characteristics [42], [46] and [67].[3]

In Figure 13, we have shown the impact of the number of actors and the realistic wireless channel on the overall event delivery ratio. As shown in Figure 13, irrespective of the number of actors and wireless channel model, the packet delivery ratio remains approximately constant, when the reporting rate is low and decreases sharply after a certain reporting rate. This behavior is similar to the packet delivery ratio observations presented in Section 2.3.2. Note that, when a realistic wireless channel is taken into account, 100% packet delivery ratio cannot be provided due to adverse wireless channel effects even if network load is very low. Therefore, in WSANs, to

[3]In our simulation experiments, we have used η=3.0 and σ=3.8, which are typical values found by experiments in [67] for indoor environments.

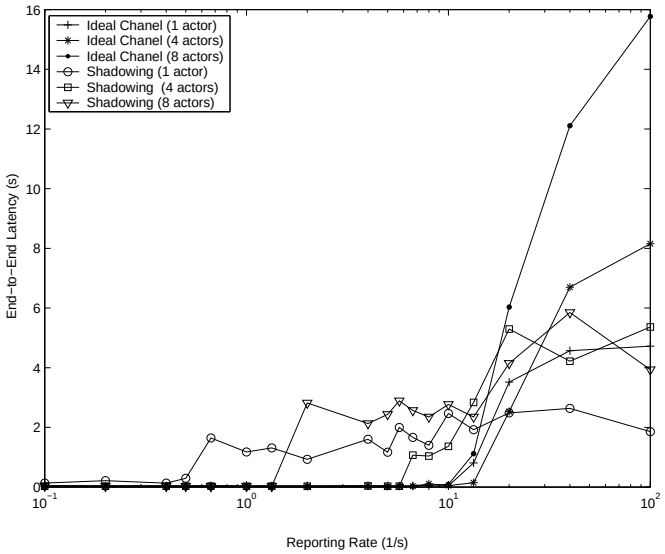

Figure 14: End-to-end latency vs. reporting rate in case of realistic wireless channel.

provide application specific reliability requirements, channel coding and transport layer reliability mechanisms are required in addition to efficient congestion control algorithms. Furthermore, in Figure 13, when the number of actors in the deployment field is increased, it is observed that the network experiences congestion in higher reporting rates compared to single actor scenarios. This is because in multiple actor cases, network load is distributed among actor nodes and thus, network resilience against congestion and contention is increased, leading to high values of dr_{th}^{low}.

In Figure 14, we also observe the average end-to-end latency of the event packets when the realistic wireless channel is modelled. As shown in Figure 14, the average packet latency is low in the non-congested region for both single actor and multiple actor scenarios. Beyond dr_{th}^{low}, the packet latency starts to increase. This behavior is obvious because the increased network load due to higher reporting rate leads to increase in the buffer occupancy and network channel contention. Thus, the average forwarding packet delay along the path from the sensors field to the actor node starts to increase. This observation is also consistent with the end-to-end latency observations shown in the previous sections. Note also that, as the reporting rate is increased,

the increase in the average packet delay is observed regardless of the number of actor nodes and wireless channel model.

In Figure 13 and 14, it is also interesting to note that when the number of actors is increased from 4 to 8, the network is started to experience congestion in lower reporting rates compared to 4 actor scenarios. This is because when the number of actors is high, the exchange of several routing packets between sensors and multiple actors overloads the network unnecessarily, which decreases the network performance in terms of reliability and end-to-end latency. Hence, realizing the full potential of multiple actors in the deployment field requires careful network engineering including adaptive and lightweight data forwarding protocols.

2.3.7 Reasons for Packet Drops

In this section, we investigate the distribution of packet drops for different reporting rates. As shown in Figure 15, the distribution of packet drops depends on the reporting rate. As explained in Section 2.3.2, the reporting rate determines the region the network is in. As the reporting rate is low, i.e., non-congested region, the packet drops are due to two sources: MAC layer failures, and routing layer failures. MAC layer failures consist of packet drops due to excessive number of unsuccessful retransmission attempts. Hence, the effect of wireless medium is also included. The routing layer failures are packet drops due to routing protocol timeouts, which occur when the next hop to the actor cannot be reached. It is observed that, in the non-congested region, the packet drops are mainly due to MAC layer errors. However, as the reporting rate increases, network congestion occurs since the wireless medium cannot support the injected load. As a result, buffer overflows start to dominate the packet drops. Note that, although the share of MAC failures in the overall packet drops decrease as the reporting rate is increased, the actual number of packet drops due to MAC failures remain constant. Hence, this constant value shows the limitations of the underlying

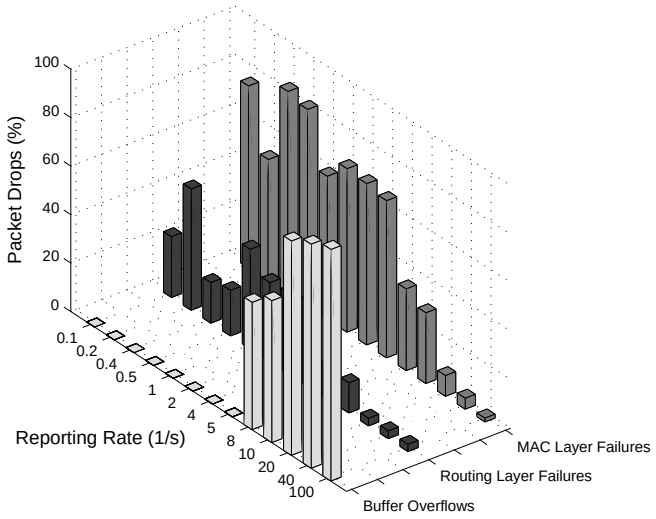

Figure 15: Distribution of packet drops due to buffer overflows, routing layer failures and MAC layer failures for different values of reporting rate.

wireless medium. The dynamic change in packet drop distribution reveals that adaptive techniques for reliability mechanisms is required considering both the local and end-to-end reliability based on the traffic load in the network.

2.3.8 Energy Efficiency

In WSN, energy efficiency is crucial due to constrained energy resources of the sensors. The developed protocols should consider the energy efficiency in the network while accomplishing their application-specific objectives. Hence, the tradeoffs in energy consumption due to interactions among sensors is highly important to be investigated. In this section, we provide insightful results for the effects of different network parameters, such as number of actors, event radius, buffer size, MAC layer retransmission limit and contention window size on average energy consumption per sensor node.

The results of our simulations for different number of actors, event radius, buffer sizes, and initial contention window size CW_{min} are shown in Figure 16 (a)-(e), respectively. In these figures, the average energy consumption per node per second in

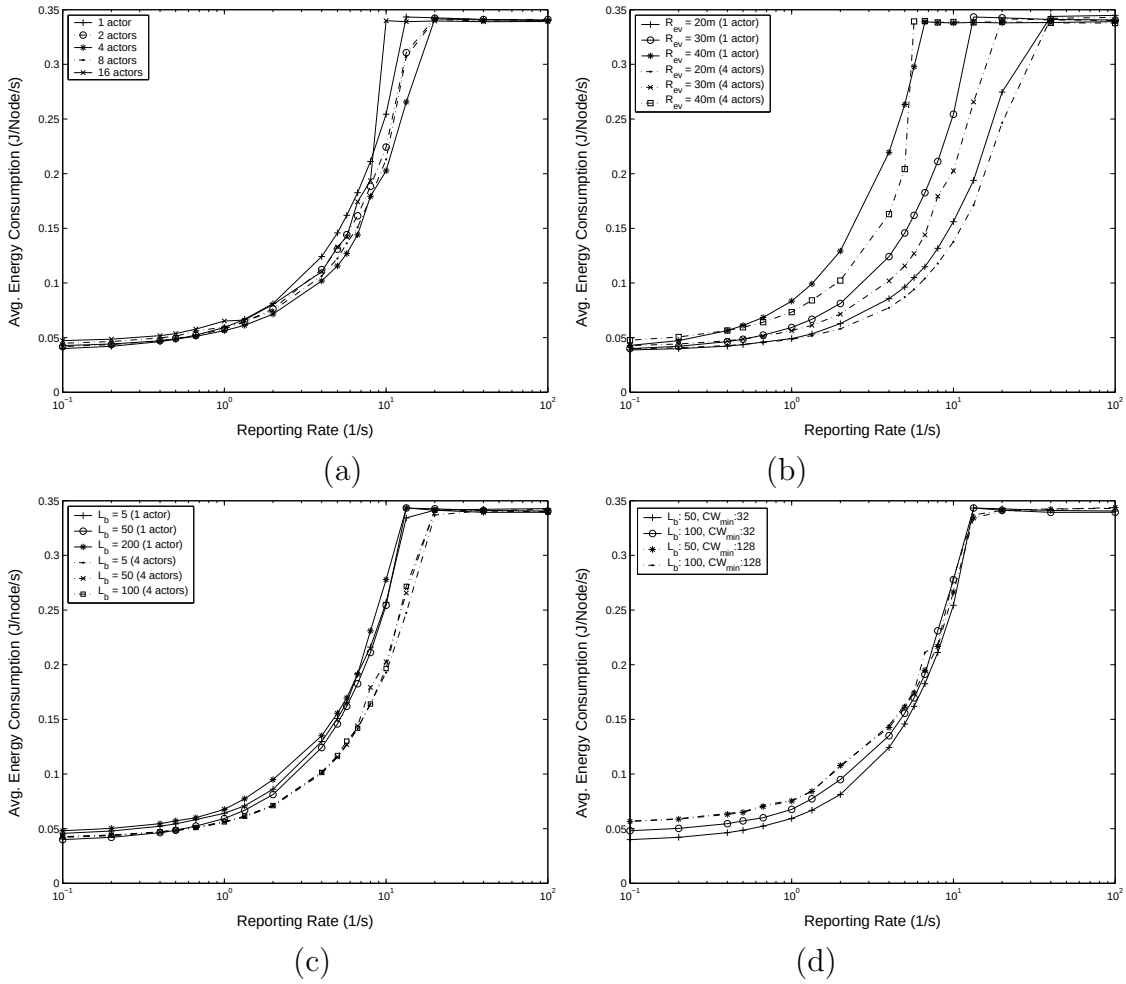

Figure 16: Average energy consumption per node for different (a) number of actors, (b) event radius, (c) buffer size, and (d) initial contention window.

the WSAN is shown. As seen in these figures, an initial increase is observed as the reporting rate is increased. Moreover, a subsequent constant level of energy consumption is obtained above a certain a dr_{th}^{low} value. Such a constant and saturated energy consumption is regardless of network parameters and is due to the limited capacity of the shared wireless medium. As the wireless medium capacity is saturated, the number of packets sent by the sensor nodes remains constant leading to constant energy consumption. However, note from our earlier discussions that, the packets drops due to various reasons such as increased level of collisions or buffer overflows lead to inefficiency in the network although same energy consumption is observed.

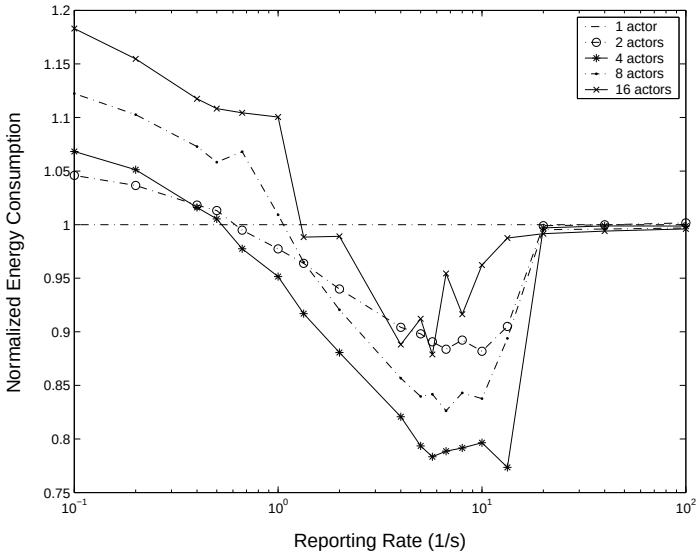

Figure 17: Average energy consumption normalized to the energy consumption of a single actor scenario.

We first investigate the effect of actors on the energy consumption. As shown in Figure 16 (a), the energy consumption for different number of actors is similar. However, there are still differences for each number of actors. In order to clearly illustrate the effect of number of actors, in Figure 17, we plot the energy consumption normalized to the case of a single actors. This figure clearly shows the advantage of WSANs on WSNs, since the case with a single actor can be regarded as a WSN. As can be observed from Figure 17, increasing the number of actors has positive impact on energy consumption above a certain reporting rate. The significance of impact the reporting rate at which energy savings start depend on the number of actors. Consistent with our earlier observations, 4 actors result in lowest energy consumption when compared to other cases. Moreover, 4 actors start to be more efficient than the single actor case at lower reporting rates. Consequently, decrease of 80% in the overall energy consumption is possible. Moreover, note that this saving is possible at lower reporting rates, where congestion is not observed. Another interesting result is that 2 actors result in lower energy consumption than 16 actors. This clearly shows that using many actors in a WSAN is not energy efficient. Rather an optimal number of

actors has to be found considering the dynamics of the WSAN.

In Figure 16(b), the average energy consumption per node is shown for various event radius values. The event radius specifies the number of source nodes sending information about an event to the actor. As shown in Figure 16(b), as the event radius increases, the dr_{th}^{low} value, above which the energy consumption is saturated, occurs at lower reporting rate. This is due to the fact that as the event radius increases, the number of sources also increases. This results in network congestion and saturated energy consumption to start at lower reporting rates. Moreover, a higher number of actors conserve energy as observed from the dotted lines in Figure 16(b).

An interesting result obtained from Figure 16(c) is that the average energy consumption per node is not significantly affected when the buffer length is changed. However, as discussed in Section 2.3.3, these parameters have significant impact on network performance metrics. Hence, it is clear that buffer length can be adjusted in WSAN protocols according to the application specific requirements without hampering the energy consumption of the nodes. On the other hand, Figure 16(d) reveals that, increasing initial contention window size CW_{min} increases average consumed energy especially in the non-congested region. However, as discussed in Section 2.3.5, increasing initial contention window size is advantageous for higher reporting rates. This reveals that an adaptive solution for the initial contention window size is required to both achieve higher reliability and efficient energy consumption.

Overall, the careful adjustments in various network parameters such as number of actor nodes, buffer size, retransmission limit or contention window size can lead to efficient protocols in terms of event reliability, end-to-end latency, or energy consumption in WSANs. Therefore, the parameters of the developed protocols should be carefully determined based on the specifics of the applications.

CHAPTER III

REAL-TIME AND RELIABLE TRANSPORT IN WIRELESS SENSOR AND ACTOR NETWORKS

In this chapter, a real-time and reliable transport $(RT)^2$ protocol is presented to address the need for real-time and reliable data transport in WSANs. $(RT)^2$ is a novel transport solution that seeks to *achieve reliable and timely event detection with minimum possible energy consumption and no congestion.* It enables the applications to perform right actions in a timely manner by exploiting both the correlation and the collaborative nature of WSANs. The $(RT)^2$ protocol was first presented in [25]. In Section 5.1, a review of related work in transport layer protocols in WSANs are presented. In Section 3.2, the design principles and functionalities of the $(RT)^2$ protocol are described in detail. The protocol operation of $(RT)^2$ for sensor-actor and actor-actor communication is described in Section 3.3 and 3.4, respectively. Performance evaluation and simulation results are presented in Section 3.5.

3.1 Motivation and Related Work

Recently, there has been considerable amount of research efforts, which have yielded many promising communication protocols for wireless sensor networks (WSNs) [15], [18], [59], [58]. The common feature of these protocols is that they mainly address the energy-efficient and reliable data communication requirements of WSN. However, in addition to the energy-efficiency and communication reliability, many proposed WSAN applications have strict delay bounds and hence mandate timely transport of the event features from the sensor field to the actor nodes [16]. Consequently, the unique features and application requirements of WSANs call for a real-time and

reliable data transport solution. The functionalities and design of a such solution for WSANs are the main issues addressed in this work [25].

In this work, to address communication challenges of WSANs outlined in chapter I, a real-time and reliable transport $(RT)^2$ protocol is presented for WSANs. $(RT)^2$ is a novel transport solution that seeks to *achieve reliable and timely event detection with minimum possible energy consumption and no congestion.* It enables the applications to perform right actions timely by exploiting both the correlation and the collaborative nature of WSANs. Furthermore, $(RT)^2$ addresses heterogenous reliability requirements of both sensor-actor and actor-actor communication. More specifically, for sensor-actor communication, unlike traditional end-to-end reliability notions, $(RT)^2$ defines *delay-constrained event reliability* notion based on both *event-to-action delay bounds* and event reliability objectives. On the other hand, for actor-actor communication, it introduces 100% packet-level reliability mechanisms to avoid inaccurate action decisions in the deployment field. In this way, the $(RT)^2$ protocol simultaneously addresses event transport reliability and timely action performance objectives of WSANs.

In general, compared to the existing transport layer proposals in the related literature, the main contribution of $(RT)^2$ is that *it concurrently provides real-time communication support and addresses heterogeneous transport reliability requirements* for typical WSAN applications involving reliable event detection and timely action objectives within a certain delay bound. To this end, the notion of *delay-constrained event reliability* distinguishes $(RT)^2$ from other existing transport solutions proposed for wireless ad hoc and sensor networks. To the best of our knowledge, reliable event transport has not been studied from this perspective before and hence $(RT)^2$ is the first solution attempt simultaneously addressing the real-time and reliable event transport and action performance objectives of WSANs.

3.2 $(RT)^2$ Protocol Design Principles

Unlike traditional networks, the sensor/actor network paradigm necessitates that the event features are collaboratively estimated within a certain reliability and real-time delay bound. To achieve this objective with maximum resource efficiency, the $(RT)^2$ protocol exploits both the correlation and the collaborative nature of the network. In the following sections, we first describe the characteristics and challenges of both sensor-actor and actor-actor communication and then based on these characteristics, we discuss the main design components of the $(RT)^2$ protocol in detail. We also present a case study to gain more insight regarding the challenges of sensor/actor network.

3.2.1 Reliable Event Transport

The $(RT)^2$ protocol is equipped with different reliability functionalities to address heterogenous requirements of both sensor-actor and actor-actor communication. Next, the main features of these reliability functionalities are described.

3.2.1.1 Sensor-Actor Transport Reliability

In WSANs, sensor-actor transport is characterized by the dense deployment of sensors that continuously observe physical phenomenon. Because of the high density in the network topology, sensor observations are highly correlated in the space domain. In addition, the nature of the physical phenomenon constitutes the temporal correlation between each consecutive observation of the sensor. Because of these spatial and temporal correlations along with the collaborative nature of the WSANs, sensor-actor transport does not require 100% reliability [15], [56].

Consequently, for sensor-actor communication, conventional end-to-end reliability definitions and solutions would only lead to over-utilization of scarce sensor resources. On the other hand, the absence of reliable transport mechanism altogether can seriously impair event detection. Thus, the sensor-actor transport paradigm requires a

collective *event transport reliability* notion rather than the traditional end-to-end reliability notions. The $(RT)^2$ protocol also considers the new notion of *event-to-action delay bound* (described in Section 3.2.2) to meet the application-specific deadlines. Based on both event transport reliability and event-to-action delay bound notions, we introduce the following definitions:

- The *observed delay-constrained event reliability* (DR_i) is the number of received data packets within a certain delay bound at the actor node in a decision interval i. In other words, DR_i counts the number of correctly received packets complying with the application-specific delay bounds and the value of DR_i is measured in each decision interval i.

- The *desired delay-constrained event reliability* (DR^*) is the minimum number of data packets required for reliable event detection within a certain application-specific delay bound. This lower bound for the reliability level is determined by the application and based on the physical characteristics of the event signal being tracked.

- The *delay-constrained reliability indicator* (δ_i) is the ratio of the observed and desired delay-constrained event reliabilities, i.e., $\delta_i = DR_i/DR^*$.

Based on the packets generated by the sensor nodes in the event area, the event features are estimated and DR_i is observed at each decision interval i to determine the necessary action. If the observed delay constrained event reliability is higher than the reliability bound, i.e., $DR_i > DR^*$, then the event is deemed to be reliably detected within a certain delay bound. Otherwise, appropriate action needs to be taken to assure the desired reliability level in sensor-actor communication. For example, to increase the amount of information transported from the sensors to the actor, reporting frequency of the sensors can be increased properly while avoiding congestion in the

network. Therefore, sensor-actor transport reliability problem in WSANs is to *configure the reporting rate, f, of source nodes so as to achieve the required event detection reliability, DR^*, at the actor node within the application-specific delay bound.* The details of the $(RT)^2$ protocol operation for sensor-actor communication is described in Section 3.4.

3.2.1.2 Actor-Actor Transport Reliability

In WSANs, a reliable and timely actor-actor ad hoc communication is also required to collaboratively perform the right action upon the sensed phenomena [16]. The $(RT)^2$ protocol simultaneously incorporates *adaptive rate-based transmission control and (SACK)-based reliability mechanism* to achieve 100% packet reliability in the required ad hoc communication. To achieve this objective, $(RT)^2$ protocol relies upon new feedback based congestion control mechanisms and probe packets to recover from subsequent losses and selective-acknowledgments (SACK) to detect any holes in the received data stream. These algorithms are shown to be beneficial and effective in recovering from multiple packet losses in one round-trip time (RTT) especially [55]. The details of adaptive rate-based transmission and congestion control algorithms for actor-actor ad hoc communication are explained in Section 3.4. Next, event-to-action delay bound notion of $(RT)^2$ protocol is explained in detail.

3.2.2 Real-Time Event Transport

To assure accurate and timely action on the sensed phenomena, it is imperative that the event is sensed, transported to the actor node and the required action is performed within a certain delay bound. We call this *event-to-action delay bound*, Δ_{e2a}, which is specific to application requirements and must be met so that the overall objective of the sensor/actor network is achieved. The event-to-action delay bound Δ_{e2a}, has three main components as outlined below:

1. *Event transport delay (Γ^{tran}):* It is mainly defined as the time between when the event occurs and when it is reliably transported to the actor node. In general, it involves the following delay components:

   (a) *Buffering delay ($t_{b,i}$):* It is the time spent by a data packet in the routing queue of an intermediate forwarding sensor node i. It depends on the current network load and transmission rate of each sensor node.

   (b) *Channel access delay ($t_{c,i}$):* It is the time spent by the sensor node i to capture the channel for transmission of the data packet generated by the detection of the event. It depends on the channel access scheme in use, node density and the current network load.

   (c) *Transmission delay ($t_{t,i}$):* It is the time spent by the sensor node i to transmit the data packet over the wireless channel. It can be calculated using transmission rate and the length of the data packet.

   (d) *Propagation delay ($t_{p,i}$):* It is the propagation latency of the data packet to reach the next hop over the wireless channel. It mainly depends on the distance and channel conditions between the sender and receiver.

2. *Event processing delay (Γ^{proc}):* This is the processing delay experienced at the actor node when the desired features of event are estimated using the data packets received from the sensor field. This may include a certain decision interval [15] during which the actor node waits to receive adequate samples from the sensor nodes.

3. *Action delay (Γ^{act}):* The action delay is the time it takes from the instant that event is reliably detected at the actor node to the instant that the actual action is taken. It is composed of the *task assignment delay*, i.e., time to select the

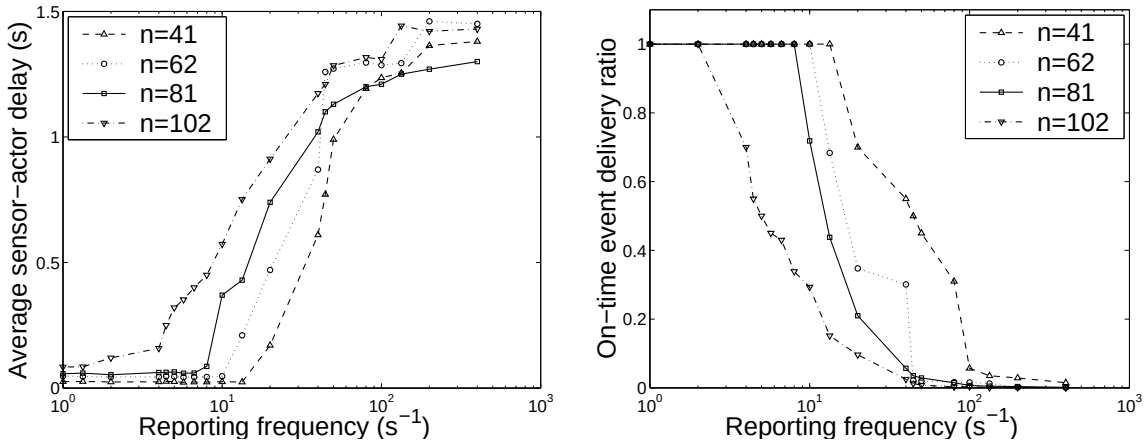

(a) (b)

Figure 18: The effect of varying reporting frequency of source nodes on (a) average sensor-actor delay and (b) on-time event delivery ratio.

best[1] set of actors for the task and the *action execution delay*, i.e., time to actually perform the action.

More specifically, while event transport delay (Γ^{tran}) and event processing delay (Γ^{proc}) occur during sensor-actor communication, action delay (Γ^{act}) is resulted from actor-actor communication in the deployment field. Let Δ_{e2a} be the event-to-action delay bound for the data packet generated by the detection of event. Then, for a timely action, it is necessary that the following relation holds:

$$\Delta_{e2a} \geq \Gamma^{tran} + \Gamma^{proc} + \Gamma^{act} \tag{2}$$

Note that Γ^{tran} is directly affected by the current network load and the congestion level in the network. In addition, the network load depends on the event reporting frequency, f, which is used by the sensor nodes to send their readings of the event. Specifically, the buffering delay, i.e., $t_{b,i}$, directly depends on the transport rate, and on the queue management and service discipline employed at each sensor in the network.

[1]The best set of actors refers to the actors which are close to the event area, or which has high capability and residual energy, or which has small action completion time upon the sensed phenomenon [16].

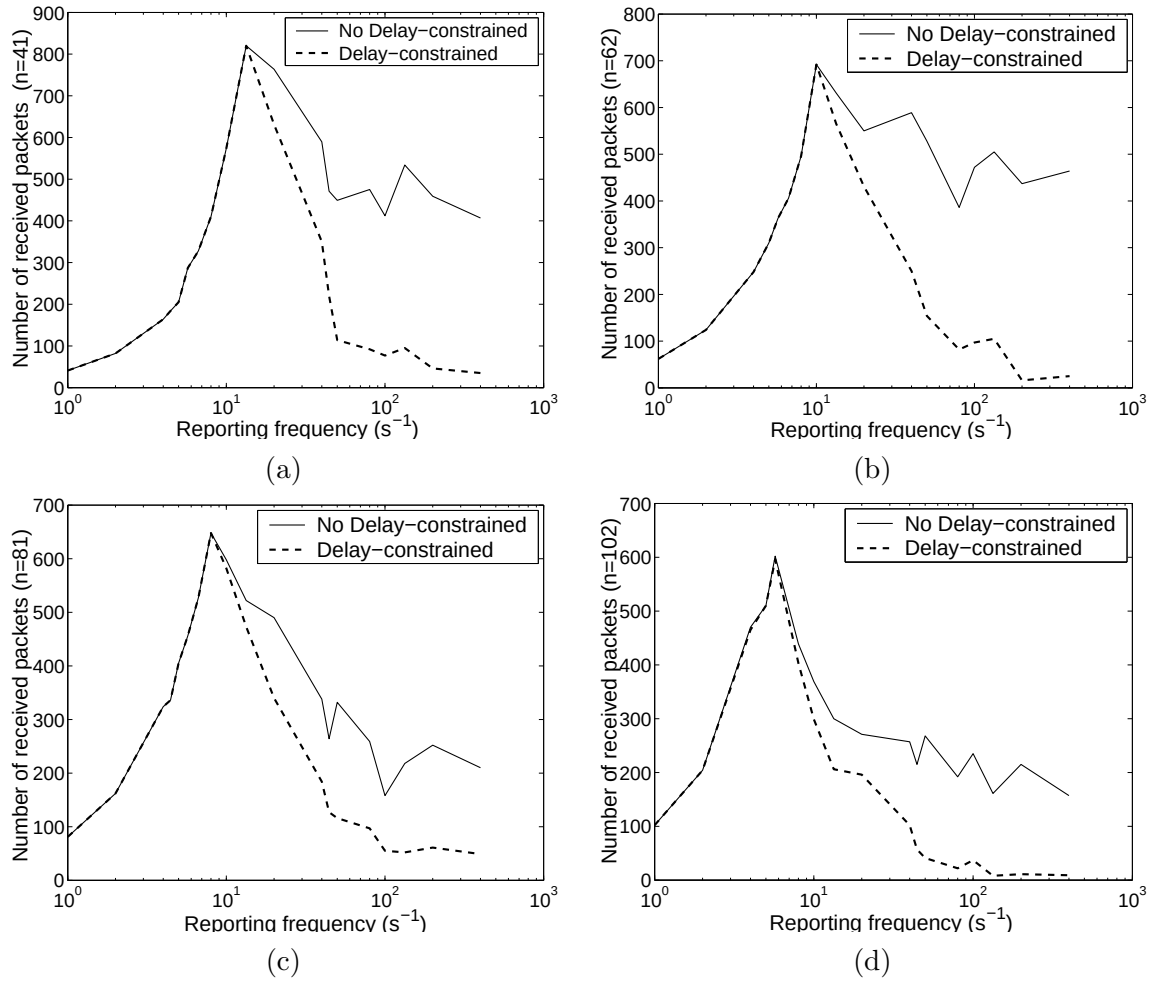

Figure 19: The number of received packets at the actor node in a decision interval, when the number of sources, (a)$n = 41$, (b)$n = 62$, (c)$n = 81$, (d)$n = 102$.

In addition, since events occurring at further distances from the actor node are in general characterized by a higher average number of hops to reach the actor node, it is more difficult to provide event-to-action delay bounds. Considering that the per-hop propagation delay, i.e., $t_{p,i}$, does not vary, the buffering delay must be controlled in order to compensate for the increase in the event transport delay. To accomplish this objective, we introduce *Time-Critical Event First* (TCEF) scheduling policy. TCEF applies the general principles of earliest deadline first service discipline on each sensor node, which is shown to be the optimal scheduling policy, i.e., to have the widest scheduling region, when real-time deadlines in a system are considered [48].

To update the remaining time to deadline without a globally synchronized clock in the network, we measure the elapsed time for a packet at each sensor and piggyback the elapsed time to the event packet so that the following sensor can determine the remaining time to deadline without a globally synchronized clock. Then, by using these elapsed time measurements, the event packets are given high priority at the sensor nodes, as their remaining time to deadline decreases. In this way, time critical sensor data obtain high priority along the path from the event area to the actor node and is served first, which is crucial to meet the application deadlines.

Note that although TCEF policy makes it possible to meet deadlines in the normal operating conditions of the network, in case of severe network congestion, it may become insufficient to provide delay-constrained event reliability. Hence, in addition to TCEF scheduling, the $(RT)^2$ protocol considers the event-to-action delay bounds and congestion conditions in its reporting rate update policies to assure timely and reliable event transport in WSANs (see Section 3.3). It is also important to note that the measured elapsed time at each sensor node can give an idea of congestion level experienced in the network, since it represents both the buffering delay and the channel contention around the sensor node (see Section 3.2.4).

3.2.3 Case Study

To investigate the relationship between the event-to-action delay and the event reporting rate, we develop an evaluation environment using *ns*-2 [8]. The parameters used in our case study are listed in Table 2. In our simulations, 200 sensor nodes were randomly positioned in a 200m x 200m sensor field. Node parameters such as radio range and IFQ (interface queue) length were carefully chosen to mirror typical sensor mote values [7]. Event centers (X_{ev}, Y_{ev}) were randomly chosen and all sensor nodes within the event radius behave as sources for that event. In this case study, the actor node receiving the data is placed in the middle of the lower side of the

deployment area. To communicate source data to the actor node, we employed a simple CSMA/CA based MAC protocol. For each simulation, we run 10 experiments and take the average of the measured values.

Table 2: NS-2 simulation parameters.

Area of sensor field	200x200 m^2
Number of sensor nodes	200
Radio range of a sensor node	20 m
Packet length	30 bytes
Interface queue (IFQ) length	65 packets
Transmit Power	0.660 W
Receive Power	0.395 W
Doze Power	0.035 W
Decision interval (τ)	1 s

First, we investigate the impact of event reporting frequency on average sensor-actor communication delay and *on-time event delivery ratio*. Here, on-time event delivery ratio represents the fraction of data packets received within sensor-actor delay bound (which we refer to reliable packets) over all data packets received in a decision interval. The results of our study are shown in Figure 18 for different number of source nodes, i.e, $n = 41, 62, 81, 102$. Note that each of these curves was obtained by varying the event reporting frequency, f, for a randomly chosen event center (X_{ev}, Y_{ev}) and corresponding number of sources, n. These values are tabulated in 3.

Table 3: Randomly selected event centers used in the simulations.

Number of source nodes	**Event center** (X_{ev},Y_{ev})	**Event radius**
41	(75.2, 72.3)	30m
62	(52.1, 149.3)	30m
81	(59.2, 68.1)	40m
102	(90.6, 119.1)	40m

As shown in Figure 18(a) and 18(b), it is observed that as the event reporting

frequency, f, increases, average sensor-actor transport delay remains constant and on-time event delivery is ensured, until a certain $f = f_{max}$ at which network congestion is experienced. After this point, the average sensor-actor transport delay starts to increase and on-time event delivery cannot be provided. This is obvious because the increased network load due to higher reporting frequency leads to increase in the buffer occupancy and network channel contention. Moreover, as the number of sources increases, on-time event delivery ratio cannot be provided even at lower reporting frequencies.

To further elaborate the relationship between observed delay-constrained event reliability, DR_i, and the event reporting frequency, f, we have observed the number of packets received at the actor node in a decision interval, τ. We make the following observations from Figure 19:

i. Until a certain $f = f_{max}$, observed delay-constrained event reliability and no delay-constrained event reliability[2] coincides, beyond which delay-constrained event reliability significantly deviates from no delay-constrained event reliability.

ii. The observed delay-constrained event reliability, DR_i, shows a linear increase (note the log scale) with source reporting rate, f, until a certain $f = f_{max}$, beyond which the observed delay-constrained event reliability drops. This is because the network is unable to handle the increased injection of data packets and packets are dropped because of congestion.

iii. Such an initial increase and a subsequent decrease in observed delay-constrained event reliability is observed regardless of the number of source nodes, n.

iv. f_{max} decreases with increasing n, i.e., network congestion occurs at lower reporting frequencies with greater number of source nodes.

[2]No delay-constrained event reliability represents the number of event packets received at the actor irrespective of their packet delay.

v. After $f{=}f_{max}$, delay-constrained event reliability starts to drop significantly due to network congestion. Therefore, an accurate congestion detection mechanism is required to both provide delay-constrained reliability and an effective congestion control in the network.

In summary, with increasing reporting frequency, a general trend of an initial increase and a subsequent decrease (due to network congestion) in delay-constrained event reliability is observed in our preliminary studies, as shown in Figure 18. Furthermore, when the application-specific delay bounds are considered, the observed delay-constrained event reliability decreases significantly with the network congestion, regardless of the number of source nodes. These observations confirm the urgent need for a delay-constrained reliable event transport solution with an efficient congestion detection and control mechanism in WSANs. In the following section, combined congestion detection mechanism of the $(RT)^2$ protocol is described in detail.

3.2.4 Congestion Detection and Control Mechanism

In WSANs, because of the memory limitations of the sensor nodes and limited capacity of shared wireless medium, congestion might be experienced in the network. Congestion leads to both waste of communication and energy resources of the sensor nodes and also hampers the event detection reliability because of packet losses [15]. Hence, it is mandatory to address the congestion in the sensor field to achieve real-time and reliable event detection and minimize energy consumption. However, the conventional sender-based congestion detection methods for end-to-end congestion control purposes cannot be applied here. The reason lies in the notion of delay-constrained event reliability rather than end-to-end reliability. Only the actor node, and not any of the sensor nodes, can determine the delay-constrained reliability indicator $\delta_i = DR_i/DR^*$, and act accordingly.

In addition, for efficient congestion detection in WSANs, the sensor nodes should

be aware of the network channel condition around them, since the communication medium is shared and might be congested with the network traffic among other sensor nodes in the neighborhood [34]. Therefore, because of shared communication medium nature of WSANs, the sensor nodes can experience congestion even if their buffer occupancy is small.

To investigate the impact of the channel contention on the congestion level of the neighboring nodes, we perform a simulation study using ns-2 [8]. The network configuration is shown in Figure 20, in which node 0 and 1 (sources) send data to node 4 and 5 (destinations), respectively. During the time period between 4 and 6 s, the node 0 increases its transmission rate, which creates a hot-spot around node 2. In Figure 21 (a) and (b), the resulting packet delay and buffer occupancy at the nodes 2 and 3 are shown, respectively. As seen in Figure 21 (a), we observe that at node 2 both buffer occupancy ratio and average packet delay between 4 and 6 s increase significantly and these metrics reflect the congestion level at node 2 accurately. On the other hand, as shown in Figure 21 (b), we observe that even if the buffer occupancy at node 3 is small during 4 and 6 s (buffer occupancy ratio is almost 20%), average packet delay increases significantly between 4 and 6 s. This is because in this time period, although the incoming traffic does not change, the increased channel contention around the node 3 causes packet collisions and retransmissions resulting in increased packet delay. Note that at node 3, it is difficult to detect the level of congestion solely based on the buffer occupancy. Therefore, for an efficient congestion detection in WSANs, a combined approach is required.

In this regard, the $(RT)^2$ protocol uses a *combined congestion detection* mechanism based on both average node delay calculation and local buffer level monitoring of the sensor nodes to accurately detect congestion in the network. Note that average node delay at the sensor node gives an idea about the contention around the sensor node, i.e., how busy the surrounding vicinity of the sensor node. To compute the average

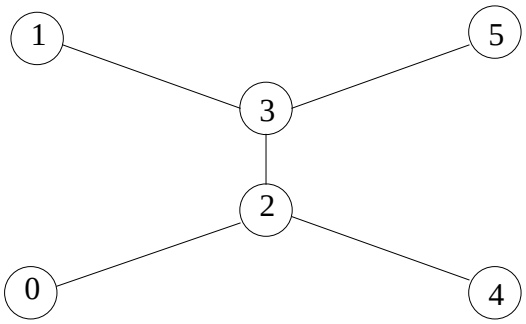

Figure 20: A simple wireless ad hoc network of 6 nodes. Only the nodes connected by a line are within each other' s communication range.

node delay at the sensor node i, the sensor node takes exponential weighted moving average of the elapsed time. Recall that with the proposed mechanism in Section 3.2.2, the calculation of the average node delay can be performed without globally synchronized clock in the network.

In combined congestion detection mechanism of the $(RT)^2$ protocol, any sensor node whose buffer overflows due to excessive incoming packets or average node delay is above a certain delay threshold value is said to be congested and it informs the congestion situation to the actor node. More specifically, the actor node is notified by the upcoming congestion condition in the network by utilizing the *Congestion Notification* (CN) bit in the header of the event packet transmitted from sensors to the actor node. Therefore, if the actor node receives event packets whose CN bit is marked, it infers that congestion is experienced in the last decision interval. In conjunction with the delay-constrained reliability indicator, δ_i, the actor node can determine the current network condition and dynamically adjust the reporting frequency of the sensor nodes.

To achieve timely execution of the right action upon the environment, actor-actor ad hoc communication must also be efficiently handled. In this respect, congestion control is also imperative for reliable and timely actor-actor ad hoc communication. Hence, combined congestion mechanism of the $(RT)^2$ protocol is also utilized for actor-actor ad hoc communication. The details of adaptive rate-based transmission

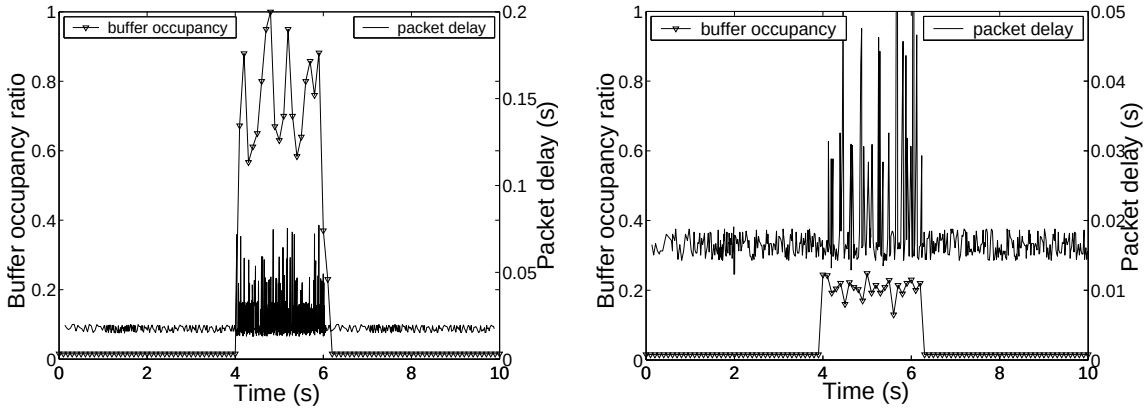

Figure 21: Buffer occupancy and packet delay at (a) node 2 and (b) node 3.

and congestion control algorithms for actor-actor ad hoc communication are explained in Section 3.4.

3.3 (RT)^2 Protocol Operation for Sensor-Actor Communication

In this section, we describe the (RT)^2 protocol operation during sensor-actor communication. Recall that in the previous sections, based on the delay-constrained event reliability and the event-to-action delay bound notions, we had defined a new delay-constrained reliability indicator $\delta_i = DR_i/DR^*$, i.e., the ratio of observed and desired delay-constrained event reliabilities. To determine proper event reporting frequency update policies, we also define T_i and T_{sa}, which are the amount of time needed to provide delay-constrained event reliability for a decision interval i and the application-specific sensor-actor communication delay bound, respectively. In conjunction with the congestion notification information (CN bit) and the values of f_i, δ_i, T_i and T_{sa}, the actor node calculates the updated reporting frequency, f_{i+1}, to be broadcast to source nodes in each decision interval. This updating process is repeated until the optimal operating point is found, i.e., adequate reliability and no congestion condition is obtained. In the following sections, we describe the details of the reporting

frequency update policies and possible network conditions experienced by the sensor nodes.

3.3.1 Early Reliability and No Congestion Condition

In this condition, the required reliability level specific to application is reached before the sensor-actor communication delay bound, i.e., $T_i \leq T_{sa}$, and no congestion is observed in the network, i.e., $CN = 0$. However, the observed delay-constrained event reliability, DR_i, is larger than desired delay-constrained event reliability, DR^*. This is because source nodes transmit event data more frequently than required. The most important consequence of this condition is excessive energy consumption of the sensors. Therefore, the reporting frequency should be decreased cautiously to conserve energy. This reduction should be performed cautiously so that the delay-constrained event reliability is always maintained. Therefore, the actor node decreases the reporting frequency in a controlled manner. Intuitively, we try to find a balance between saving energy and maintaining reliability. Hence, the updated reporting frequency can be expressed as follows:

$$f_{i+1} = f_i \frac{T_i}{T_{sa}} \tag{3}$$

3.3.2 Early Reliability and Congestion Condition

In this condition, the required reliability level specific to application is reached before the sensor-actor communication delay bound, i.e., $T_i < T_{sa}$, and congestion is observed in the network, i.e., $CN = 1$. However, the observed delay-constrained event reliability, DR_i, is larger than the desired delay-constrained event reliability, DR^*. In this situation, the $(\mathrm{RT})^2$ protocol decreases reporting frequency to avoid congestion and save the limited energy of sensors. This reduction should be in a controlled manner so that the delay-constrained event reliability is always maintained. However, the reporting frequency can be decreased more aggressively than the case where there is

no congestion and the observed delay-constrained event reliability, DR_i, is larger than the desired delay-constrained event reliability, DR^*. This is because in this case, we are farther from optimal operating point. Here, we try to avoid congestion as soon as possible. Hence, the updated reporting frequency can be expressed as follows:

$$f_{i+1} = min(f_i \frac{T_i}{T_{sa}}, f_i^{(T_i/T_{sa})}) \tag{4}$$

3.3.3 Low Reliability and No Congestion Condition

In this condition, the required reliability level specific to application is not reached before sensor-actor communication delay bound, i.e., $T_i > T_{sa}$, and no congestion is observed in the network, i.e., $CN = 0$. However, the observed delay-constrained event reliability, DR_i, is lower than the desired delay-constrained event reliability, DR^*. This can be caused by i) packet loss due to wireless link errors, ii) failure of intermediate relaying nodes, iii) inadequate data packets transmitted by source nodes. Packet loss due to wireless link errors might be observed in WSANs due to energy inefficiency of powerful error correction and retransmission techniques. However, regardless of the packet error rate, the total number of packets lost due to link errors is expected to scale proportionally with the reporting frequency, f. Here, we make the assumption that the net effect of channel conditions on packet loss does not deviate significantly in successive decision intervals. This is reasonable with static sensor nodes, slowly time-varying and spatially separated communication channels [15]. Furthermore, when intermediate nodes fail, packets that need to be routed through these nodes are dropped. This can cause a reduction in reliability even if enough number of data packets is transmitted by source nodes. However, fault-tolerant routing/re-routing in WSN is provided by several existing routing algorithms [18]. The $(RT)^2$ protocol can work with any of these routing schemes. Therefore, to achieve required event reliability, we need to increase the data reporting frequencies

of source nodes. Here, we exploit the fact that the DR vs. f relationship in the absence of congestion, i.e., for $f < f_{max}$, is linear (see Section 3.2.3). In this regard, we use the multiplicative increase strategy to calculate updated reporting frequency, which is expressed as follows:

$$f_{i+1} = f_i \frac{DR^*}{DR_i} \tag{5}$$

3.3.4 Low Reliability and Congestion Condition

In this condition, the required reliability level specific to application is not reached before sensor-actor communication delay bound, i.e., $T_i > T_{sa}$, and congestion is observed in the network, i.e., $CN = 1$. However, the observed delay-constrained event reliability, DR_i, is lower than the desired delay-constrained event reliability, DR^*. This situation is the worst possible case, since desired delay-constrained event reliability is not reached, network congestion is observed and thus, limited energy of sensors is wasted. Hence, the $(\mathrm{RT})^2$ protocol aggressively reduces reporting frequency to reach optimal reporting frequency as soon as possible. Therefore, to assure sufficient decrease in the reporting frequency, it is exponentially decreased and the new frequency is expressed by:

$$f_{i+1} = f_i^{\frac{DR_i}{(DR^* * k)}} \tag{6}$$

where k denotes the number of successive decision intervals for which the network has remained in the same situation including the current decision interval, i.e., $k \geq 1$. Here, the purpose is to decrease reporting frequency with greater aggression, if a network condition transition is not detected.

3.3.5 Adequate Reliability and No Congestion Condition

In this condition, the network is within β tolerance of the optimal operating point, i.e., $f < f_{max}$ and $1 - \beta \leq \delta_i \leq 1 + \beta$, and no congestion is observed in the network. Hence, the reporting frequency of source nodes is left constant for the next decision interval:

$$f_{i+1} = f_i \tag{7}$$

Here, our aim is to operate as close to $\delta_i = 1$ as possible, while utilizing minimum network resources and meeting event delay bounds. For practical purposes, we define a tolerance level, β, for optimal operating point. If at the end of decision interval i, the delay-constrained reliability indicator δ_i is within [1-β,1+β] and if no congestion is detected in the network, then the network is in (Adequate reliability, No congestion) condition. In this condition, the event is deemed to be reliably and timely detected and the reporting frequency remains unchanged. Thus, a greater proximity to the optimal operating point can be achieved with small β. However, the smaller the β, the greater the convergence time needed to reach corresponding (Adequate reliability, No congestion) condition. Therefore, a good choice of β is the one that balances the tolerance and convergence requirements and hence is mainly dependent on the application-specific requirements in terms of convergence time, the degree of energy conservation, expected lifetime, as well as desired delay-constrained reliability level.

To this end, for a given set of application requirements, the optimal value of β can be either found analytically (which is left as a future work) or determined by the simulation experiments through parameter-tuning.

The entire $(RT)^2$ protocol operation is presented in the pseudo-algorithm given in Figure 22.

$k = 1$;
(RT)^2()
  If (CONGESTION)
    If ($\delta < 1$)
    /*Low Reliability and Congestion*/
      $f_{i+1} = f_i^{\frac{DR_i}{(DR^* * k)}}$;
      $k = k + 1$;
    else if ($\delta > 1$)
    /*Early Reliability and Congestion*/
      $k = 1$;
      $f_{i+1} = min(f_i \frac{T_i}{T_{sa}}, f_i^{(T_i/T_{sa})})$;
    end;
  else if (NO_CONGESTION)
    $k = 1$;
    If ($\delta < 1 - \beta$)
    /*Low Reliability and No Congestion*/
      $f_{i+1} = f_i \frac{DR^*}{DR_i}$;
    else if ($\delta > 1 + \beta$)
    /*Early Reliability and No Congestion*/
      $f_{i+1} = f_i \frac{T_i}{T_{sa}}$;
    end;
    else if ($1 - \beta \leq \delta \leq 1 + \beta$)
    /*Adequate Reliability and No Congestion*/
      $f_{i+1} = f_i$;
    end;
end;

Figure 22: Algorithm of the (RT)^2 protocol during sensor-actor communication.

3.4 (RT)^2 Protocol for Actor-Actor Communication

In WSANs, as discussed before, after receiving event information, actors need to communicate with each other to make decisions on the most appropriate way to perform the action. Thus, to timely initiate the right actions upon the sensed phenomena, the (RT)^2 protocol also addresses efficient actor-actor communication. In this section, we first describe the main design principles of the (RT)^2 protocol for actor-actor communication. Then, we describe the details of the (RT)^2 protocol operation during actor-actor communication.

3.4.1 $(RT)^2$ Protocol Overview for Actor-Actor Communication

In this section, we make an overview of the key design elements of the $(RT)^2$ protocol for actor-actor communication:

1. *Cross-layer interactions:* In the current literature on wireless ad hoc networks, some protocols providing an efficient coordination between communication layers are developed to react the network dynamics both accurately and timely [32], [64]. The $(RT)^2$ protocol also benefits from both cross-layer interactions and intermediate node feedback information to i) capture route failures accurately and timely, ii) get congestion notification and transmission rate feedback for both initial start up phase and steady state phase.

2. *Distinguishing cause of packet loss:* The $(RT)^2$ protocol distinguishes congestion and non-congestion related losses by the feedback information from both receiver and the intermediate nodes. In this context, the $(RT)^2$ protocol uses a *combined congestion detection* mechanism based on both the average node delay calculation and the local buffer level monitoring of the actor nodes to accurately detect congestion in the network (see Section 3.2.4). When the actor node is notified about the congestion condition, it decreases the transmission rate accordingly to relieve the congestion as soon as possible.

3. *SACK-based reliability:* To provide reliable actor-actor communication, the $(RT)^2$ protocol relies upon probe packets to recover from subsequent losses and selective-acknowledgments (SACK) packets to detect any holes in the received data stream. Furthermore, to prevent congestion in the reverse path, SACK packets are delayed in the receiver, i.e., one SACK packet for every d data packets received. Hence, this delayed SACK strategy of $(RT)^2$ protocol enables the receiver to control the amount of the reverse path traffic accordingly.

4. *Adaptive rate-based transmission:* The $(RT)^2$ protocol periodically adjusts transmission rate based on bottleneck node information, i.e., congestion notification (CN), packet delay and the number flows passing through the node. Here, the packet delay represents the sum of queuing, channel access time and transmission time at the bottleneck node along the path. Note that we also compute exponential average of packet delays, i.e., D_i, at the intermediate nodes and the receiver to fine tune the fluctuations of the observed delay values, i.e., $Avg(D_i)=\alpha*Avg(D_i)+(1-\alpha)*Current(D_i)$. Moreover, based on the number of flows passing through the same node, a simple fair sharing principle is employed to equally distribute the network resources. Note that $(RT)^2$ can also work with other service disciplines such as per-flow quality-of-service (QoS) based disciplines, which can further improve the performance and are beyond the scope of this study. In addition, to meet the application-specific delay bounds, the minimum transmission rate (R_{min}) is also determined according to the remaining time to event-to-action delay bound (see eq. 8). In this way, the data rate is dynamically adjusted based on both the current conditions of the data path and event-to-action delay bounds.

5. *Flow control:* The $(RT)^2$ protocol performs flow control by observing the application processing rate R_p, which represents the application reading rate from the receiver buffer. Here, our objective is to limit the amount of data transmitted by the sender to a certain rate that the receiver can manage. In this regard, if R_p is smaller than the rate feedback R_f provided by intermediate nodes, the receiver sends R_p to the sender as a rate feedback. Thus, $(RT)^2$ also provides flow control at the receiver while dynamically adjusting transmission rate.

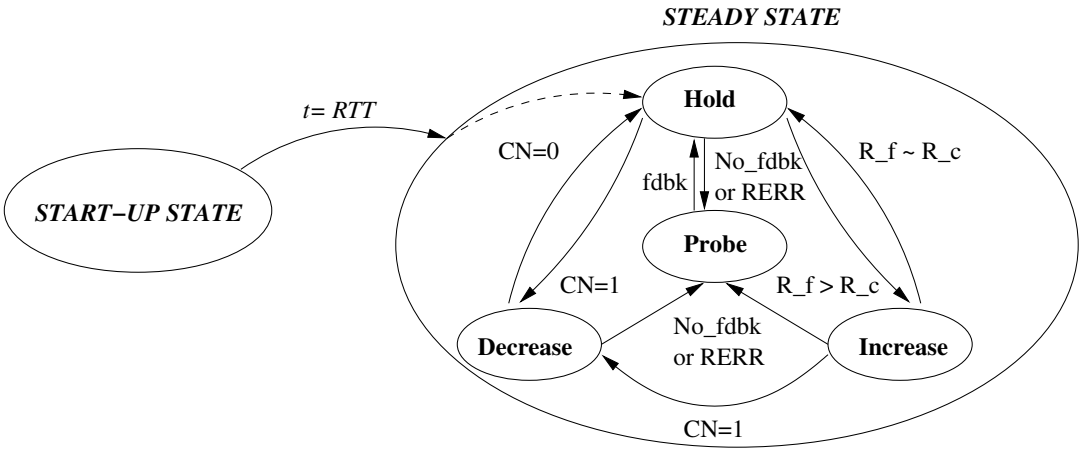

Figure 23: $(RT)^2$ state transition diagram for actor-actor communication.

3.4.2 $(RT)^2$ Protocol Operation for Actor-Actor Communication

In this section, we describe the protocol operation of $(RT)^2$ during actor-actor communication. The protocol operation is composed of two main states: i) start-up state, ii) steady state. In Figure 23, the $(RT)^2$ protocol state diagram for actor-actor communication is shown. In the following paragraphs, the operations at each state is described in detail.

1. *Start-Up State:* When establishing new connection between sender and receiver, the sender transports a probe packet towards the receiver to capture the the available transmission rate quickly. Each intermediate node between the sender and receiver intercepts the probe packet and updates the bottleneck delay field of the probe packet, if the current value of delay information is higher than that of the intermediate node. Initially, the delay value of probe packet is assigned to zero. Therefore, after one round-trip-time, the sender gets estimated rate feedback from the receiver, which results in quick convergence to available transmission rate. Furthermore, this probing mechanism of start up phase is also applied after route changes.

2. *Steady State:* This state consists of four substates: i) Increase, ii) Decrease, iii) Hold and iv) Probe. In the following, we describe the $(RT)^2$ protocol operations in each substate:

   (a) *Increase:* In this state, the sender increases its transmission rate according to the feedback coming from the receiver. Once an increase decision for sender transmission rate is taken, only m fraction of the difference between transmission rate feedback (R_f) and sender current transmission rate (R_c) is performed. The appropriate fraction value (m) for the transmission rate increase is obtained as follows: If the hop count along the data path is greater than or equal to 4 for that connection, m is set to 4. Otherwise, if the hop count is less than 4, then m is set to the actual hop count value along the path. The inherent spatial reuse property of underlying CSMA/CA based MAC protocol requires this normalization in transmission rate. The details can be found in [22],[38]. Note also that to prevent fluctuations, transmission rate is only increased when a certain threshold (Δ_{rate}) is exceeded.

   (b) *Decrease:* In this state, the sender reduces its transmission rate according to the feedback coming from the receiver. Note that the transmission rate is decreased until the minimum transmission rate (R_{min}) is reached. R_{min} represents the minimum transmission rate requirement to transfer a certain amount of data within event-to-action delay bound. R_{min} can be calculated as follows:

$$R_{min} = \frac{B}{\Delta_{re2a}} \tag{8}$$

   where B represents the amount of packets that should be transmitted to the actor and Δ_{re2a} is remaining event-to-action deadline, which is the

residual time of event-to-action delay bound Δ_{e2a} (see Section 3.2.2), after the sensor-actor communication is performed.

(c) *Hold:* In this state, the required transmission rate is reached. Sender does not change the transmission rate unless route failure or congestion occurs in the network.

(d) *Probe:* In this state, the sender sends a probe packet to the receiver so as to monitor the available transmission rate in the network as in start up phase. This phase might occur due to route errors (RERR), which is common in ad hoc communication networks. When the route error is observed, i.e., RERR information is received from intermediate nodes, sender freezes its transmission and periodically starts to send the probe packet to get transmission rate feedback from the receiver.

Overall, the $(RT)^2$ protocol dynamically shapes data traffic based on both delay bounds and the current conditions of the network. Note that, in the protocol operation, the sender adjusts its transmission rate in response to the rate feedbacks from the receiver, which are sent with the period of T_{fdbk}. To prevent the sender from over-flooding the network in case all the feedback packets from the receiver are lost, the $(RT)^2$ protocol also performs a multiplicative decrease of transmission rate for each feedback periods, in which the sender does not receive feedback from the receiver up to a maximum of two feedback periods. After the second feedback period, if the sender still does not receive any feedback packet, it enters into probe state so as to monitor the available transmission rate in the network. In this respect, the periods of feedback (T_{fdbk}) and probe packets (T_p) should be larger than one round-trip-time (RTT) and small enough to capture the network dynamics.

For this purpose, the period of feedback packets (T_{fdbk}) and probe packets (T_p) are selected as $2 * RTT$. Note also that if the receiver rate feedback changes more than

a certain threshold (Δ_{fdbk}), then the receiver immediately sends the rate feedback information to the sender without waiting for a feedback timer timeout event. Thus, the sender can adjust the transmission rate accordingly even for long RTT values.

Note that actor-actor communication in WSANs is similar to the communication paradigm of ad hoc networks due to the small number of resource-rich actor nodes being loosely deployed. In the related literature, there are several transport protocols dealing with ad hoc networks [20]. In general, these solutions are either window-based [32], [39] or rate-based protocols [55]. Although these solutions may improve TCP performance to a certain extent, they do not address the unique requirements of WSANs completely. To evaluate the performance of $(RT)^2$ during actor-actor communication, we also compare $(RT)^2$ with these ad hoc transport solutions in the following section.

3.5 $(RT)^2$ Performance Evaluation

Here, we present the performance evaluation of the $(RT)^2$ protocol. In Section 3.5.1, we report the performance results for the sensor-actor communication, while in Section 3.5.2, we discuss the performance results for the actor-actor communication.

3.5.1 Sensor-Actor Communication

To evaluate the performance of the $(RT)^2$ protocol during sensor-actor communication, we developed an evaluation environment using ns-2 [8]. For sensor-actor communication scenario, the number of sources, sensor-actor delay bound and tolerance level were selected as $n = 81$, $1s$ and $\epsilon = 5\%$, respectively. The event radius was fixed at $40m$. We run 10 experiments for each simulation configuration. Each data point on the graphs is averaged over 10 simulation runs. We use the same sensor node and simulation configurations provided in 2 in Section 3.2.3.

Moreover, in this simulation scenario, the actor nodes, which receive data packets from sensors, stop their movements once they start to receive data. In this way,

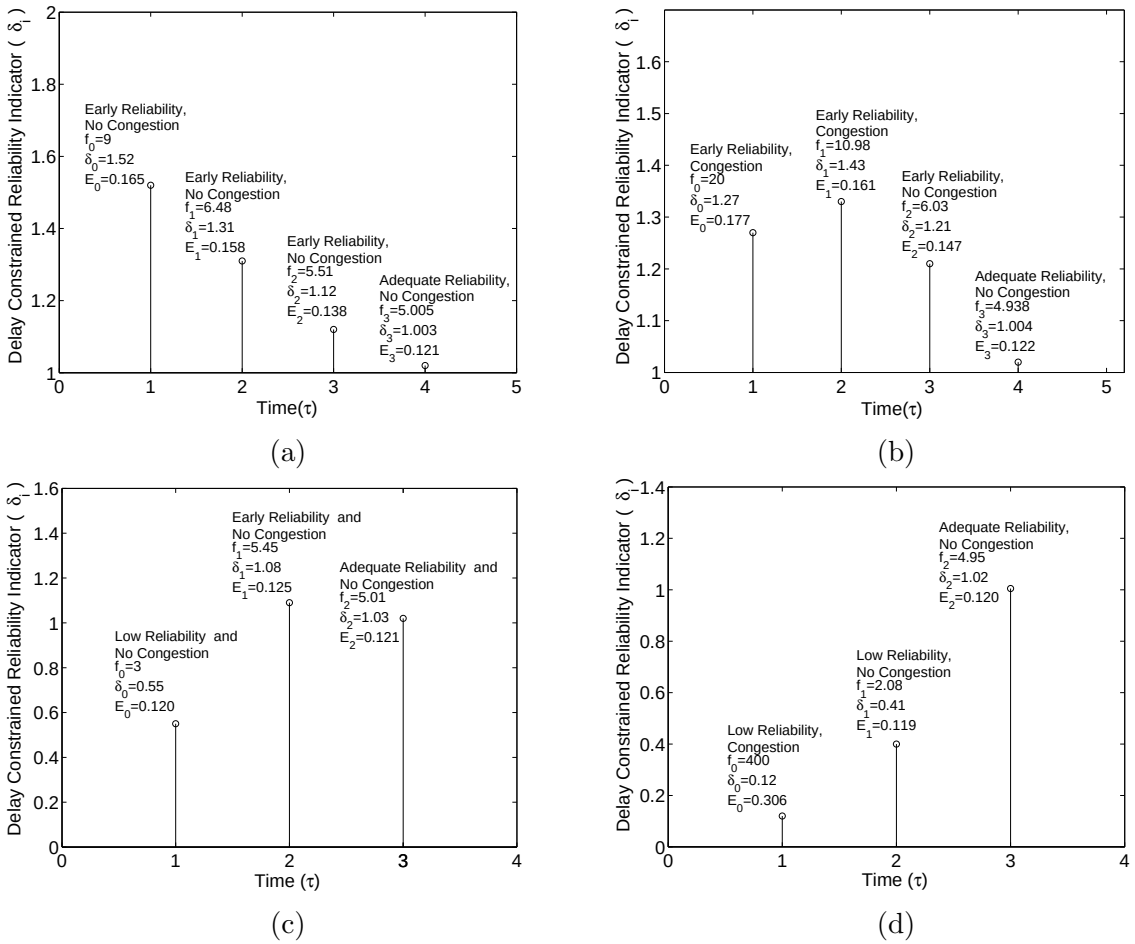

Figure 24: $(RT)^2$ trace for (a) early reliability and no congestion, (b) early reliability and congestion, (c) low reliability and no congestion, (d) low reliability and congestion.

the possible packet losses and extensive message exchange due to the associated actor node movement are avoided. Thus, the limited energy resources of the sensors are saved. Note that the other actor nodes, which can involve the action but do not receive data from sensors, may continue their mobility and the impacts of the actor mobility on network performance are investigated in Section 3.5.2 in detail. For sensor-actor communication case, the main performance metrics that we use to measure the performance of $(RT)^2$ protocol are the convergence time to (adequate reliability, no congestion) condition from any other initial network conditions and average energy consumption per packet (E_i) for each decision interval i.

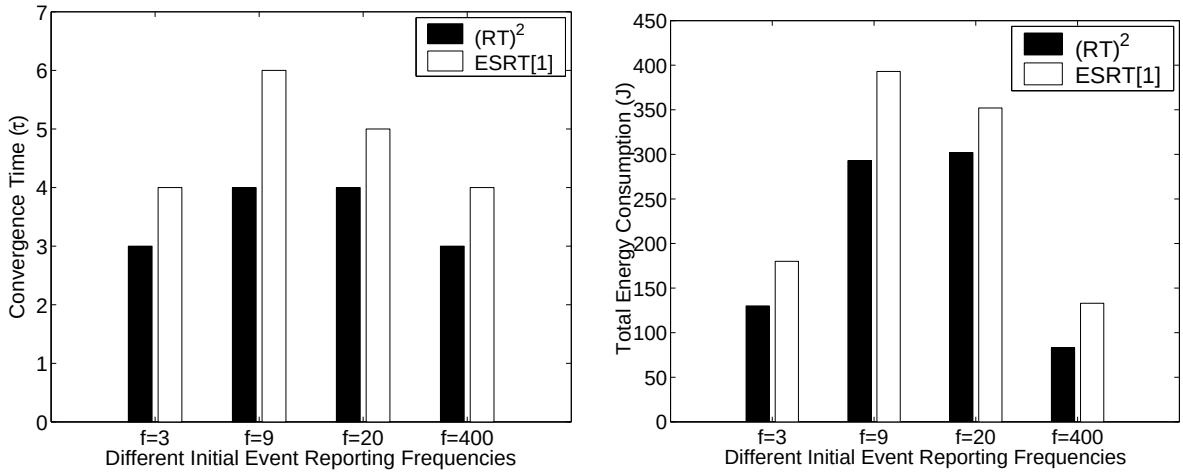

(a) (b)

Figure 25: The comparison of $(RT)^2$ and ESRT[15] for sensor-actor communication in terms of a) convergence times to (Adequate reliability, No congestion) condition, and b) total energy consumption.

The $(RT)^2$ protocol convergence results are shown in Figure 24 for different initial network conditions. As observed in Figure 24, $(RT)^2$ protocol converges to (Adequate reliability, No congestion) condition starting from any of the other initial network conditions discussed in Section 3.3. Thus, $(RT)^2$ is self-configuring and can perform efficiently under random, dynamic topology frequently encountered in WSAN applications. Moreover, the average energy consumed per packet during sensor-actor communication, i.e., (E_i), is also observed. As shown in Figure 24, E_i decreases as the (no congestion, adequate reliability) state is approached which shows that energy consumption of the sensor nodes is also decreased while providing reliability constraints and delay bounds. Due to energy limitations of sensors, this result is also important for the proper operation of WSAN. Performance of reporting frequency update policies for sensor-actor communication are given as the trace values and states listed within Figure 24.

To further investigate $(RT)^2$ protocol convergence results, we have compared $(RT)^2$ protocol and ESRT [15] protocol in terms of convergence time to (Adequate reliability,

No congestion) condition and total energy consumption. The reason for comparison with ESRT is that both of them is based on event transport reliability notion unlike the other transport layer protocols addressing conventional end-to-end reliability in WSNs. As shown in Figure 25, the convergence time and total energy consumption of the $(RT)^2$ protocol are much smaller than those of ESRT for different initial network conditions. This is because ESRT does not consider application-specific delay bounds while avoiding network congestion and adjusting reporting rate of sensor nodes.

To elaborate the relationship between the event-to-action delay notion and the $(RT)^2$ protocol operation, in Figure 26, we have also observed the delay distributions of the event packets received at the sink, when there is a transition from (Low reliability, Congestion) condition to (Adequate reliability, No congestion) condition. As seen in Figure 26, when the (Adequate reliability, No congestion) condition is approached, the delay of the event data packets also decreases. This is because the $(RT)^2$ protocol takes event-to-action delay bounds into account, while adjusting reporting rate of sensor nodes and avoiding network congestion.

3.5.2 Actor-Actor Communication

In this section, we present the performance results of the $(RT)^2$ protocol during actor-actor communication. For the simulations, we set up an evaluation environment using ns-2 [8]. The simulations for this scenario are performed for a 200m x 200m field with 10 actor nodes, distributed randomly over the field. In addition, to take into account the mobility of the actors during actor-actor communication, we have used the random way-point model. In this mobility model, we consider maximum speeds of $1m/s$, $5m/s$, $10m/s$, $15m/s$ and $20m/s$ for mobile actor nodes. The packets are 1000 bytes. Other simulation parameters are the same as those listed in 2 in Section 3.2.3.

For actor-actor communication scenario, the performance of the $(RT)^2$ protocol is

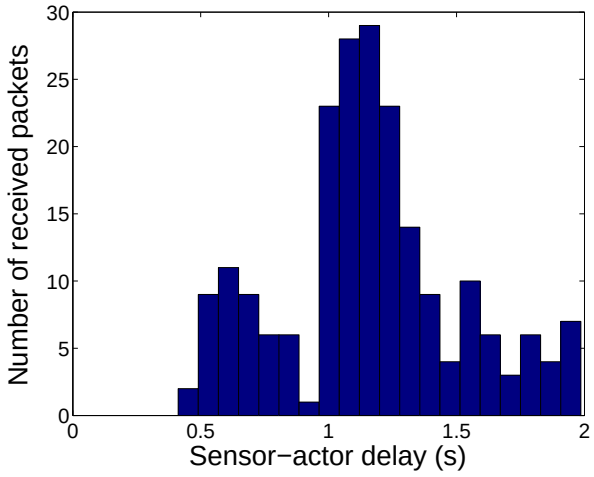

(a)

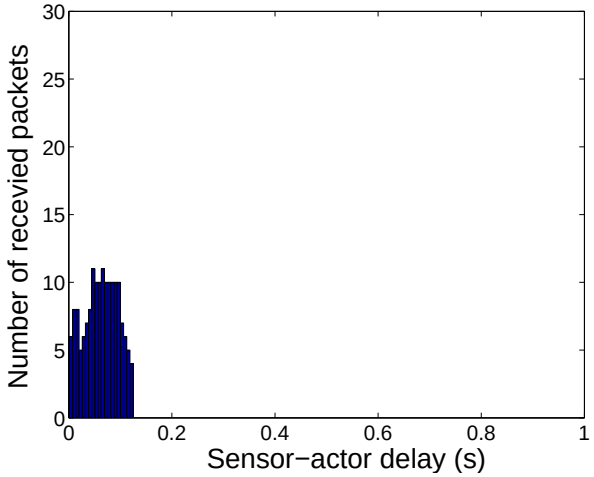

(b)

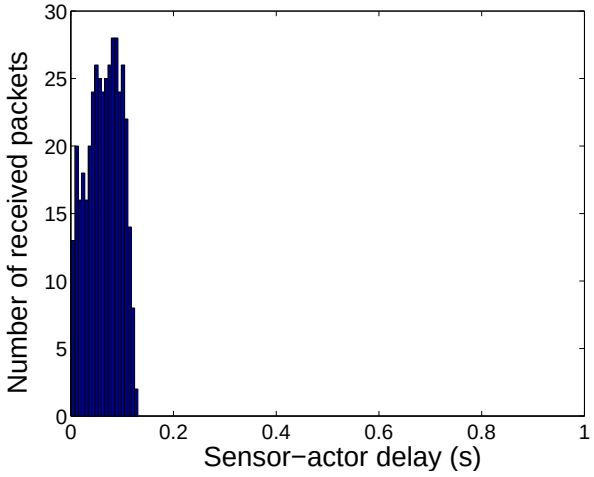

(c)

Figure 26: Packet delay distribution in (a) (Low reliability, Congestion), (b) (Low reliability, No congestion), (c) (Adequate reliability, No congestion), conditions.

evaluated and compared against TCP-NewReno, TCP-ELFN [32] and ATP [55]. The main performance metrics that we employ to measure the performance of the $(RT)^2$ protocol are aggregate throughput, and average packet delay. Here, the aggregate throughput reflects the number of packets successfully received at the destination. By average packet delay, we refer to average latency of data packets during actor-actor communication. All the simulations last for 1000 s. We run 10 experiments for each simulation configuration and each data point on the graphs is averaged over 10 simulation runs.

3.5.2.1 Aggregate Throughput

In Figure 27, we present the aggregate throughput results of the $(RT)^2$ protocol and other ad hoc transport protocols, i.e., TCP-NewReno, TCP-ELFN [32] and ATP [55]. Here, different number of flow connections are used and source-destination pairs are randomly chosen from 10 actor nodes. In terms of aggregate throughput, the $(RT)^2$ protocol outperforms other transport protocols under comparison, since $(RT)^2$ dynamically shapes data traffic according to the channel condition and intermediate node feedbacks. In addition, proper reaction of $(RT)^2$ to congestion and non-congestion related losses, such as route failures, avoids any performance degradation during actor-actor communication. For example, for 5 flow connection and $10m/s$ speed, we obtain that the aggregate throughput achieved by $(RT)^2$ during actor-actor communication is around 40%, 30% and 15% higher than that of TCP-NewReno, TCP-ELFN and ATP, respectively. Note also that rate-based transport protocols, i.e., $(RT)^2$ and ATP, outperform window-based transport protocols, i.e., TCP-ELFN and TCP-NewReno, mainly because rate-based schemes capture the available bandwidth more quickly compared to window-based schemes.

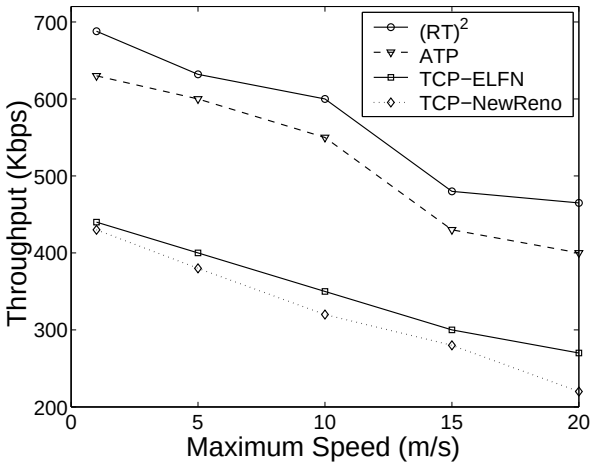

(a)

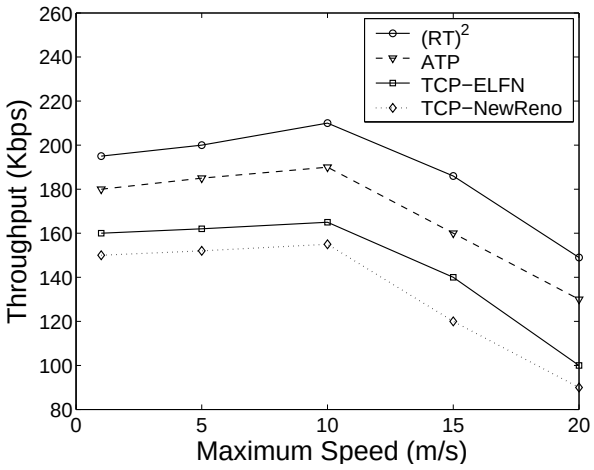

(b)

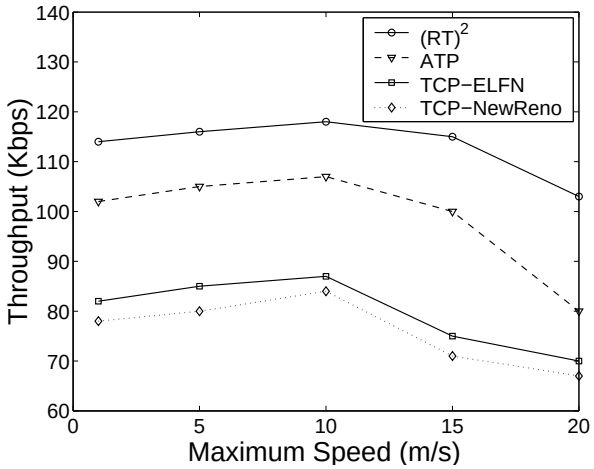

(c)

Figure 27: Aggregate throughput for (a) 1 flow connection, (b) 5 flow connection, (c) 10 flow connection, when the maximum speed of the actors are varying.

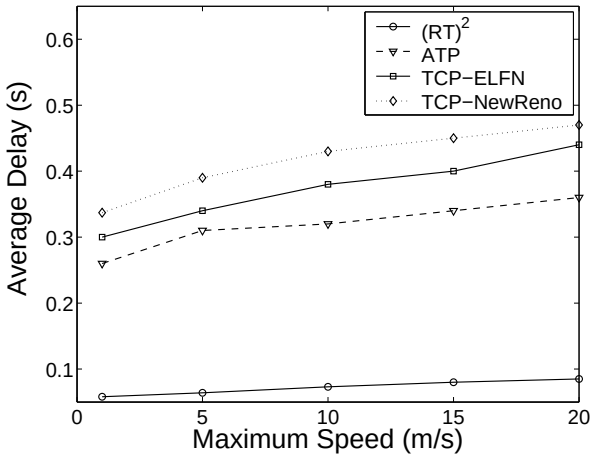

(a)

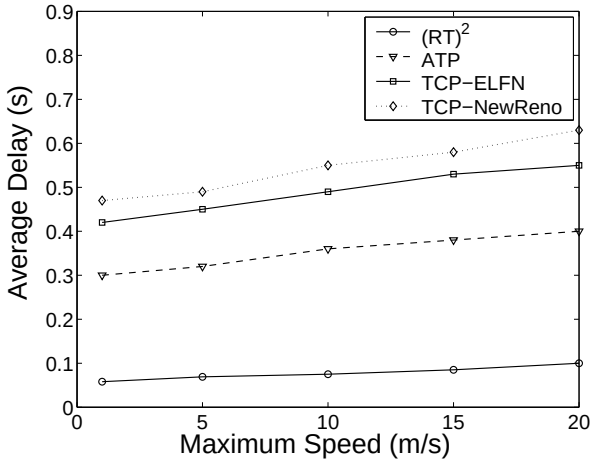

(b)

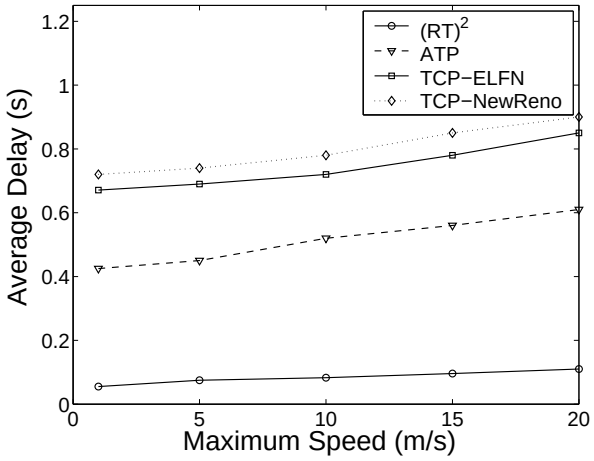

(c)

Figure 28: Average packet delay for (a) 1 flow connection, (b) 5 flow connection, (c) 10 flow connection, when the maximum speed of the actors are varying.

3.5.2.2 Average Delay

In Figure 28, we also show the average packet delay results of the $(RT)^2$ and the other transport protocols. As shown in Figure 28, for all simulation configurations, the average packet delay values of $(RT)^2$ are much lower than those of other protocols, since $(RT)^2$ captures the available bandwidth in the network quickly and does not allow a burst of packet transmissions with explicit congestion notification and rate feedback based mechanisms. For example, for 10 flow connection and $15m/s$ speed, the average packet delays achieved by $(RT)^2$ are approximately eight, seven and five times lower than that of TCP-NewReno, TCP-ELFN and ATP, respectively. This is so crucial because of timely event detection and action performance objectives of the WSANs.

Note that, in these experiments, we do not assume that the underlying layer protocols, i.e., network, MAC, and physical layer protocols, provide any additional support for meeting application-specific real-time delay requirements. Intuitively, we anticipate that the performance of $(RT)^2$ protocol further improves, when deployed on top of lower layer communication protocols, which also provide real-time support. The evaluation of such scenario is left as a future study mainly due to lack of space.

CHAPTER IV

RESOURCE-AWARE AND LINK-QUALITY-BASED ROUTING IN WIRELESS SENSOR AND ACTOR NETWORKS

In this chapter, a resource-aware and link-quality-based (RLQ) routing protocol is described for wireless sensor and actor networks (WSANs). The RLQ protocol is a new routing layer solution that adapts to varying wireless channel conditions while exploiting the heterogeneous capabilities in WSANs. In addition, it balances the energy expenditure and network load across available paths, accounting for energy drain of individual nodes. The RLQ protocol was first presented in [28]. In Section 5.1, a comprehensive review of the related work on link-quality estimation in WSANs is described. In Section 4.2, the target application is introduced while a case study is presented in Section 4.3 to gain more insight regarding the network characteristics and communication challenges in WSANs. The RLQ protocol overview along with the detailed operations of the protocol algorithms is explained in Section 4.4. The performance evaluation of the RLQ protocol and the test-bed experiments are presented in Section 4.5.

4.1 Motivation and Related Work

Recent experimental studies [37], [65], [52] and [66] have shown that in real sensor network deployments, wireless link quality varies over space and time, deviating to a large extent from the idealized unit disc graph models used in network simulation tools. Based on these empirical studies and measurements, it is also found that the coverage area of sensor radios is neither circular nor convex, and packet losses due to

fading and obstacles are common at a wide range of distances and keep varying over time. These studies provide valuable and solid foundations for several sensor network protocols [19], [30], [36], [50], [62], and have guided design decisions and tradeoffs for a wide range of sensor network applications [18], [17], [49], [23], and [60].

Although these early studies made many important observations for the problems of reliable data transmission in wireless sensor networks, the challenges of integrating battery-powered sensors with resource-rich actor nodes are yet to be efficiently studied and addressed. First of all, all these experimental studies do not take node heterogeneity into account when making routing decisions; they assume that all nodes are identical in capabilities. This assumption clearly leads to waste of valuable network resources in heterogenous sensor networks, especially in WSANs.

Second, since all these studies were conducted, the design space of sensor platforms and their radio hardware have advanced significantly. Recently, many sensor platforms, including Tmote Sky [7] and MicaZ [3], have gravitated towards an international sensor network standard (IEEE 802.15.4 [12]) and even a single radio chip (CC2420), which provides an additional radio hardware link quality indicator (LQI) to several network services [1]. This newer technology differs significantly from earlier radios and thus, these recent 802.15.4 based sensor platforms may behave differently compared to earlier sensor platforms [44], [53]. Consequently, all these new advances in sensor radio hardware as well as link quality variations and node heterogeneities in WSANs call for new empirical measurements on recent sensor platforms and the design of resource-aware protocols for WSANs.

In this chapter, a resource-aware and link quality based (RLQ) routing protocol is presented for WSANs. The primary objective of the RLQ routing protocol is to adapt to varying wireless channel conditions while exploiting the heterogeneous capabilities in WSANs. To accomplish this objective, the RLQ routing protocol biases the use of resource-rich actor nodes over energy-constrained sensor nodes for packet forwarding

and processing in the network. Specifically, the proposed link-cost metric captures the expected energy cost to transmit, receive, and re-transmit a packet while considering the residual energy levels of the sensor nodes. Also, unlike most of the existing simulation-based studies, this research effort is guided by extensive field experiments of link-quality dynamics at various locations over a long period of time using recent sensor network platforms.

4.2 Target Application

In this study, we focus on indoor wireless sensor/actor network applications, such as *advanced building automation systems*. In such an integrated system, several sensor nodes monitor the ambient conditions of the indoor environment to determine when to start or stop heaters and chillers, modulate air dampers, activate pumps for freeze protection. After the sensors detect an event occurring in an indoor building environment, the event data is distributively processed and transmitted to the terminal equipment controllers, which gather, process, and eventually reconstruct the event data and communicate with actors to initiate the actions upon the environment. Due to ever increasing installation and maintenance costs, energy efficient and reliable configuration of such systems significantly reduces the operational expenses. Although these systems bring significant advantages over traditional sensing and facilitate fine-grained monitoring and control of indoor environments within a limited budget, in a case study made by Siemens Building Technologies [35], it is observed that wireless link quality varies over space and time and it has a significant impact on network performance, including network throughput, network lifetime and resource utilization. Therefore, the design of reliable and energy efficient communication protocols is of great importance to provide several economic and operational benefits. This motivated us to design of resource-aware and link quality based routing metrics for WSAN. Note also that although our research effort is motivated by the challenges

of building automation applications, the wireless link quality variations and energy limitations are common in several WSAN applications [16] and thus other real-world applications can benefit from our experimental observations and findings.

4.3 Link-Quality Measurements in WSANs

In WSANs, rapid variations in the wireless channel preclude an efficient mechanism for knowing instantaneous link-quality at the time of transmission, thus making it difficult to estimate the instantaneous value of the cost metric. Moreover, in bandwidth-limited and battery-operated sensor networks, there is a trade-off between keeping the communication overhead and energy expense at a minimum (which calls for wireless channel measurements with long periods) and obtaining a reliable estimate of link quality (which requires frequent channel measurements). Striking a good balance in this trade-off requires a good understanding of the behavior of wireless channel quality during the operation of the network. This motivates us to explore whether it is possible to obtain a good estimate of the true link-cost metric based on only a few hardware measurements.

In this study, we first focused on how to characterize and measure link-quality in WSANs. We conducted experiments with TMote Sky sensor nodes to obtain insights to answer this question [28]. TMote Sky nodes use the CC2420 radio component, and support the IEEE 802.15.4, an emerging wireless sensor network standard [12]. Based on our link-quality measurements and observations, we also implemented a resource-aware and link-quality-based (RLQ) routing algorithm in TinyOS. In our experiments, to measure the link-quality during the operation of the network, two useful link-quality metrics were implemented: (i) link-quality indicator (LQI) and (ii) received signal strength indicator (RSSI). More specifically, RSSI is the estimate of the signal power and is calculated over eight symbol periods, while LQI can be viewed as a chip-error rate and is calculated over eight bits following the start frame delimiter

(SFD). LQI values are usually between 110 and 50 and correspond to maximum and minimum quality frames, respectively.

In link-quality measurements, we used a pair of TMote Sky nodes in an indoor environment, one as the sender and the other as the receiver. We varied the distance from the receiver to the sender from 1 m to 30 m, in steps of 1 m. At each distance, the transmitter sends 100 data packets at a rate of two packets per second. To avoid any potential interference and network congestion, we deliberately chose a low data rate so that the effect of unreliable links could be isolated from the effects of network congestion.

In Figure 29, we present our preliminary experiment results to elaborate on the relationship between packet-reception rate and link-quality metrics. Here, packet-reception rate (PRR) represents the ratio of the number of successful packets to the total number of packets transmitted over a certain number of transmissions.

In Figure 29 (a), we observe a strong correlation between the average LQI values and packet-reception rates at the receiver. Statistical analysis shows that the Pearson correlation coefficient is around 0.80 between these two variables. Note that there are still some inconsistencies observed, especially when the received signal is weak. These inconsistencies explain why the Pearson's coefficient is not 1.0. Nevertheless, the observed correlation is still quite interesting, since LQI is calculated only from those packets that are received, whereas the packet reception probability takes into account those packets that are dropped. This correlation implies that average LQI is a good measurable indicator of the packet reception probability. In Figure 29 (a), we also fitted a curve to the average LQI vs. PRR and observed that although the curve fits the data quite well, there are still a few outliers, which can be caused by environmental changes and interference from 802.11 networks in the deployment field.

In Figure 29 (b), we observe that there is a much smaller correlation between RSSI and the packet reception probability. The Pearson correlation coefficient is only

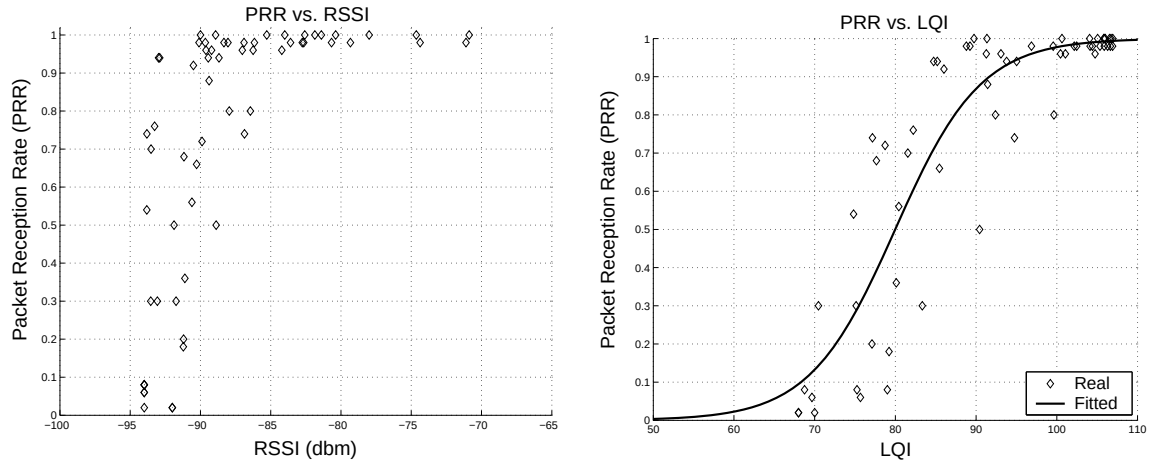

(a) (b)

Figure 29: (a) Packet-reception rate vs. LQI, and (b) Packet-reception rate vs. RSSI.

0.55 between the packet reception probability and the RSSI value. Furthermore, it is found that when the signal is weak (especially when it is around the sensitivity threshold (-94 *dbm*)), even though there is a considerable variation in the packet loss rate, RSSI does not provide any correlated behavior with PRR. On the other hand, when the signal is higher than the sensitivity threshold, RSSI is a promising link-quality estimator, since it shows small variance compared to LQI measurements. Therefore, to minimize the estimation error and link-measurement costs, one can use LQI measurements as a link-quality metric as long as its variances are factored out.

4.4 Resource-Aware and Link-Quality-Based Routing in WSANs

In WSANs, the wireless link quality between pairs of nodes varies during the lifetime of a network based on distance, transmit power, radio interference, and environmental factors (such as obstructions and people in the sensor network field attenuating radio signals)[65]. Even if the locations of nodes in the network are fixed and each node is configured with an identical transmit power, node inter-connectivity changes during the lifetime of the network. Moreover, the energy limitations of the sensors exacerbate

the challenge of reliable wireless communication in WSANs.

To alleviate these drawbacks, the RLQ routing protocol uses a link-cost metric, which is based on both energy efficiency and link-quality statistics [28]. In this way, our objective is to adapt to varying wireless channel conditions while exploiting the heterogeneous capabilities in the network. Specifically, the proposed link-cost metric captures the expected energy cost to transmit, receive, and retransmit a packet while considering the residual energy levels of the sensor nodes. Moreover, for nodes that have high energy resources, e.g., actors[1], the transmission and reception of packets have negligible energy cost, which is also reflected in the link-cost metric.

To calculate link cost, let us assume each node uses the CSMA/CA MAC protocol with DATA/ACK exchange, which is supported by IEEE 802.15.4. Then, the energy cost (C_{link}) for a reliable transmission of a data packet over a single hop can be typically calculated as follows:

$$C_{link} \;=\; \eta_{tx}\;\alpha_{tx} \;+\; \eta_{rx}\;\alpha_{rx} \tag{9}$$

, where η_{tx} and η_{rx} represent the normalized energy cost for the transmitter and receiver, respectively. The variables α_{tx} and α_{rx} are 1, if the transmitter or receiver is energy constrained, i.e., battery powered, and 0 otherwise. In addition, normalized energy costs η_{tx} and η_{rx} are calculated as follows:

$$\eta_{tx} \;=\; [(C_{tx-data} \;+\; C_{rx-ack})\;E_{link}]^x \;\left[1 \;+\; (1 \;-\; \frac{E_{tx-res}}{E_{tx-init}})\right]^y \tag{10}$$

$$\eta_{rx} \;=\; [(C_{rx-data} \;+\; C_{tx-ack})\;E_{link}]^x \;\left[1 \;+\; (1 \;-\; \frac{E_{rx-res}}{E_{rx-init}})\right]^y \tag{11}$$

[1]Note that the actors in WSANs have long battery life compared to sensor nodes, since the order of magnitude of the energy required for actions is much higher than that required for sensing and communication.

, where C_{tx} and C_{rx} represent the energy consumption during transmission and reception, respectively. Also, $E_{tx-init}$ and $E_{rx-init}$ are the initial and remaining energy of the transmitter, and $E_{rx-init}$ and E_{rx-res} are the initial and remaining energy of the receiver, respectively. Here, E_{link} represents the expected number of transmissions, which is calculated as follows:

$$\sum_{i=0}^{K} i\ (1\ -\ PRR)^i\ PRR \tag{12}$$

, where PRR represents the packet-reception rate and K is the maximum number of retransmissions before the packet is ignored. To calculate P_s of a link in terms of packet-reception rate, RLQ routing protocol utilizes the link-quality indication (LQI) reported by the physical layer of IEEE 802.15.4 [12]. In this way, the nodes dynamically adapt to changing wireless network conditions and select the paths with high-quality links. In addition, with the use of normalized energy cost, when the sensors have plenty of residual energy, e.g., at the beginning of the network deployment, the energy consumption term in equations (10) and (11) is emphasized, while if the residual energy of a node becomes lower, then the residual energy term is more emphasized. In this way, we balance the energy expenditure and network load across available paths, thus accounting for the energy drain of individual nodes.

It is also important to note that in equations (10) and (11), the variables x and y are the weighting factors that can be adjusted to find the minimum energy path or the path with nodes having the most energy or a combination of the above. For example, if x=y=0, the shortest cost path is the minimum hop path and if $x = 1$ and $y = 0$, the shortest cost path is the minimum total energy consumption path. Thus, these weighting factors provide flexibility to the user based on the application-specific requirements. In the energy cost calculation of a link, if both the transmitter and receiver are not battery powered, equation (1) becomes equal to zero. To avoid a link-energy cost of zero, we also take the maximum of the calculated cost and a small

constant for these cases. Overall, with the use of the proposed cost metric, the RLQ routing protocol chooses paths that contain as few battery-powered data transmissions and receptions as possible and utilizes resource-rich nodes in the deployment field to maximize the network lifetime.

4.5 Performance Evaluation

To gain more insight into link-quality variations and energy limitations in WSANs, we first investigated the effects of link-quality indicator (LQI) on the overall network performance. In the first set of experiments, all the nodes in the network were battery-powered. Then, we evaluated the impact of energy heterogeneity in the network, where some nodes (actor nodes) were line powered and other nodes were battery powered.

Furthermore, we compared the performance of different routing metrics on a physical test-bed, including 21 TMote Sky nodes. The experiments were carried out in a large office floor with obstructions and the 802.11b networks to mimic the realistic operating network conditions. The parameters used in our performance measurements are listed in Table 4.

Table 4: Network parameters used in the experiments.

Area of sensor field	20x30 m^2
Number of nodes	21
Packet length	30 bytes
Buffer size	64 packets
Re-transmission threshold (K)	5
Traffic type	CBR
Transmission power	-25 dbm
Weighting factors (x, y)	(1,1)

To communicate the sensor data to the sink node, we employed the CSMA/CA MAC protocol with DATA/ACK exchange supported by the IEEE 802.15.4 standard.

In our experiments, we also considered energy heterogeneity in the network and non-ideal battery behaviors. In the evaluations, we investigated the following performance metrics:

- *Throughput* is the number of unique packets received at the sink node divided by the interval between the start and the end of the experiment.
- *Packet-reception rate* is the ratio between the total number of unique packets received at the sink node and the total number of packets generated by all the sensor nodes.
- *Network lifetime* is defined as the smallest time that it takes for at least one node in the network to drain its energy beyond the point where it can function normally.

In our experiments, each sensor node sent packets toward a sink node at a rate of one packet per second. To avoid any potential interference and network congestion, we deliberately chose a low data rate so that the effect of unreliable links could be isolated from the effects of network congestion. Multiple trials were used in all experiments and the duration of each experiment trial was at least 20 minutes. In the performance evaluations, we used the multi-hop LQI routing algorithm in TinyOS. Using the multi-hop LQI routing algorithm, we also implemented four different routing algorithms: (i) the shortest path routing algorithm, which we call $Shortest\_Path$; (ii) the multi-hop routing algorithm using instantaneous LQI measurements, which we call $LQI\_Instant$; (iii) the multi-hop routing algorithm using moving average of LQI measurements, which we call LQI_MovAvg; (iv) the multi-hop routing algorithm using the proposed RLQ metric, which we call RLQ.

In the $Shortest\_Path$ routing algorithm, each sensor node uses a hop-count metric as the link-cost metric and prefers a shorter path over very poor radio links rather than a longer path over high-quality links. Specifically, when link quality varies

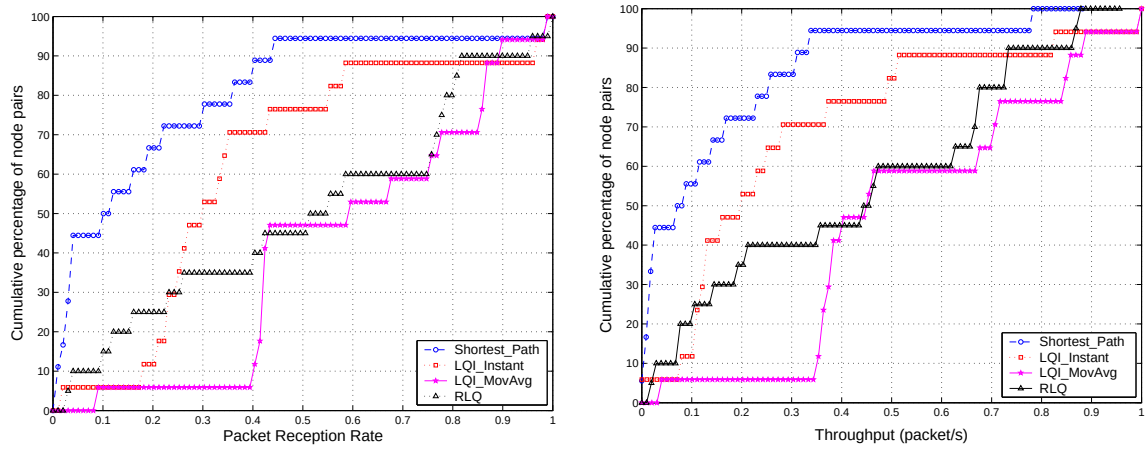

(a) (b)

Figure 30: Performance results: (a) CDF vs. PRR, (b) CDF vs. Throughput.

significantly, it leads to low network throughput, because it limits the bandwidth to be consumed by retransmissions. In the *LQI_Instant* and *LQI_MovAvg* routing algorithms, each sensor node maintains a recent history of the LQI measurements to its neighbors and uses the link-quality estimations to select the parent with the lowest cost path to the sink node.

The only difference between the *LQI_Instant* and *LQI_MovAvg* algorithms is that the *LQI_MovAvg* algorithm uses a moving average of LQI measurements with a window size of 50 to factor out the variances of the LQI measurements from the measured data. In the *RLQ* routing algorithm, the routing metric captures expected energy cost to transmit, receive, and retransmit a packet while considering the residual energy levels of the sensor nodes.

Figures 30 (a) and (b) show the cumulative distributive function (CDF) of the packet-reception rate and throughput performance of the routing metrics under comparison for the set of 20 paths, respectively.

As shown in Figures 30 (a) and (b), compared to the *LQI_MovAvg* algorithm, the *LQI_Instant* and *Shortest_Path* algorithms are noticeably worse, with median packet-reception rates of 30% and 10% and with median average network throughputs

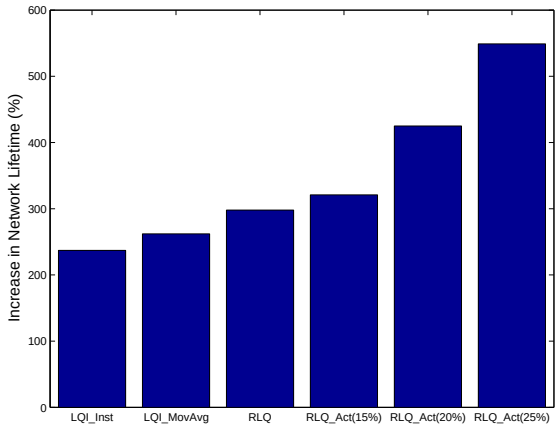

Figure 31: The effect of line powered actor nodes on network lifetime.

of 48*bps* and 26*bps*, respectively. It is also important to note that the network performance of the *RLQ* routing algorithm is slightly lower than that of LQI_MovAvg. This is due to the fact that when the residual energy of a node along the high-quality path becomes lower, the *RLQ* algorithm changes the path to improve the network lifetime. In this way, the *RLQ* algorithm aims to balance the energy expenditure and network load across the available paths, thus accounting for the energy drain of the individual nodes. Overall, these test-bed results show that the routing selection metric has a major impact on the overall network performance. The LQI_MovAvg and *RLQ* routing algorithms provide high network performance using a simple model mapping from average *LQI* measurements to the packet-reception rates.

In the second set of experiments, we also investigated the effect of routing metrics and energy heterogeneity on network lifetime. Figure 31 shows the normalized network lifetime performance of the different routing metrics under comparison. As shown in Figure 31, when there is no line-powered actor nodes in the network, the proposed *RLQ* metric achieves the best performance compared to the LQI_MovAvg and $LQI\_Instant$ routing metrics. For example, the average network lifetime increase achieved by the *RLQ* metric is 25% and 15% higher than that of the $LQI\_Instant$ and LQI_MovAvg algorithms, respectively. When the line-powered actor nodes are

included in the network ($RLQ\_Act(x\%)$ cases), it is observed that the network lifetime increases significantly. For example, when 20% of the nodes in the network are line-powered, we obtain that the average network lifetime increases 40% compared to the case when the RLQ metric is used. In our experiments, we have also observed that the selection of the position of the line-powered actor nodes affects the overall network performance. Therefore, in addition to the resource-aware and link-quality-based routing metrics, optimal deployment strategies should be developed to fully utilize the potential of the network heterogeneity.

CHAPTER V

WIRELESS SENSOR AND ACTOR NETWORK APPLICATIONS AND EXPERIMENTS FOR ELECTRIC UTILITY AUTOMATION

In this chapter, a statistical characterization of the wireless channel in different electric utility environments is presented. Field tests have been performed on 802.15.4 compliant wireless sensor/actor networks in both a 500 kV substation as well as an underground network transformer vault to measure background noise, channel characteristics, and attenuation in the 2.4 GHz frequency band. This study was first presented in [26]. In Section 5.1, a review of the related work on electric utility monitoring systems is described. In Section 5.2, the electric utility automation applications are introduced along with its challenges. The channel measurements and the test-bed experiments are presented in Section 4.5.

5.1 Motivation and Related Work

In today's competitive electric utility marketplace, electric utilities face growing demands to produce reliable power, comply with environmental regulations and meet corporate financial objectives. Given the increasing age of many electrical systems and the dynamic electric utility market, intelligent and low cost monitoring and control systems are required in order to improve the productivity and efficiency of such systems [21], [24] and [27]. Traditionally, electric utility monitoring systems are realized through wired communications. However, the wired monitoring systems require expensive communication cables to be installed and regularly maintained and thus they are not widely implemented in power plants because of their high cost [11],[13].

Therefore, there is an urgent need for cost-effective wireless power utility monitoring systems that enable significant savings and reduce air pollutant emissions by optimizing the management of coal-based power generation systems.

With the recent advances in wireless sensor and actor networks (WSANs), the realization of low-cost embedded electric utility monitoring systems have become feasible [18]. In these monitoring systems, wireless tiny sensor nodes are installed on electric utility equipment and monitor the parameters critical to each equipment's efficiency based on a combination of measurements such as vibration, temperature, pressure and power quality. This data is then transmitted to an actor node that analyzes the data from each sensor. Any potential problems are notified to plant personnel as an advanced warning system. This enables plant personnel to repair or replace equipments, before their efficiency drops or they fail entirely. In this way, catastrophic equipment failures and the associated repair and replacement costs can be prevented, while complying with strict environmental regulations.

Accurate wireless channel models are extremely important for the design of WSAN-based utility communication architectures. These channel models provide utility network designers with the ability to predict the performance of the communication system for specific propagation environment, channel modulation, and frequency band. Although there exists radio propagation measurements in urban areas, office buildings, and factories [42], [46], [45] [51], and [67], the propagation characteristics in utility systems are yet to be efficiently studied and addressed. In this study, a statistical characterization of the wireless channel in different electric utility environments is presented. Field tests have been performed on 802.15.4 compliant wireless sensor/actor networks in both a 500 kV substation as well as an underground network transformer vault to measure background noise, channel characteristics, and attenuation in the 2.4 GHz frequency band. Various communication links, including both line-of-sight (LOS) and non-LOS (NLOS) scenarios, are also considered. In addition,

the use of external antennas in WSANs is investigated to improve the communication range in the network. In this context, extensive measurements are made to quantify the use of external antennas in indoor, outdoor and underground utility environments.

5.2 WSAN Applications for Electric Utility Automation

Wireless sensor and actor networks can enhance the performance of the electric utility operations by enabling wireless automatic meter reading and reliable monitoring systems for electric utilities. In the following, the WSAN applications for electric system automation are described in detail.

5.2.1 Reliable Electric System Monitoring

Due to several reasons such as equipment failures, lightning strikes, accidents and natural catastrophes, power disturbances and outages in electric systems occur and often result in long service interruptions [27], [63]. Thus, the electric systems should be properly controlled and monitored in order to take the necessary precautions accurately and timely. In this respect, Wireless Sensor and Actor Networks (WSANs) can provide cost effective real-time and reliable monitoring system for the electric utilities. Efficient monitoring system constructed by smart sensor nodes can reduce the time for detection of the faults and resumption of electric supply service in distribution networks.

In addition, electricity regulators monitor the performance of the electricity distribution network operators utilizing a range of indices relating to customer service. Distribution network operators have targets and incur penalties related to the length of time of service interruptions, i.e., both outage frequency and duration [9] and [47]. Continuity of electricity service is also crucial in today's competitive electric utility marketplace from the perspective of customer satisfaction.

In order to evaluate the performance of the electric system, several Quality of Service (QoS) indices can be obtained utilizing WSANs for real-time and reliable

monitoring system. For example, average duration of service interruption and average repairing time can be computed [27]. Typically, for densely deployed urban areas, these performance indices are correlated with the time for remote or manual switching of supply circuits. In this context, smart sensor nodes deployed in the electric utility can provide rapid identification of service interruptions and timely restoration of the electric utility services and thus, WSANs can help electric utilities to maintain regulatory targets for the performance indices.

5.2.2 Wireless Automatic Meter Reading

Currently, traditional manual electricity meter reading is the most common method for the electric utility measurement systems. These systems require visual inspection of the electric utility meters and do not allow flexible management systems for the electric utilities. In addition, network connections between traditional meters and data collection points are basically non-existent; thus, it is impossible to implement a remotely controlled flexible management system based on energy consumption statistics by using traditional measurement systems.

With the recent advances in Micro Electro-Mechanical Systems (MEMS) technology, wireless communications and digital electronics; the development of low cost smart sensor networks, that enables wireless automatic meter reading (WAMR) systems for electric utilities, has become feasible. As the deregulation and competition in electric utility marketplace increase, so does the importance of WAMR systems. Wireless collection of electric utility meter data is a very cost-efficient way of gathering energy consumption data to the billing system and it adds value in terms of new services such as remote deactivation of a customer's service, real-time price signals and control of customers' applications. The present demand for more data in order to make cost-effective decisions and to provide improved customer service has played a major role in the move towards WAMR systems.

WAMR systems offer several advantages to electric utilities including reduced electric utility operational costs by eliminating the need for human readers and real-time pricing models based on real-time energy consumption of the customers. Real-time pricing capability of WAMR systems can also be beneficial for the customers. For example, using the real-time pricing model, the electric utility can reward the customers shifting their demand to "off-peak" times. Therefore, electric utility can work with customers to shift loads and manage prices efficiently by utilizing WAMR systems instead of once a month on-site traditional meter reading.

Real-time pricing model of the electric utilities requires real-time and reliable two-way communication between electric utility and the customer's metering equipment. WSN technology addresses this requirement efficiently by providing low cost and low power wireless communication.

Wireless Sensor and Actor Networks (WSANs) with wireless automatic meter reading capability provide several functionalities for electric system automation applications. Some of these functionalities are described below:

- *Automatic meter reading functionalities:* WSANs enable real-time automatic measurement of energy consumption of the customers. The automatic meter measurements can also be classified as individual meter measurements, cluster meter measurements and global meter measurements. Here, the objective is to provide flexible management policies with different real-time monitoring choices for electric utilities.

- *Telemetry functionalities:* The electric utility control centers can obtain real-time data from smart sensor nodes and control some elements located at selected points of the distribution network, e.g. control of the status of the switches [41]. Thus, distributed sensing and automation enhance electric utility services by reducing failure and restoration times.

- *Dynamic configuration functionality:* In electric system automation applications, reliability of the measurements should be ensured even in case of route failures in the network [54]. Thus, it is extremely significant to dynamically adjust the configuration of the network, e.g., dynamic routing, in order to provide reliability requirements of the applications. In this respect, self-configuration capability of WSANs enables dynamic reconfiguration of the network.

- *Status monitoring functionality:* Monitoring the status of the metering devices is another functionality of WAMR systems which are embedded by smart sensors. This functionality can be very helpful to determine sensor node failures in the network accurately and timely. In addition, status monitoring functionality can be utilized in case of vandalization of the metering devices. For example, if someone tries to vandalize a metering device, the system can notify the police automatically [27]. This reduces the considerable costs of sending service crews out to repair vandalized metering devices.

As advances in WAMR technologies continue, these systems will become less expensive and more reliable. Most utility and billing companies have recognized that with the invention of low-cost, low-power radio sensors, wireless RF communication is by far the most cost-efficient way to collect utility meter data.

5.3 Experimental Setup and Channel Measurements

In this study, we conducted experiments with 802.15.4 compliant TMote Sky sensor nodes to characterize radio propagation in electric utility environments. These nodes have Chipcon CC2420 radio chips that are compliant with the 802.15.4 standard [12]. Specifically, Tmote-Sky motes operate in the 2.4 GHz ISM band with an effective data rate of 250 kbps, which is a much higher data rate than older radios. The higher data rate allows shorter active periods further reducing energy consumption. Tmote-Sky motes also integrate programming, computation, communication and sensing onto a

Table 5: Comparison of commercial off-the-shelf sensor platforms.

Features	TMote-Sky	MicaZ	Mica2
CPU type @[MHz]	16bit TI @ 8	8bit Atmel @8	8bit Atmel @8
Memory (SRAM [kB])	10	4	4
Radio Frequency	2.4 GhZ	2.4 GhZ	900 MHz
Bandwidth [Kbps]	250	250	40
Current Consumption Listening / Rx / Tx [mA]	1/20/18	8/20/18	8/10/17
Power Sleep [uA]	6	27	19

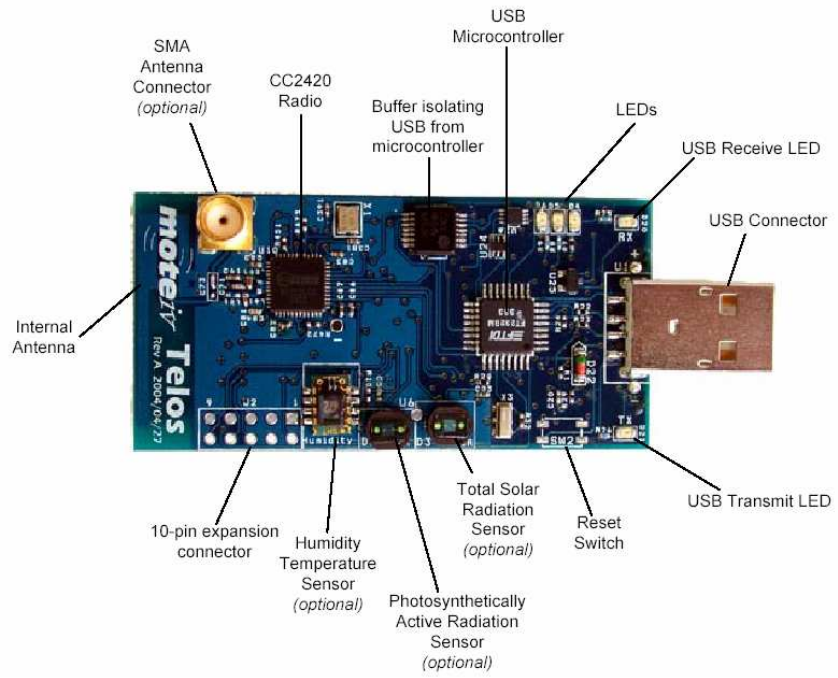

Figure 32: Tmote Sky sensor node used in the field tests.

single device [44]. The integrated design provides an easy to use sensor mote with increased robustness, which is crucial for electric system automation applications. In Figure 32, we present TMote sky module used in the field tests. To provide a better understanding of current sensor network technologies, we also compared various sensor platforms in Table 5.

Specifically, field tests have been performed to measure background noise, wireless channel characteristics, and attenuation in an indoor power control room, a 500

(a)

(b)

(c)

Figure 33: Experimental sites a) outdoor b) indoor, and c) underground utility environments.

kV substation and an underground network transformer vault. We also measured the impact of the interference from 802.11b networks and electronic devices on the performance of 802.15.4 networks. In addition, we investigated the use of external antennas in WSANs to improve the communication range in the network. In Figure 33, we present our experimental sites.

5.3.1 Wireless Channel Model

It is well-known that when an electromagnetic signal propagates, it may be diffracted, reflected and scattered. Reflection occurs when an electromagnetic signal encounters an object, such as a building, that is larger than the signal's wavelength. Diffraction occurs when the signal encounters an irregular surface, such as a stone with sharp edges. Scattering occurs when the medium through which the electromagnetic wave propagates contains a large number of objects smaller than the signal wavelength. All these effects have two important consequences on the signal strength. First, the signal strength decays exponentially with respect to distance. Second, for a given distance d, the signal strength is random and log-normally distributed about the mean distance dependent value. In addition, low antenna heights of the sensor nodes (10s of cms) and near ground communication channels exacerbate these effects.

In this research effort, we modelled the wireless channel using log-normal shadowing path loss model through a combination of analytical and empirical methods. This model is used for large and small coverage systems and moreover, experimental studies have shown that it provides more accurate multi-path channel models than Nakagami and Rayleigh models for indoor wireless environments with obstructions [67]. In this model, the signal to noise ratio $\gamma(d)$ at a distance d from the transmitter is given by:

$$\gamma(d)_{dB} = P_t - PL(d_0) - 10\eta log_{10}\Big(\frac{d}{d_0}\Big) - X_\sigma - P_n \tag{13}$$

Table 6: Mean power loss and shadowing deviation in electric utility environments.

Propagation Environment	**Path Loss** (n)	**Shadowing Deviation** (σ)
500 kv Substation (LOS)	2.42	3.12
500 kv Substation (NLOS)	3.51	2.95
Underground Transformer Vault (LOS)	1.45	2.45
Underground Transformer Vault (NLOS)	3.15	3.19
Main Power Room (LOS)	1.64	3.29
Main Power Room (NLOS)	2.38	2.25

where P_t is the transmit power in dBm, $PL(d_0)$ is the path loss at a reference distance d_0, η is the path loss exponent, X_σ is a zero mean Gaussian random variable with standard deviation σ, and P_n is the noise power in dBm.

In Table 6, we present the radio propagation parameters for different electric utility distribution environments. Note that in Table 6, the values of n and σ were calculated from the measured data in electric utility environments, using linear regression such that the difference between the measured and estimated path losses is minimized in a mean square error sense over a wide range of measurement locations and transmitter-receiver separations. These experiments were conducted over a period of several days for various locations and network configurations, including line-of-sight (LOS) and non-LOS (NLOS) scenarios.

5.3.2 Noise and Interference Measurements

In this section, we first investigate the impact of background noise on the overall performance of 802.15.4 sensor networks in different utility environments. Then, we study the effect of interference from 802.11b (Wi-Fi) networks and electronic appliances on 802.15.4 sensor networks.

To measure background noise, we wrote a TinyOS [2] application that samples RF energy at 62.5 Hz by reading the RSSI register of the CC2420 radio. The register

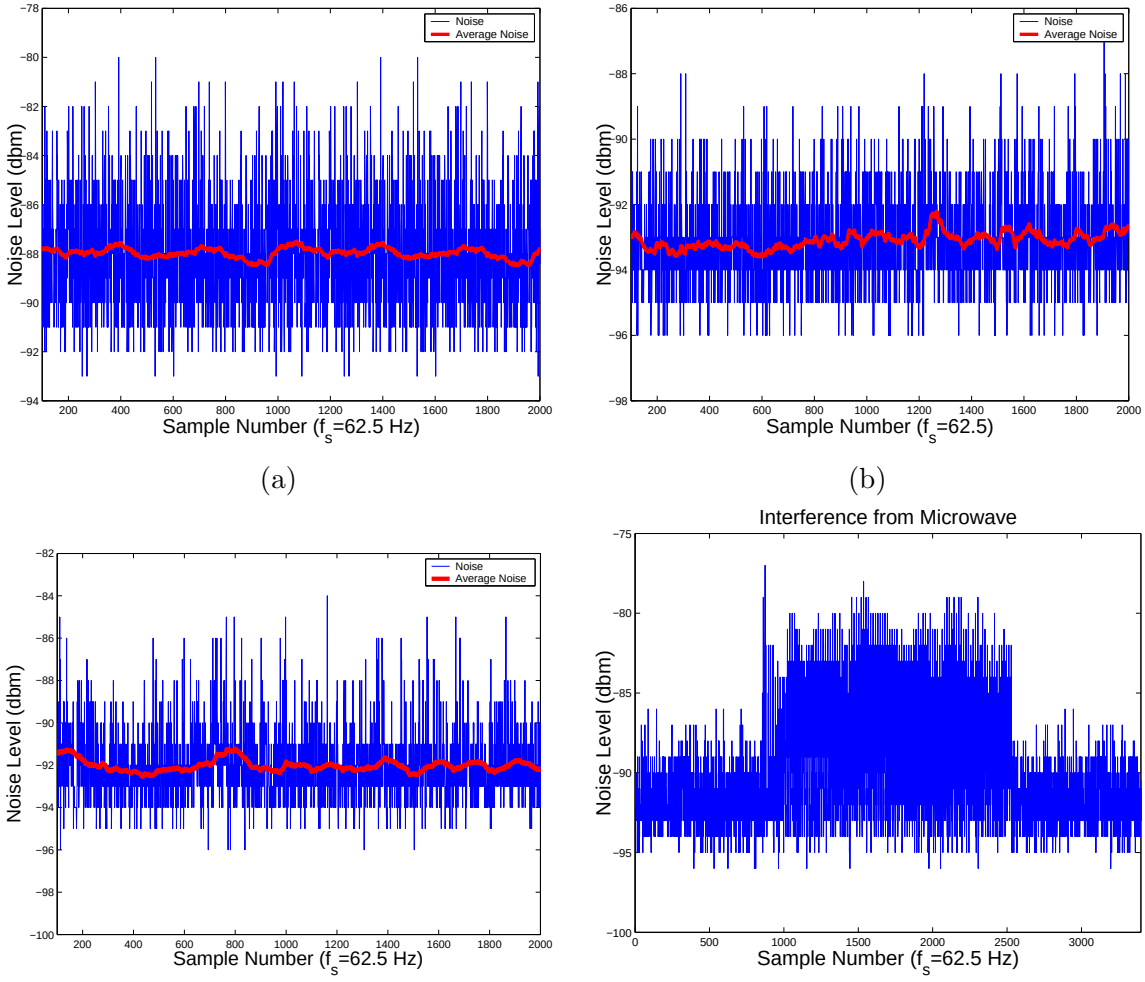

Figure 34: Background noise measurements in (a) an indoor power control room, (b) a 500 kV substation, (c) an underground transformer vault, and (d) an indoor room, when microwave is on.

contains the average RSSI over the past 8 symbol periods. We sampled noise on different radio channels in a wide range of environments, including indoor power control room, a 500 kV substation and an underground network transformer vault. Figure 34 presents our noise measurements and the effect of electric appliance (microwave) on 802.15.4 network. From the field measurements, the average noise level is found to be around -90 dbm, which is significantly higher than that of outdoor environments, i.e., -105 dbm background noise is found in outdoor environments. We also observe that background noise continuously change over time, which can be caused by temperature changes and interference levels. In Figure 34 (d), we also show that the effect of microwave interference on the noise floor measured by TMote Sky module. As shown in Figure 34, it is shown that the interference from an existing microwave leads to 15 dbm interference in the 2.4 GHz frequency band.

To decrease the effect of noise and interference problems in the 2.4 GHz frequency band, Tmote Sky nodes use direct sequence spread spectrum (DSSS) encoding scheme. To evaluate the DSSS's strength in real situations, we also measured the packet reception rate, when a pair of Tmote Sky motes are deployed close to an microwave operating in 2.4 GHz. The performance measurements show that the packet reception rate varies from 100% to 35%, when the microwave is turned on and off, respectively. This experimental observation reveals that DSSS addresses the crowded spectrum issue in some degree, but is still far from enough.

In addition to background noise measurements, we also conducted several experiments to quantify the impact of 802.11b interference on 802.15.4 networks. In Figure 35, we present the 802.15.4 and 802.11b spectrum usage. Here, it is important to note that some of the 802.15.4 frequencies overlap with 802.11b frequencies increasing the effects of external interference on link quality [33]. In our performance measurements, we observe that only channel 26 in 802.15.4 spectrum is not affected by 802.11b interference. Thus, to minimize 802.11b interference in electric utility

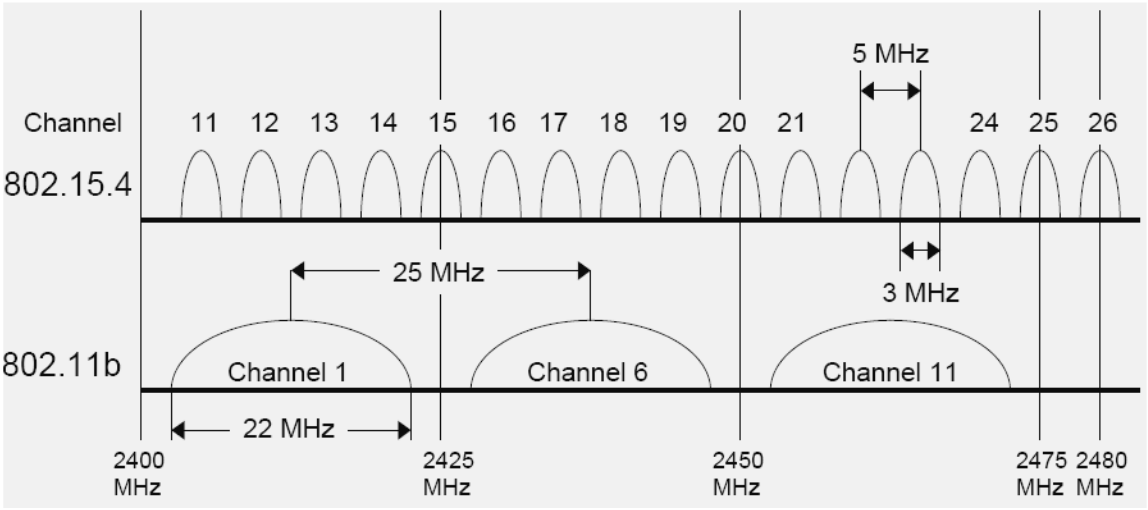

Figure 35: 802.15.4 and 802.11b spectrum usage.

automation applications, e.g., wireless automatic meter reading systems, the default 802.15.4 channel can be set to 26. However, it is important to note that multi-channel radios are often optimized for the center channel, so selecting by default a channel at one extreme may significantly lower the radio performance. Hence, the utilities need to conduct large-scale field tests to decide the optimal channel for 802.15.4 sensor networks.

5.3.3 Link Quality Measurements

In this section, we focused on how to characterize and measure link quality in sensor networks deployed in utility environments. We have conducted experiments with Tmote Sky nodes. In our experiments, to measure the radio link quality, two useful radio hardware link quality metrics were used: i) link quality indicator (LQI) and received signal strength indicator (RSSI). Specifically, RSSI is the estimate of the signal power and is calculated over 8 symbol periods, while LQI can be viewed as chip error rate and is calculated over 8 symbols following the start frame delimiter (SFD). LQI values are usually between 110 and 50 and correspond to maximum and minimum quality frames, respectively. The details of LQI metric can be found in the

IEEE 802.15.4 standard [12].

In our experiments, we use a pair of TMote Sky nodes in different utility environments, one as the sender and the other as the receiver. We vary the distance from the receiver to the sender from 1 m to 20 m, in steps of 1 m. The output power level of each sensor node and the packet size were set to be -25 dBm and 30 byte, respectively. At each distance, the transmitter sends 100 data packets with a rate of two packets per second. We deliberately chose a low rate to avoid any potential interference, so that the effect of unreliable links can be isolated from that of congestion.

In Figure 36, we also present our preliminary experiment results to elaborate the relationship between packet reception rate (PRR) and link quality metrics. Here, packet reception rate represents the ratio of the number of successful packets to the total number of packets transmitted over a certain number of transmissions. In Figure 36, it has been observed that a strong correlation exists between the average LQI measurements and packet reception probabilities. This observation is also consistent with the results in presented the previous chapter. Hence, to minimize the estimation error and link-measurement costs, one can use LQI measurements as a link-quality metric as long as its variances are factored out.

5.3.4 Integration of External Antennas into Sensor Motes

In our experiments, we observed that the integration of the external antennas into sensor modules greatly improve the communication range, leading to single-hop communication between the sensor module and the sink node (base station). It is worth noting that this may simplify the network architecture and protocol design and implementation in some sensor network scenarios. The use of external antennas can also increase the number of nodes, which are one hop away from the sink node. Since the one-hop nodes from the sink node are burdened with relaying data from other nodes further away, these one-hop nodes in the network are typically the bottleneck in terms

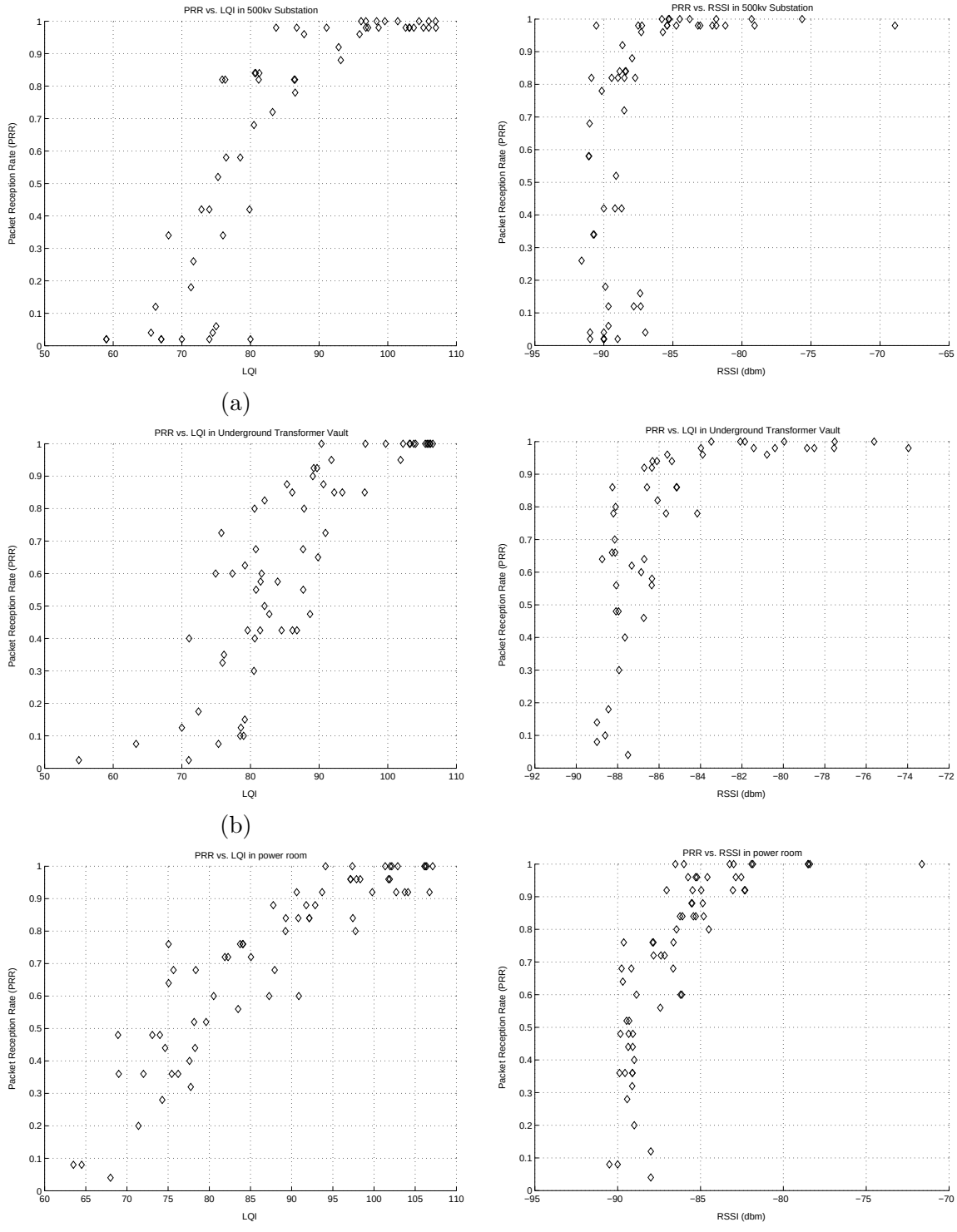

Figure 36: PRR vs. LQI and PRR vs. RSSI measurements in (a) a 500 kV substation, (b) an underground transformer vault, and (c) an indoor power control room.

of energy consumption, and hence in terms of the network lifetime. Intuitively, it can be useful to increase the number of one-hop nodes with the use of external antennas. This would provide the opportunity for distributing the data relaying functionality over a larger set of nodes and thus improve network lifetime.

Some possible concerns with the use of external antennas are the relatively large form-factor involved, and the equipment cost. For 2.4 GHz operation, high gain parabolic grid antennas, sector antennas, or even omni-directional antennas can be 0.5-1m in length and weigh 0.5-5kg. The cost of antennas also changes depending on the gain and functionality [4], [5], [6]. In sensor network applications, it is also important to note that the sink node does not particularly have any form factor or cost constraints. Moreover, while external antennas for 2.4 GHz operation are manageable, those for lower frequencies (433 MHz, 900 MHz) are likely to be much larger due to the larger wave-length. Commercially available external antennas for lower frequencies are also more expensive.

To quantify the use of external antennas in WSANs, we conducted experiments with TMote-Sky motes. To connect the external antennas to the TMote-Sky motes, we soldered an SMA (Sub-Miniature ver-A) connector to the circuit board, while also disconnecting the internal antenna and changing the location of one capacitor on the board. Note that the Tmote Sky motes come with 3.1 dBi internal antennas. In our experiments, we integrated two different external antennas: i) HyperLink 8 dBi omni-directional antenna [6], and Titanis 4 dBi omni-directional antenna [5].

In our measurements, we used a pair of TMote-Sky motes, one as the sender and the other as the receiver. The transmitter was also programmed to continuously transmit a configurable number of packets with 1 sec inter packet arrivals. We also vary the transmit power from -25 dBm to 0 dBm, the maximum allowed power level by the Chipcon CC2420 radio. The data packet size was set to 30 Bytes. The external antennas were also fixed at a distance of 1.7m above the ground to prevent the channel

Table 7: Communication range measurements vs. transmission power in outdoor and indoor environments.

Antenna Type and Environment	Tx Power (dBm)	Communication Range (m)	Current Consumption (mA)
Internal - 3.1 dBi (Outdoor)	-25	15	8.5
	-15	20	9.9
	-7	50	12.5
	-3	60	15.2
	0	75	17.4
External - 4 dBi (Outdoor)	-25	20	8.5
	-15	25	9.9
	-7	80	12.5
	-3	90	15.2
	0	100	17.4
External - 8 dBi (Outdoor)	-25	50	8.5
	-15	60	9.9
	-7	110	12.5
	-3	120	15.2
	0	150	17.4
External - 4 dBi (Indoor)	-25	12	8.5
	-15	15	9.9
	-7	18	12.5
Internal - 3.1 dBi (Indoor)	-25	10	8.5
	-15	12	9.9
	-7	15	12.5
External - 8 dBi (Indoor)	-25	15	8.5
	-15	17	9.9
	-7	20	12.5

impairments caused by the ground reflections. For each type of antenna, we took readings at several receiver locations. We also stopped measuring at a distance where the receiver received signal strength fell to about -85 dBm or worse.

In Table 7, we present the communication range measurements vs. different transmission power levels in different deployment environments. Note that in indoor environments, we could not make measurements with higher transmission power levels since the length of the indoor corridor was limiting our communication range measurements. Hence, we continued further range studies in outdoor environments.

In the outdoor measurements, we observed that the communication ranges are

improved by external antennas significantly. For example, for 0 dBm transmission power, the communication range of the sensor mote is increasing from 75 m (i.e., internal antenna with 3.1 dBi gain) to 150 m (external antenna with 8 dBi gain). Hence, the use of an external antenna in an outdoor environment can halve the number of hops to the sink node. However, the relative performance improvements in indoor and underground environments are not very significant. This is because in indoor and underground environments exhibit widely varying characteristics varies over space and time because of obstructions and RF noise. In our experiments, we also observed that the communication range of low power TMote-Sky modules can be up to 12 m in an underground environment. To this end, the electric utilities need to use link-quality-based and energy-aware multi-hop routing solutions [28] to achieve real-time and reliable communication in an underground environment. We also want to point that these communication range measurements should be taken as providing a rough idea, rather than exact measurements. The exact values are likely to vary depending on the environment.

CHAPTER VI

CONCLUSIONS AND FUTURE RESEARCH DIRECTIONS

In this thesis, first the characteristics and challenges of wireless sensor and actor networks (WSANs) are investigated and then based on these characteristics, new and efficient communication protocols are proposed. Specifically, the following four areas are investigated under this research:

1. On the Cross-Layer Interactions between Congestion and Contention in WSANs
2. Real-Time and Reliable Transport in WSANs
3. Resource-Aware and Link-Quality-Based Routing in WSANs
4. WSAN Applications and Experiments for Electric Utility Automation

6.1 Research Contributions

6.1.1 On the Cross-Layer Interactions between Congestion and Contention in WSANs

Recently, a number of congestion detection and control algorithms have been proposed for wireless sensor networks [15],[34], and [59]. The majority of these algorithms state that cross-layer interactions between transport layer and MAC layer are imperative for efficient congestion detection and hence congestion control. Despite the considerable amount of research on several aspects of congestion detection and control in sensor networks, the interdependence of congestion and contention in WSANs is yet to be efficiently studied and addressed.

In Chapter 2, the interactions between contention resolution and congestion control mechanisms as well as the physical layer effects in wireless sensor and actor

networks (WSANs) were investigated in detail. An extensive set of simulations was performed in order to quantify the impacts of several network parameters on the overall network performance. In addition, the main sources of network congestion in WSANs were identified as (i) channel contention and interference, (ii) source reporting rates, (iii), many-to-one network nature, (iv) number of event sources, and (v) packet collisions. The results of this analysis confirm the urgent need for a delay-constrained reliable event transport solution with an efficient congestion detection and control mechanism in WSANs.

6.1.2 Real-Time and Reliable Transport in WSANs

The existing and potential applications of WSANs span a very wide range, including real-time target tracking and surveillance, homeland security, and biological or chemical attack detection [16]. Realization of these currently designed and envisioned applications, however, directly depends on real-time and reliable communication capabilities of the deployed sensor/actor network.

In Chapter 3, a real-time and reliable transport $(RT)^2$ protocol was proposed to address the communication challenges introduced by the coexistence of sensors and actors in WSANs. The $(RT)^2$ protocol is a novel transport solution that seeks to achieve reliable and timely event detection with minimum possible energy consumption. It includes a combined congestion control mechanism that serves the dual purpose of achieving reliability and conserving energy. The $(RT)^2$ protocol operation is determined by the current network state based on the delay-constrained event reliability and congestion condition in the network. If the delay-constrained event reliability is lower than required, $(RT)^2$ adjusts the reporting frequency of source nodes aggressively to reach the desired reliability level as soon as possible. If the reliability is higher than required, then $(RT)^2$ reduces the reporting frequency conservatively to conserve energy while still maintaining reliability. This self-configuring nature of

$(RT)^2$ makes it robust to random, dynamic topology in WSANs. Furthermore, to address the different reliability requirements of actor-actor communication, $(RT)^2$ incorporates adaptive rate-based transmission control and (SACK)-based reliability mechanism during actor-actor communication. Performance evaluation via simulation experiments shows that $(RT)^2$ achieves high performance in terms of reliable event detection, communication latency and energy consumption in WSANs.

6.1.3 Resource-Aware and Link-Quality-Based Routing in WSANs

In Chapter 4, to address energy limitations and link quality variations in WSANs, a resource-aware and link-quality-based (RLQ) routing protocol was developed for WSANs. The RLQ routing protocol uses a link-cost metric, which is based on both energy efficiency and link quality statistics. The primary objective of the RLQ routing protocol is to adapt to varying wireless channel conditions, while exploiting the heterogeneous capabilities in WSANs. To accomplish this objective, the RLQ routing protocol biases the use of resource-rich actor nodes over energy-constrained sensor nodes for packet forwarding and processing in the network. Specifically, the proposed link cost metric captures the expected energy cost to transmit, receive and retransmit a packet, while considering the residual energy levels of the sensor nodes. Moreover, for nodes that have high energy resources, e.g., actor nodes, the transmission and reception of packets have negligible energy cost, which is also reflected in the link cost metric.

Unlike most of the existing simulation-based studies, this research effort is guided by extensive field experiments of link-quality dynamics at various locations over a long period of time using recent sensor/actor network platforms. Through these experiments, significant performance improvements of the RLQ protocol over existing routing protocols have been demonstrated in terms of packet reception rate, throughput, and network lifetime.

6.1.4 WSAN Applications and Experiments for Electric Utility Automation

In today's competitive electric utility marketplace, electric utilities face growing demands to produce reliable power, comply with environmental regulations and meet corporate financial objectives. Given the increasing age of many electrical systems and the dynamic electric utility market, intelligent and low cost monitoring and control systems are required in order to improve the productivity and efficiency of such systems.

With the recent advances in wireless sensor and actor networks (WSANs), the realization of low-cost embedded electric utility monitoring systems have become feasible. In this regard, accurate wireless channel models are extremely important for the design of WSAN-based electric utility communication architectures. These channel models provide utility network designers with the ability to predict the performance of the communication system for specific propagation environment, channel modulation, and frequency band. Although there exists radio propagation measurements in urban areas, office buildings, and factories [46], [67], the propagation characteristics in utility systems are yet to be efficiently studied and addressed.

In Chapter 5, a statistical characterization of the wireless channel in different electric utility environments is presented. Field tests have been performed on 802.15.4 compliant wireless sensor/actor networks in both a 500 kV substation as well as an underground network transformer vault to measure background noise, channel characteristics, and attenuation in the 2.4 GHz frequency band. Various communication links, including both line-of-sight (LOS) and non-LOS (NLOS) scenarios, are also considered. In addition, the use of external antennas in WSANs is investigated to improve the communication range in the network. In this context, extensive measurements are made to quantify the use of external antennas in indoor, outdoor and underground utility environments.

6.2 Future Research Directions

- **Analytical Wireless Sensor and Actor Network Modelling:** To meet the requirements and constraints of practically deployable WSAN applications, an analytical sensor/actor network modelling should be developed based on general features identified through a careful analysis of existing and envisioned WSAN applications. This analytical model can facilitate the design of WSANs by characterizing them according to these general features and providing a set of performance objectives. The specification of each network's performance requirements within this analytical model can also enable the design of efficient communication protocols.

- **Integration of WSANs with Next Generation Wireless Internet (NGWI):** In WSANs, to achieve anywhere, anytime seamless service to the end users, it is required to integrate sensor/actor nodes with the NGWI architectures. However, the memory, power and processing constraints of WSANs, coupled with the limitations of wireless environments, call for unified and adaptive communication protocols. The impact of these protocols on the overall performance of the integrated architecture of WSANs and NGWI should also be investigated through extensive field experiments.

- **Spatial-Temporal Correlation-based Communication in WSANs:** Wireless Sensor and Actor Networks (WSANs) are characterized by the collaborative operation of sensors and actors. In addition to the collaborative nature of WSANs, the spatio-temporal correlation among the sensor observations is another unique characteristic of WSANs. Although the $(RT)^2$ protocol achieves reliable event detection with no congestion, it can be extended to exploit the correlation and to balance the tradeoffs between accuracy of real-time reporting and minimizing the consumption of network resources through aggregation,

processing, and approximation functions over space and time.

- **Dynamic Spectrum Management Techniques for WSANs:** With the rapid development and continuous expansion of WSANs, it is expected that in the next decade the world will be full of wireless sensor/actor networks. Due to the inefficiency in the spectrum usage and the diverse quality of service (QoS) requirements of the WSAN applications, the limited radio frequency spectrum will be extremely crowded. This spectrum crowding and scarcity will necessitate employing dynamic spectrum management and sharing techniques for WSANs to exploit the existing wireless spectrum opportunistically. Therefore, cross-layer spectrum management functionalities, such as spectrum sensing, spectrum decision, and spectrum mobility, as well as the influence of these functionalities on the overall performance of the WSANs should be investigated.

REFERENCES

[1] "Chipcon - CC2420 Radio Chip." http://www.chipcon.com, January 2007.

[2] "Component-based Operating System for Wireless Sensor Networks - TinyOS." www.tinyos.net/tinyos-1.x, May 2007.

[3] "Crossbow Technology - MicaZ Node." htttp://www.xbow.com, April 2007.

[4] "FAB-Corp Wireless Networking Hardware." http://www.fab-corp.com, May 2007.

[5] "GigaAnt Antenna Solutions." http://www.gigaant.com, May 2007.

[6] "HyperLink Technologies." http://www.hyperlinktech.com, May 2007.

[7] "Moteiv Corporation - Tmote Sky Node." http://www.moteiv.com, May 2007.

[8] "The Network Simulator, ns-2." http://www.isi.edu/nsnam/ns/index.html, January 2007.

[9] "Quality of Electricity Supply Initial Benchmarking on Actual Levels, Standards and Regulatory Strategies." Council of European Energy Regulators, Working Group on Quality of Electric Supply, 2001.

[10] "Wireless LAN medium access control (MAC) and physical layer (phy) specifications." IEEE 802.11 Standard, 2001.

[11] "Industrial Wireless Technology for the 21^{st} Century." U.S. Department of Energy, Office of Energy and Renewable Energy Report, 2002.

[12] "Wireless Medium Access Control (MAC) and Physical Layer (PHY) Specifications for Low-Rate Wireless Personal Area Networks (LR-WPANs)." IEEE 802.15.4 Standard, Oct. 2003.

[13] "Assessment Study on Sensors and Automation in the Industries of the Future." U.S. Department of Energy, Office of Energy and Renewable Energy Report, 2004.

[14] Aad, I. and Castelluccia, C., "Differentiation Mechanisms for IEEE 802.11," in *Proceedings of IEEE INFOCOM 2001*, (Anchorage, AK), 2001.

[15] Akan, O. and Akyildiz, I. F., "Event-to-Sink Reliable Transport in Wireless Sensor Networks," *IEEE/ACM Transactions on Networking*, vol. 13, pp. 1003–1017, October 2005.

[16] Akyildiz, I. F. and Kasimoglu, I. H., "Wireless Sensor and Actor Networks: Research Challenges," *Ad Hoc Networks (Elsevier)*, vol. 2, pp. 351–367, October 2004.

[17] Akyildiz, I. F., Melodia, T., and Chowdhury, K., "A Survey on Wireless Multimedia Sensor Networks," *Computer Networks (Elsevier)*, vol. 51, pp. 921–960, March 2007.

[18] Akyildiz, I. F., Su, W., Sankarasubramaniam, Y., and Cayirci, E., "Wireless Sensor Networks: A Survey," *Computer Networks (Elsevier)*, vol. 38, pp. 393–422, March 2002.

[19] Akyildiz, I. F., Vuran, M. C., and Akan, O. B., "A Cross Layer Protocol for Wireless Sensor Networks," in *Proceedings of CISS 2006*, (Princeton, NJ), March 2006.

[20] Chlamtac, I., Conti, M., and Liu, J., "Mobile Ad-hoc Networking: Imperatives and Challenges," *Ad Hoc Networks Journal (Elsevier)*, vol. 1, pp. 13–64, July 2003.

[21] Cleveland, F. and Ehlers, R., "Guidelines for Implementing Substation Automation using UCA-SA (Utility Communications Architecture-Substation Automation)," in *Electric Power Research Institute Technical Report-1002071*, 2003.

[22] Fu, Z., Zerfos, P., Luo, H., Lu, S., Zhang, L., and Gerla, M., "The Impact of Multihop Wireless Channel on TCP Throughput and Loss," in *Proceedings of IEEE INFOCOM 2003*, April 2003.

[23] G. Simon, A.Ledeczi, M., "Sensor Network-Based Countersniper System," in *Proceedings of ACM SENSYS 2004*, (Baltimore, MD, USA), November 2004.

[24] Goodman, F. and et al., "Technical and System Requirements for Advanced Distribution Automation," in *Electric Power Research Institute Technical Report-1010915*, June 2004.

[25] Gungor, V. C., Akan, O. B., and Akyildiz, I. F., "A Real-Time and Reliable Transport Protocol for Wireless Sensor and Actor Networks," *to appear in IEEE/ACM Transactions on Networking for publication*, June 2008.

[26] Gungor, V. C. and et al., "Wireless Channel Measurements and Experiments for Electric Utility Automation," in *preparation*, 2007.

[27] Gungor, V. C. and Lambert, F. C., "A Survey on Communication Networks for Electric System Automation," vol. 50, pp. 877–897, May 2006.

[28] Gungor, V. C., Sastry, C., Song, Z., and Integlia, R., "Resource-Aware and Link-Quality-Based Routing in Wireless Sensor and Actor Networks," in *Proceedings of IEEE ICC*, (Scotland, UK), June 2007.

[29] Gungor, V. C., Vuran, M. C., and Akan, O. B., "On the Cross-Layer Interactions between Congestion and Contention in Wireless Sensor and Actor Networks," *to appear in Ad Hoc Networks Journal (Elsevier)*, August 2007.

[30] Gungor, V. and Akan, O., "Delay-Aware Reliable Transport in Wireless Sensor Networks," *International Journal of Communication Systems (Wiley)*, January 2007.

[31] Hashemi, H., "The Indoor Radio Propagation Channel," *Proceedings of the IEEE*, pp. 943–968, July 1993.

[32] Holland, G. and Vaidya, N., "Analysis of TCP Performance over Mobile Ad Hoc Networks," in *Proceedings of ACM MOBICOM 1999*, (Seattle, WA, USA), August 1999.

[33] Howitt, I. and Gutierrez, J., "IEEE 802.15.4 Low Rate-Wireless Personal Area Network Coexistence Issues," in *Proc. of IEEE WCNC 2003*, March 2003.

[34] Hull, B., Jamieson, K., and Balakrishnan, H., "Techniques for Mitigating Congestion in Sensor Networks," in *Proceedings of ACM SENSYS 2004*, (Baltimore, MD, USA), November 2004.

[35] Kevan, T., "Case Study: When Renovation Includes Building Automation," in *Proc. of Sensors Magazine*, May 2006.

[36] Krishnamurthy, L. and et al., "Design and Deployment of Industrial Sensor Networks: Experiences from a Semiconductor Plant and the North Sea," in *Proceedings of ACM SENSYS 2005*, (CA, USA), November 2005.

[37] Lal, D. and et al., "Measurement and Characterization of Link Quality Metrics in Energy Constrained Wireless Sensor Networks," in *Proceedings of IEEE GLOBECOM 2003*, (San Francisco, USA), December 2003.

[38] Li, J., Blake, C., Couto, D. D., Lee, H., and Morris, R., "Capacity of Ad Hoc Wireless Network," in *Proceedings of ACM MOBICOM 2001*, (Rome, Italy), 2001.

[39] Liu, J. and Singh, S., "ATCP: TCP for Mobile Ad Hoc Networks," *IEEE Journal on Selected Areas in Communications*, vol. 19, pp. 1300–1315, July 2001.

[40] Melodia, T., Pompili, D., Gungor, V. C., and Akyildiz, I. F., "A Distributed Coordination Framework for Wireless Sensor and Actor Networks," in *Proceedings of ACM MOBIHOC 2005*, (Urbana-Champaign, IL), May 2005.

[41] Molina, F. J. and et al., "Analyzing the Transitional Region in Low Power Wireless Links," in *Proceedings of ADHOC-NOW 2003*, (Canada), 2003.

[42] Parsons, J., "The Mobile Radio Propagation Channel," in *Pentech Press*, 1992.

[43] Petriu, E. and et al., "Sensor-Based Information Appliances," in *Proceedings of IEEE Instrumentation and Measurement Magazine*, pp. 31–35, 2000.

[44] Polastre, J., Szewczyk, R., and Culler, D., "Telos: Enabling Ultra-low Power Wireless Research," in *Proceedings of IEEE ISPN 2005*, April 2005.

[45] Rappapport, T., "Indoor Radio Communications for Factories of the Future," *IEEE Communications Magazine*, pp. 15–24, May 1989.

[46] Rappapport, T., "Wireless Communications: Principles and Practice," in *Prentice Hall*, 2002.

[47] Roman, J. and et al., "Regulation of Distribution Network Business," *IEEE Transactions on Power Delivery*, vol. 14, pp. 662–669, August 1999.

[48] Schwartz, M., "Mobile Wireless Communications," in *Cambridge University Press,*, (New York, USA), 2004.

[49] Schwiebert, L., Gupta, S. K. S., and Weinmann, J., "Research Challenges in Wireless Networks of Biomedical Sensors," in *Proceedings of ACM MOBICOM 2001*, (Rome, Italy), 2001.

[50] Seada, K., Zuniga, M., Helmy, A., and Krishnamachari, B., "Energy-Efficient Forwarding Strategies for Geographic Routing in Lossy Wireless Sensor Networks," in *Proceedings of IEEE SECON 2004*, (Santa Clara, CA, USA), October 2004.

[51] Sohrabi, K., Manriquez, B., and Pottie, G., "Near Ground Wideband Channel Measurement," in *Proceedings of IEEE Vehicular Technology Conference*, 1999.

[52] Son, D., Krishnamachari, B., and Heidemann, J., "Experimental Analysis of Concurrent Packet Transmissions in Low-Power Wireless Networks," in *Proc. of ACM SENSYS 2006*, November 2006.

[53] Srinivasan, K. and Levis, P., "RSSI is Under Appreciated," in *Proc. of EMNET 2006*, May 2006.

[54] Stephenson, M. and et al., "Exploiting Emerging Tools in Short Range Wireless Technologies," in *Proceedings of International Conference on 3G Mobile Communication Technologies*, June 2003.

[55] Sundaresan, K., Anantharaman, V., Hsieh, H.-Y., and Sivakumar, R., "ATP: A Reliable Transport Protocol for Ad-hoc Networks," in *Proceedings of ACM MOBIHOC 2003*, (Annapolis, MD USA), June 2003.

[56] Vuran, M. C., Akan, O. B., and Akyildiz, I. F., "Spatio-Temporal Correlation: Theory and Applications for Wireless Sensor Networks," *Computer Networks Journal (Elsevier)*, vol. 45, pp. 245–259, June 2004.

[57] Vuran, M. C., Gungor, V. C., and Akan, O. B., "On the Interdependency of Congestion and Contention in Wireless Sensor Networks," in *Proc. of ICST SenMetrics 2005*, (San Diego, CA), July 2005.

[58] Wan, C. Y., Campbell, A. T., and Krishnamurthy, L., "PSFQ: A Reliable Transport Protocol for Wireless Sensor Networks," in *Proceedings of WSNA 2002*, (Atlanta, GA, USA), September 2002.

[59] Wan, C. Y., Eisenman, S. B., and Campbell, A. T., "CODA: Congestion Detection and Avoidance in Sensor Networks," in *Proceedings of ACM SENSYS 2003*, (CA, USA), Nov. 2003.

[60] Werner-Allen, G. and et al., "Deploying a Wireless Sensor Network on an Active Volcano," in *Proceedings of IEEE Internet Computing*, March/April 2006.

[61] Woo, A. and Culler, D. E., "A Transmission Control Scheme for Media Access in Sensor Networks," in *Proceedings of ACM MOBICOM*, (Rome, Italy), July 2001.

[62] Woo, A., Tong, T., and Culler, D. E., "Taming the Underlying Challenges of Reliable Multihop Routing in Sensor Networks," in *Proceedings of ACM SENSYS 2003*, (CA, USA), November 2003.

[63] Xie, Z. and et al., "An Information Architecture for Future Power Systems and Its Reliability Analysis," *IEEE Transactions on Power Systems*, vol. 17, pp. 857–863, August 2002.

[64] Yu, X., "Improving TCP Performance over Mobile Ad Hoc Networks by Exploiting Cross-Layer Information Awareness," in *Proceedings of ACM MOBICOM 2004*, (PA, USA), 2004.

[65] Zhao, J. and Govindan, R., "Understanding Packet Delivery Performance in Dense Wireless Sensor Networks," in *Proceedings of ACM SENSYS*, (CA, USA), November 2003.

[66] Zhou, G., He, T., Stankovic, J., and Abdelzaher, T., "RID: Radio Interference Detection in Wireless Sensor Networks," in *Proceedings of IEEE INFOCOM*, (Miami, USA), March 2005.

[67] Zuniga, M. and Krishnamachari, B., "Analyzing the Transitional Region in Low Power Wireless Links," in *Proceedings of IEEE SECON 2004*, (Santa Clara, CA, USA), October 2004.

VITA

Vehbi Cagri Gungor was born on September 5, 1979, in Ankara, Turkey. He received his B.Sc. and M.Sc. degrees in Electrical and Electronics Engineering from Middle East Technical University, Ankara, Turkey, in 2001 and 2003, respectively. He attended the doctoral program at the School of Electrical and Computer Engineering of Georgia Institute of Technology, Atlanta, GA, from January 2004 to August 2007. At the same time, he was a research assistant in the Broadband and Wireless Networking Laboratory (BWN-LAB), Georgia Tech. He is also the recipient of the IEEE International Symposium On Computer Networks (ISCN) 2006 Best Paper Award. In August 2007, he received his Ph.D. in Electrical and Computer Engineering from Georgia Institute of Technology.